Drying and Fermentation of Cocoa Pod Husk for Increasing Total Crude Protein Content

Nattawut Sianoun

A Thesis Submitted in Partial Fulfillment of the Requirements for the Degree of Doctor of Philosophy in Chemical Engineering (International Program) Prince of Songkla University 2024

Drying and Fermentation of Cocoa Pod Husk for Increasing Total Crude Protein Content

Nattawut Sianoun

A Thesis Submitted in Partial Fulfillment of the Requirements for the Degree of Doctor of Philosophy in Chemical Engineering (International Program) Prince of Songkla University 2024

Thesis Title   Drying and Fermentation of Cocoa Pod Husk for Increasing

       Total Crude Protein Content

Author   Mr. Nattawut Sianoun

Major Program Chemical Engineering (International Program)

Major Advisor   **Examining Committee**:

……………………………..   …...………......................Chairperson

(Assoc. Prof. Dr. Juntima Chungsiriporn) (Asst. Prof. Dr. Nirattisai Rakmak)

…...………………………..Committee

(Assoc. Prof. Dr. Pakamas Chetpattananondh)

…...………………………..Committee

(Asst. Prof. Dr. Pornsiri Kaewpradit)

…...………………………..Committee

(Asst. Prof. Dr. Parinya Khongprom)

…...………………………..Committee

(Assoc. Prof. Dr. Juntima Chungsiriporn)

   The Graduate School, Prince of Songkla University, has approved this

thesis as partial fulfillment of the requirements for the Doctor of Philosophy Degree in

Chemical Engineering (International Program)

       …………………………………………...

       (Asst. Prof. Dr. Kawinbhat Sirikantisophon)

       Acting Dean of Graduate School

This is to certify that the work here submitted is the result of the candidate's own investigations. Due acknowledgement has been made of any assistance received.

..……………………………….Signature

(Assoc. Prof. Dr. Juntima Chungsiriporn)

Major Advisor

………………………..…….Signature

(Mr. Nattawut Sianoun)

Candidate

I hereby certify that this work has not been accepted in substance for any degree, and is not being currently submitted in candidature for any degree.

..………………………..……. Signature

(Mr. Nattawut Sianoun)

Candidate

ชื่อวิทยานิพนธ์	การศึกษาลักษณะการอบแห้งเปลือกฝักโกโก้และการหมักเพื่อเพิ่มปริมาณโปรตีนโดยการออกแบบการทดลองแบบพื้นผิวตอบสนอง
ผู้เขียน	นาย ณัฐวุฒิ เศียรอุ่น
สาขาวิชา	วิศวกรรมเคมี (หลักสูตรนานาชาติ)
ปีการศึกษา	2565

บทคัดย่อ

กระบวนการเก็บเกี่ยวผลโกโก้เพื่อนำเมล็ดไปผลิตเป็นช็อคโกแลตหรือผงโกโก้แห้ง พบว่ามีของเสียเกิดขึ้นในปริมาณที่ค่อนข้างสูง เปลือกฝักโกโก้คิดเป็น 70-80% ของผลโกโก้ทั้งหมด โดยปกติเปลือกฝักโกโก้จะถูกกำจัดโดยการนำไปทิ้งที่โคนต้นไม้เพื่อทำปุ๋ยหมัก จากการวิเคราะห์องค์ประกอบทางเคมีของเปลือกฝักโกโก้ พบว่าประกอบไปด้วยโปรตีนประมาณ 5.0 - 6.2% ไขมัน 1.5% เถ้า 6.7% ใยอาหาร 36.6% ซึ่งเปลือกฝักโกโก้มีความน่าสนใจในการนำไปแปรรูปเพื่อเพิ่มมูลค่า โดยเฉพาะใช้เป็นวัตถุดิบตั้งต้นในกระบวนการผลิตอาหารสัตว์ เนื่องจากมีราคาถูกและมีโปรตีนสูงเทียบเคียงได้กับข้าวโพดสำหรับเลี้ยงสัตว์ การศึกษานี้มีวัตถุประสงค์เพื่อเพิ่มมูลค่าเปลือกฝักโกโก้ แต่การที่จะนำของเสียดังกล่าวไปแปรรูปเพื่อเพิ่มมูลค่า จำเป็นต้องมีการศึกษากระบวนการอบแห้ง เพื่อให้มีความชื้นสุดท้ายเหมาะสมสำหรับการจัดเก็บให้สัตว์ได้กินในช่วงที่หญ้าสำหรับเลี้ยงสัตว์ขาดแคลน นอกจากนี้การหมักยังจะช่วยลดปริมาณสารธีโอโบรมีนในเปลือกฝักโกโก้เนื่องจากสารดังกล่าวมีคุณสมบัติออกฤทธิ์เช่นเดียวกับคาเฟอีน รวมไปถึงการเพิ่มปริมาณโปรตีนดิบและสารแอนติออกซิเดนท์เพื่อให้เหมาะแก่เป็นอาหารสดสำหรับสัตว์อีกด้วย

ส่วนที่ 1 เป็นการศึกษาการทำแห้งเปลือกฝักโกโก้โดยที่เปลือกฝักโกโก้ซึ่งมีความชื้นเริ่มต้น 5.40 ±0.05 กิโลกรัมน้ำ/ กิโลกรัมของเปลือกฝักโกโก้แห้ง ทำการอบแห้งที่อุณหภูมิ 50, 60 และ 70 องศาเซลเซียส โดยกำหนดอัตราการระบายอากาศที่ 3 ลิตร/นาที แบบจำลองทางคณิตศาสตร์กึ่งทฤษฎี 12 แบบถูกนำมาใช้ในการทำนายอัตราความชื้นที่เปลี่ยนไปของเปลือกฝักโกโก้ที่อุณหภูมิการอบแห้งต่างๆ แบบจำลองทางคณิตศาสตร์ที่เหมาะสมสำหรับอธิบายพฤติกรรมการอบแห้งเปลือกฝักโกโก้จำเป็นต้องมีค่าทางสถิติที่ดีที่สุดโดยการเปรียบเทียบค่าทางสถิติ ได้แก่ ความแปรผันของตัวแปรตอบสนอง ค่าไคสแควร์ที่ลดลง ความคลาดเคลื่อนกำลังสองเฉลี่ยของราก และผลรวมของข้อผิดพลาดกำลังสอง จากการทดลองพบว่าแบบจำลองทางคณิตศาสตร์โดย Midilli และคณะ สามารถอธิบายลักษณะทางกายภาพของการอบแห้งเปลือกฝักโกโก้ได้ดีที่สุด โดยมีความแปรผันของตัวแปรตอบสนองสูงสุด ในขณะที่ค่าไคสแควร์ที่ลดลง กำลังสองเฉลี่ยของความคลาดเคลื่อน และผลรวมของความคลาดเคลื่อนกำลังสองมีค่าต่ำที่สุดเมื่อเทียบกับแบบจำลองทางคณิตศาสตร์อื่นๆ จาก

การพิจารณาความสัมพันธ์โดยสมการของอาร์เรเนียสพบว่าค่าสัมประสิทธิ์การแพร่กระจายที่มี ประสิทธิผลของการถ่ายเทความชื้นมีค่าระหว่าง 7.979×10^{-10} - 13.298×10^{-10} ตารางเมตรต่อ วินาที ที่อุณหภูมิการทำแห้ง 50, 60 และ 70 องศาเซลเซียส นอกจากนี้ยังพบว่า พลังงานกระตุ้นของ เปลือกฝักโกโก้มีค่าเท่ากับ 70.48 กิโลจูลต่อโมล

ส่วนที่ 2 จะเป็นการทดลองเพื่อลดสารธีโอโบรมีน โดยหาสภาวะในการหมักเพื่อเพิ่ม องค์ประกอบของโปรตีนทั้งหมด การผสมกากน้ำตาลลงในกระบวนการหมักโดยเปรียบเทียบความ แตกต่างกับกระบวนการหมักแบบใช้ด่างโดยการมีเติมจุลินทรีย์ Aspergillus N. เพื่อให้กระบวนการ หมักมีความสมบูรณ์ โดยสภาวะที่ให้ปริมาณสารธีโอโบรมีนต่ำสุดในขณะที่ความสามารถในการยับยั้ง สารต้านอนุมูลอิสระมีค่าสูงที่สุดคือ สภาวะที่มีการเติมกากน้ำตาลในกระบวนการหมัก สภาวะ ดังกล่าวถูกนำมาศึกษาต่อโดยการออกแบบการทดลองแบบระเบียบวิธีพื้นผิวตอบสนอง โดยตัวแปรที่ ทำการศึกษาได้แก่ ระยะเวลาการหมัก (7 ถึง 21 วัน) เปอร์เซ็นต์กากน้ำตาล (0 ถึง 10 เปอร์เซ็นต์) และอัตราส่วนของเหลวต่อของแข็ง (0 ถึง 15 มิลลิลิตรต่อกรัม) จากการออกแบบการทดลองทำให้ได้ สภาวะการทดลองทั้งหมด 17 สภาวะ การทำนายค่าตอบสนองโดยสมการทางคณิตศาสตร์จำเป็นต้อง มีการวิเคราะห์ความน่าเชื่อถือของแบบจำลองโดยใช้ ANOVA พบว่ามีความน่าเชื่อถือเนื่องจากมีค่า $R^2 = 0.9878$, $R^2_{adj} = 0.9804$, และค่า p <0.0001 จึงถือว่าแบบจำลองทางคณิตศาสตร์สำหรับ ทำนายปริมาณโปรตีนดิบเป็นที่ยอมรับได้ โดยสภาวะที่เหมาะสมซึ่งได้ปริมาณโปรตีนดิบรวมสูงที่สุด เท่ากับ 7.93 เปอร์เซ็นต์ ที่ระยะเวลาการหมัก 21 วัน กากน้ำตาล 10% และการหมักในสภาวะ ปราศจากของเหลว (L/S = 0) จุลินทรีย์ *A. niger* ที่มีการเติมในกระบวนการหมักมีบทบาทสำคัญใน การย่อยเปลือกฝักโกโก้ให้เป็นองค์ประกอบที่เล็กลงส่งผลให้ปริมาณโปรตีนดิบมีค่าสูงกว่าเปลือกฝัก โกโก้สดที่ไม่ผ่านกระบวนการหมัก นอกจากนี้สภาวะที่เหมาะสมยังทำให้ปริมาณสารธีโอโบรมีนลดลง เหลือ 0.58 ± 0.02 มก. ต่อ 100 กรัมมวลแห้ง พร้อมด้วยคุณสมบัติต้านอนุมูลอิสระที่เพิ่มขึ้นซึ่ง กระบวนการหมักเหมาะแก่การแปรรูปเป็นอาหารสดสำหรับสัตว์อีกด้วย

จากกระบวนการทดลองดังกล่าวพบว่าการเพิ่มมูลค่าเปลือกฝักโกโก้ได้รับความ ประสบสำเร็จทั้งในแง่ของการพิสูจน์หาแบบจำลองทางคณิตศาสตร์ที่เหมาะสมสำหรับอธิบาย กระบวนการทำแห้งเปลือกฝักโกโก้และการหมักเพื่อเพิ่มปริมาณโปรตีน อีกทั้งยังเป็นการเพิ่มปริมาณ สารที่มีคุณค่าและลดปริมาณสารที่เป็นอันตรายต่อสัตว์ ซึ่งเป็นแนวทางที่มีประโยชน์สำหรับการเพิ่ม มูลค่าให้แก่เปลือกฝักโกโก้ที่เป็นมิตรกับสิ่งแวดล้อมและยังสามารถเพิ่มรายได้ให้แก่เกษตรกรผู้ปลูก โกโก้อีกด้วย

คำสำคัญ: เปลือกฝักโกโก้ (CPH) แบบจำลองทางคณิตศาสตร์สำหรับการอบแห้งแบบชั้นบาง สารต้าน อนุมูลอิสระ ปริมาณโปรตีนดิบรวม การตอบสนองแบบพื้นผิว (RSM)

Thesis Title   Drying and Fermentation of Cocoa Pod Husk for
                          Increasing Total Crude Protein Content

Author   Mr. Nattawut Sianoun

Major program   Chemical Engineering (International Program)

Academic year   2023

ABSTRACT

Cocoa bean harvesting for chocolate or cocoa powder yields substantial waste, mainly cocoa pod husk (CPH), 70-80% of total cocoa fruit. Traditionally, CPH is composted at tree bases. Recent analysis shows CPH contains 5.0-6.2% protein, 1.5% fat, 6.7% ash, and 36.6% dietary fiber. CPH can be cheap, protein-rich animal feed, rivaling maize.

This study's objective is to elevate the value of cocoa husks, necessitating a focus on their processing to increase utility. To achieve this, a crucial aspect is the drying process, ensuring the final moisture content is suitable for prolonged storage and consumption during periods of scarce animal feed. Additionally, fermentation plays a role in reducing theobromine content, an active compound akin to caffeine in cocoa. This process not only increases crude protein and antioxidants but also renders cocoa husks more fitting for immediate animal consumption.

The initial segment delved into cocoa pod drying, commencing with an initial moisture content of 5.40 ± 0.05 kg $_{water}$/kg $_{dry\ matter}$. The CPH underwent drying at temperatures of 50, 60, and 70 °C, employing a ventilation rate of 3 L/mins. To predict moisture alteration rates across temperatures, 12 semi-theoretical mathematical models were utilized. Optimal model selection hinged on statistical values, encompassing reduced chi-square, root mean square error, and sum of squared errors. Among the models, the model by Midilli et al. emerged as the most adept, demonstrating superior response variable variation and the lowest reduced chi-square, mean square error, and sum of squared errors. The effective diffusion coefficient of moisture transfer, as per the Arrhenius equation, ranged from 7.979 x 10^{-10} to 13.298 x

10^{-10} m^2/s across drying temperatures of 50, 60, and 70 °C. Furthermore, the activation energy for cocoa pod shells was determined to be 70.48 kJ/mol.

The subsequent phase involves an experimentation to diminish theobromine content. Fermentation conditions were optimized to augment overall protein composition. A comparison between a molasses-based mixture and an alkaline fermentation process supplemented with Aspergillus N. microorganisms was undertaken. The condition yielding the lowest theobromine content while effectively suppressing antioxidant activity was the incorporation of molasses during fermentation. Through response surface methodology, encompassing fermentation period (7 to 21 days), molasses percentage (0 to 10%), and liquid to solid ratio (0 to 15 ml/g), an experimental design of 17 conditions was established. Mathematical equations provided reliable insights into responses, validated by ANOVA with $R^2 = 0.9878$, $R^2_{adj} = 0.9804$, and p-value < 0.0001. The optimized conditions yielded a peak total crude protein content of 7.93% after 21 days of fermentation, utilizing 10% molasses, and adhering to an anhydrous condition (L/S = 0). Aspergillus.N microorganisms proved instrumental, augmenting digestion, and resulting in elevated crude protein content compared to unfermented cocoa pods. Furthermore, these optimal conditions reduced the theobromine content to 0.58 ± 0.02 mg/100 g dry mass, concurrently heightening antioxidant properties. This renders the fermentation process suitable for the creation of nutritious animal feed.

This experimental endeavor successfully heightens the value of cocoa husks through the establishment of a suitable mathematical model for drying and the enhancement of protein content via fermentation. This approach increases beneficial constituents while curbing harmful substances, contributing to both eco-friendly cocoa husk utilization and the potential economic betterment of cocoa farmers.

Keywords: Cocoa Pod Husk (CPH), Thin-layer mathematical modeling, Theobromine, Antioxidants substances, Total Crude Protein (TCP) content, Response Surface Methodology (RSM)

ACKNOWLEDGEMENT

CONTENTS

CONTENTS (Continued)

CONTENTS (Continued)

CONTENTS (Continued)

LIST OF TABLES

LIST OF TABLES (Continued)

LIST OF TABLES (Continued)

LIST OF FIGURES

LIST OF FIGURES (continued)

LIST OF FIGURES (continued)

ABBREVIATION

a, b, c, g, h, n	Empirical constant	MR_{exp}	Experimental moisture ratio (dimensionless)
k, k_1, k_2	Drying rate constant (1/min)	MR_{pre}	Predicted moisture ratio(dimensionless)
D_e	Effective diffusivity (m^2/s)	SSE	Sum of square error
D_0	Pre-exponential factor (m^2/s)	N	Number of observations
DR	Drying rate ($g_{water}/g_{dry\ matter}$ min)	n	Positive integer
E_a	Activation energy (kJ/mol)	p	Number of constants
M_e	Equilibrium moisture content ($g_{water}/g_{dry\ matter}$ min)	R	Universal gas constant (kJ/kmol K)
M_0	Initial moisture content ($g_{water}/g_{dry\ matter}$ min)	RMSE	Root mean square error
M_t	Moisture content at time t ($g_{water}/g_{dry\ matter}$ min)	R^2	Coefficient of determination
MR	Moisture ratio (dimensionless)	T	Temperature (°C)
MR_{exp}	Experimental moisture ratio (dimensionless)	t	Drying time (min)
MR_{pre}	Predicted moisture ratio (dimensionless)	W_0	Initial weight of dried product (g)
SSE	Sum of square error	W_d	Weight of dried product (g)
N	Number of observations	W_t	Weight of product to be dried at any time (g)
n	Positive integer	$\chi 2$	Chi-square
p	Number of constants	SEC	Specific energy consumption

CHAPTER 1

INTRODUCTION

1.1   Source of problems and significance

Harvesting agricultural products generates large amounts of waste biomass that need to be disposed of in an environmentally friendly and cost-effective manner. The cocoa pod, which grows on the main and lateral branches of the cocoa plant, is a bulbous fruit. After the cocoa beans are removed, the remaining cocoa pod husk (CPH) accounts for 70-80% of the mature fruit's dry weight(Nair, 2010). This by-product is produced in significant quantities, with each ton of cocoa beans generating ten tons of wet CPH as organic waste. Traditionally, the CPH is dumped at the base of cocoa plants to decompose into organic fertilizer. However, the excessive volume of CPH can lead to an oversupply of fertilizer. Finding alternative uses for CPH can not only reduce the cost of waste management but also add value to agricultural waste.

CPH has been identified as a valuable energy source that can be used as a raw material for producing animal feed (Bhatia et al., 2020; Lorenci Woiciechowski et al., 2020). This can potentially replace costly ingredients such as maize, soybean meal, rice bran, grits, and fish meal. Utilizing CPH for low-cost animal feed production offers a competitive advantage, as 80% of the cost of animal feed production involves agricultural raw materials. Proximate and chemical analysis of CPH has revealed that it contains 8.6% crude protein, 1.5% lipid, 6.7% ash, and 36.6% total dietary fiber(Campos-Vega et al., 2018; Oddoye et al., 2013). Furthermore, it possesses acid detergent fiber, neutral detergent fiber, and total digestible nutrients at percentages of 43.8%, 56.6%, and 60.0%, respectively. Recent attention has been focused on using CPH as a raw material for animal feed production due to its low cost compared to other agricultural wastes.

However, the high moisture content of CPH, as determined by AOAC analysis at 84.3% (wet basis), can lead to rapid decomposition. Drying is the most used method for extending the shelf-life of materials and occurs in two stages. In the first phase, moisture evaporates from the material's surface into the surrounding hot air at a constant drying rate. In the second stage, moisture from the inner layers of the material diffuses

to the outer layers, driven by the evaporation of surface moisture. This second stage exhibits a decreasing drying rate over time. Various factors influence the drying process, including temperature, relative humidity, ventilation rate, and initial moisture content.

Thin layer drying equations categorize the drying characteristics of agricultural products into three types: theoretical, semi-theoretical, and empirical. The theoretical approach involves the diffusion equation or simultaneous heat and mass transfer equations. In contrast, the semi-theoretical and empirical approaches consider only the external resistance to mass transfer between materials and ambient air. These approaches are commonly used to avoid assumptions about the geometric, mass diffusion, and conductivity properties of materials. Semi-theoretical and empirical models based on the thin layer assumption were employed to investigate the moisture evaporation mechanism from agricultural materials. These models effectively fitted the drying experimental data based on Newton's law of cooling as applied to mass transfer. They assumed that isothermal and moisture transfer occurred only at the material's surface.

The drying processes of other agricultural materials have previously been investigated such as lemon basil leaf (Mbegbu et al., 2021), thyme leaves (Turan and Firatligil, 2019), scent leaf (Mbegbu et al., 2021), bitter leaf (Gumus, 2015) and elephant apple (Nag and Dash, 2016) using fitted mathematical models. These studies used parameters to evaluate the appropriateness of selected models defined by determination coefficients and chi-square. Moisture diffusivity during the drying process and the activation energy required to evaporate the moisture are described by Fick's first law and the Arrhenius type relationship equation, respectively. Gradually increasing the operating temperature positively impacted moisture reduction.

CPH containing antioxidant substances like polyphenols, flavonoids that offer potential health benefits, and CPH also contains theobromine ($C_7H_8N_4O_2$), a bitter alkaloid (Oduro-Mensah et al., 2020). The theobromine has physiological effects, including vasodilation, diuretic properties, potential health benefits, and mood enhancement (Brunetto et al., 2007). However, theobromine can be toxic to certain animals due to slower metabolism, which leads to its accumulation and adverse effects (B et al., 2013; Donkoh et al., 1991). Therefore, processes for theobromine reduction

are necessary to prevent harm to animals. Fermentation is a process commonly employed to reduce the theobromine content in agricultural products (Bhatia et al., 2020; Dahunsi et al., 2019a, 2019b; Jönsson and Martín, 2016). Fermentation with an alkaline environment promotes reactions and affects enzymatic activity, leading to the degradation or conversion of theobromine (Lorenci Woiciechowski et al., 2020). Molasses, which is abundant in sugars and serves as nutrients for microorganisms, is used in fermentation to break down and metabolize theobromine (Yaya et al., 2023).

Furthermore, the fermentation process also contributes to an increase in the total crude protein content (TCP) of CPH (Chebaibi et al., 2019a). Microorganisms involved in fermentation can produce proteolytic enzymes that break down proteins into smaller peptides and amino acids (Gupta et al., 2017). These modified protein structures may exhibit improved nutritional properties and higher bioavailability compared to the original proteins (KIM and KEENEY, 1984). Additionally, microorganisms such as bacteria or fungi utilized in the fermentation process have the capability to synthesize proteins through their metabolic activities and multiply during fermentation to generate new protein molecules (Gupta et al., 2017; Roelofsen, 1958).

Response Surface Methodology (RSM) is a statistical technique used to design experiments and optimize the impact of process variables. It is based on the principles of Design of Experiments (DOE), which is a field of applied statistics focused on planning, conducting, analyzing, and interpreting controlled tests to assess factors influencing parameter values (KIM and KEENEY, 1984). The Faced Central Composite Design (FCCD) extends the widely used Central Composite Design (CCD) for research in engineering and science (Mehmood et al., 2018a). It adds "face" points on the design space boundaries, improving coverage for exploring response surface curvature (Vásquez et al., 2019). The FCCD models the relationship between input variables and the response variable. By strategically collecting data, regression models describe this relationship. It combines factorial, axial, and face points to evaluate main effects, interaction effects, and curvature effects. The FCCD optimizes process exploration, aids in prediction under different conditions, and efficiently studies the impact of input variables on the response of interest (Roy et al., 2023a).

The aims of this study were to value added CPH by studying the drying characteristics, decreasing theobromine content, and increasing TCP content in CPH.

The drying characteristics of CPH were studied under operating temperatures of 50, 60 and 70°C, with a constant rate of air ventilation at 3 L/min and the assumption of thin layer drying materials. The effective diffusivity coefficients of moisture transfer and moisture diffusion from the activation energy applied from an Arrhenius type relationship equation were also determined. Statistical parameters were calculated to ensure model suitability for the CPH drying process. The fermentation technique was employed with various factors, including the addition of molasses and alkali substances to decrease the theobromine content while enhancing antioxidant substances in CPH. The increasing TCP content in CPH was performed by fermentation with independent parameters of fermentation time, % molasses, and liquid-to-solid ratio (L/S). Design of Experiment (DOE) and RSM were employed to optimize the single response variable, using a FCCD. Analysis of Variance (ANOVA) was conducted to validate the experimental results and ensure the acceptability of the developed model.

1.2 Research objectives

1. To increase the value of cocoa pod husk (CPH) by utilizing it as a raw material in the production of animal feed.

2. To investigate the drying characteristics of CPH under different operating temperatures.

3. To study the impact of various fermentation conditions on the reduction of theobromine and alterations in antioxidant substances while optimizing the total crude protein (TCP) contents using response surface methodology (RSM).

1.3 Scopes of research work

1. Investigate the chemical composition of cocoa pod husk (CPH) and identify potential methods to enhance its value.

2. Study the drying characteristics of CPH and determine the appropriate mathematical model that best describes the behavior of CPH during the drying process.

3. Study the effects of different fermentation methods (untreated, alkali-added, and molasses-added) on the reduction of theobromine and changes in antioxidant substances.

4. Study change of total crude protein (TCP) content by employing a fermentation technique that incorporates various factors. Optimization of the single response variable, Design of Experiment (DOE) and Response Surface Methodology (RSM) were utilized. The experiment was designed using a Face Centered Central Composite Design (FCCD).

1.4   Expected benefits

1. Optimizing the straightforward approach to handling cocoa pod husk (CPH) and adding value.

2. The drying process of cocoa pod husk (CPH) yielded a suitable mathematical model that effectively elucidates the behavior of CPH, and the model can be applied on a larger scale with confidence.

3. The theobromine content was reduced, while the concentration of antioxidant substances was increased through fermentation processes.

4. RSM (Response Surface Methodology) provided the optimal conditions for achieving the highest total crude protein (TCP) content, while enabling a clear understanding of the effects of fermentation conditions.

CHAPTER 2

THEORIES AND LITERATURE REVIREWS

2.1 Cocoa Pod Husk (CPH)

Cocoa pods exhibit variations in shape and color. In terms of cocoa fruit, the cocoa pod, or husk, constitutes approximately 56% of the total weight of matured fruit. Figure 2.1 depicts the fresh mature of cocoa fruit (a) and dried cocoa pod husk (b).

(a)   (b)

Figure 2.1 (a) Fresh cocoa mature fruit, and (b) Dried cocoa pod husk after beans separation.

In the early 1980s, cocoa pod husk had no perceived market value. Farmers' primary concern was the extraction of cocoa beans from the pod. Initially, when farmers had moderate harvests, pod husks were left to rot. However, as cocoa cultivation expanded and bean processing increased, heaps of pods accumulated on farms, reaching several tons in Nigeria. This practice continued for several years until decomposing pod remnants led to the outbreak of a chronic disease called "witch broom," which affected cocoa trees. Phytophthora spp. was identified as the causative

agent. Surveys conducted in the 1980s estimated that over 800,000 tons of decomposing cocoa pod husks were present in Nigeria. This situation reinforced the notion that the leftover harvest material was wasted with no value, becoming an environmental hazard harboring various pathogens and posing a threat to cocoa plants.

2.1.1 Chemical composition of CPH

Cocoa pod husk has gained significant attention due to its potential as a biomass feedstock for bioenergy production, the creation of value-added compounds, and its applications in agriculture. Researchers have been actively investigating methods to convert cocoa pod husk into useful products, aiming to minimize waste and maximize the utilization of this abundant byproduct from cocoa production. The table 2.1 below presents the chemical composition found in cocoa pod husk (CPH)

Table 2.1 Chemical composition of CPH.

Compound	Percentage
Crude protein	5.0-6.2
Crude fiber	32.1-35.0
Crude fat	0.87
Acid detergent fiber	43.8
Neutral detergent fiber	56.6
Total digestible nutrient	60.0

Based on research findings, cocoa pod husk (CPH) has been determined to contain approximately 5.0-6.2% crude protein content. This discovery indicates that CPH holds promise as a viable raw material for animal feed production. Given its substantial protein content, CPH could serve as a valuable and sustainable source of nutrients for livestock and other animals within the agricultural sector. Utilizing CPH in animal feed production has the potential to reduce waste generated from cocoa production while offering an environmentally friendly approach to enhancing the nutritional quality of animal feeds. Further investigations and exploration are necessary to comprehensively evaluate and optimize the incorporation of CPH into animal feed formulations.

Campos-Vega et al. 2018 studied the quality and functionality of cocoa pod husk (CPH) have improved through various processing methods such as fermentation, enzymatic hydrolysis, and combustion. These processes have led to the utilization of CPH in diverse applications, including the production of volatile fragrance compounds, extraction of lipase, skin whitening and hydration, sun screening, ruminant feed, vegetable gum, organic potash, antibacterial agents, and synthesis of nanoparticles with antioxidant and larvicidal properties. However, the exploration of CPH for high-value products, particularly in the food industry, remains limited, as well as its potential health benefits. Cocoa pod husk, which constitutes a significant by-product of the cocoa industry (up to 76%), represents an abundant, cost-effective, and renewable source of bioactive compounds such as dietary fiber, pectin, antioxidant compounds, minerals, and theobromine. This inherent composition justifies the need to enhance the value of CPH. Therefore, this review emphasizes the potential for value addition to this valuable industrial co-product, aiming to generate novel pharmaceutical, medical, nutraceutical, and functional food products.

2.1.2 Limitations and applications of CPH in animal feed

CPH possesses nutritive value that enables its use in animal feed materials, albeit limited by its theobromine content, which is toxic to livestock. Cattle can consume up to 7 kg of dried CPH per day without adverse effects, while pigs can consume up to 2 kg per day. Animals fed on CPH diets tend to consume more water due to the high sodium content. Water absorption in the small intestine is proportional to the rate of sodium chloride absorption. Furthermore, animals fed CPH diets tend to have a leaner body. In chickens, consumption of over 10% CPH results in darker yolks in laying hens and larger gizzards in broiler birds, both of which are desirable traits. Fresh or dried husks can be used as livestock feed, but the theobromine content (around 0.4%) restricts the proportion that can be consumed, limiting its use. While acceptability by animals is satisfactory, digestibility is considered poor and dependent on the husk. Polysaccharide digestibility limitations hinder the use of pod husks for methane production in biodigesters. Theobromine and caffeine are the two known antinutritional factors in cocoa husk, with theobromine being the most widely reported.

To address the antinutritional problem and make CPH suitable for inclusion in livestock diets, various treatments such as sun drying, and alkaline treatment have been tested. The following studies at CRIN assessed CPH inclusion in animal feed: (a) In layer mash, an optimum 20% inclusion level of CPH in the layer diet proved economically viable for laying hens. (b) For broiler mash (starter and finisher), a 10% replacement of CPH was found to be optimal for raising broiler chicks. (c) In cockerel diets, a 20% inclusion of CPH produced table-sized cockerels. (d) Raising growing quail benefited from a 14% dietary inclusion of CPH in quail feed. (e) Substituting 15% of maize with cocoa pod husk (cocoa husk endocarp) was deemed suitable for feeding catfish and tilapia in fish diets. (f) Growing land snails tolerated up to a 40% replacement level of maize with CPH. (g) Dried CPH served as a viable heat energy source for fish smoking.

Donkoh et al. 1991 explained that the cocoa pod husk (CPH) was found to contain the following nutrients per kilogram of dry matter: 76.6g crude protein, 43.7g ether extract, 325g crude fiber, 101g ash, 414g acid detergent fiber, 522g neutral detergent fiber, and 108g hemicellulose. The metabolizable energy content was determined to be 4.72 MJ/kg. In comparison to maize, CPH had lower levels of most amino acids, except for lysine. During a feeding trial, 450 one-week-old broiler chicks (AF Bosbek strain) were provided with five diets containing 0g, 50g, 100g, 150g, and 200g CPH per kilogram, with maize and fish meal as major components. The diets were offered ad libitum for a duration of 7 weeks, while water was freely accessible to the birds. The inclusion of increasing levels of CPH in the broiler diets led to a nearly 60% rise in food intake for the highest inclusion level (r = 0.97). However, it also resulted in reduced growth (r = -0.85) and decreased efficiency of food utilization compared to the control (r = 0.96). Birds fed with cocoa husk exhibited higher water consumption, with a trend of increased intake corresponding to each increment of CPH (r = 0.99). A significant negative correlation (r = -0.85) was observed between the CPH concentration in the diet and carcass dressing percentage. Importantly, no deaths could be attributed to the inclusion of CPH in the diet.

2.2 Drying process

Drying is defined as the process in which moisture is vaporized from a material and carried away from its surface. This is typically achieved by using a carrier gas, either passing through or over the material, sometimes under vacuum conditions (Keey 1992). Traditionally, drying refers to the removal of water through exposure to a hot airstream, but it can also involve the evaporation of any volatile liquid into a heated gas. In order for this defined drying process to occur, the moist material must acquire heat from its surroundings through convection, radiation, conduction, or internal generation methods such as dielectric or inductive heating. As a result, the moisture within the material evaporates, and the vapor is carried away by the carrier gas. The drying process is illustrated in Figure 2.2.
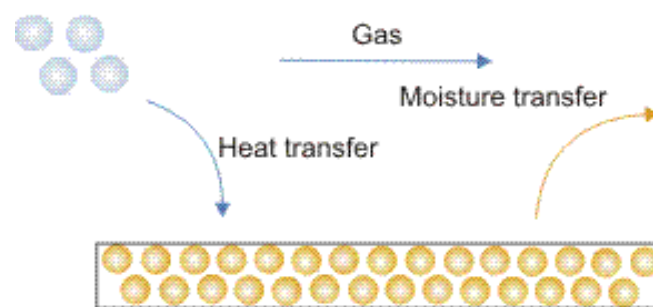
Figure 2.2 The drying process

Drying encompasses several closely related terms. Dehydration is the process of extracting water from a material or the loss of water as a constituent. In the context of food drying, dehydration refers to techniques that focus on removing moisture while retaining other volatile components that contribute to desirable aromas and flavors. Desiccation, on the other hand, implies a more thorough elimination of water. It is commonly used in food drying to indicate nearly complete dehydration for the purpose of preservation. Desiccation is also frequently used to describe the complete removal of moisture from gases.

While heat is commonly employed to remove moisture from a wet substance, moisture separation from the host material can also be achieved through pressure

differentials. This process, known as dewatering, is often utilized as an initial step for highly wet materials when the bond between moisture and solid is not strong. Dewatering can be accomplished through mechanical means such as pressing or centrifuging. However, this encyclopedia does not cover these operations as they do not involve combined heat and mass transfer processes.

Water can also be extracted through osmotic dehydration. In this process, foods are treated with concentrated solutions of salt or sugar, leading to significant water removal while limiting the uptake of solutes. The mechanism of osmotic dehydration involves the coupled diffusion of water and solutes, as described by Raoult-Wack et al. (1989). Another method of dewatering involves the use of an external direct-current field, known as electro-osmosis, which has been employed for sludge dewatering according to Yoshida and Yukawa (1992). These osmotic techniques fall outside the scope of heat and mass transfer processes.

2.2.1 Drying rate

The drying process of a material can be described as a series of steps, with the drying rate playing a crucial role. The figure below illustrates a typical drying rate curve under constant drying conditions. Point B on the curve represents the equilibrium temperature conditions of the product surface. The section from B to C, known as the constant rate period, signifies the removal of unbound water from the product. During this period, the water behaves as if the solid is not present. The surface of the product is heavily saturated with water, and the water activity is equal to one. The constant rate period continues as long as the amount of water evaporating from the surface is equal to the amount of water supplied to the material's surface.

The falling rate period is reached when the drying rate starts to decline, and the surface water activity drops below one. The rate of drying is then determined by the internal flow of liquid or vapor. This point is represented by C in the figure. At this stage, there isn't enough water on the surface to maintain a water activity value of one. The falling rate period can be further divided into two steps. The first falling drying rate occurs as the wetted spots on the surface continuously decrease until the surface is completely dried (Point D).

The second falling rate period begins at point D when the surface is entirely dry. The plane of evaporation recedes from the surface, and the heat required for moisture removal is transferred through the solid to vaporize the moisture within the material. The vapor then moves through the solid and into the air stream. The amount of water removed during this period may be relatively small compared to the constant rate and first falling rate periods. However, this period can take much longer than the constant rate period because the drying process becomes slower. The behavior of the drying rate throughout all these steps is depicted in Figure 2.3 below.
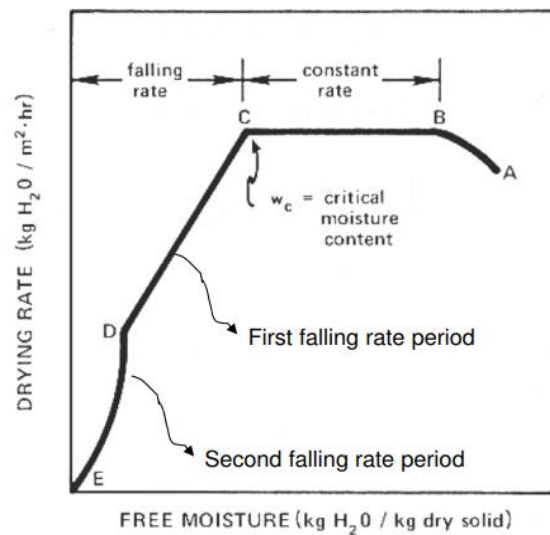
Figure 2.3 Step of drying rate behavior.

Doymaz 2005 studied a laboratory-scale hot-air dryer was used to investigate how okra air-dried under temperatures ranging from 50°C to 70°C and relative humidity ranging from 8% to 25%. The results showed that the drying process occurred during the falling rate period, indicating that moisture transfer followed Fick's diffusion model. The effective diffusivity, representing the rate of diffusion, was determined and found to increase with higher temperatures. The relationship between temperature and diffusivity was described using an Arrhenius relation, with an activation energy of 51.26 kJ/mol. To model the drying process, two mathematical models from the literature, the Page model and the simple exponential model, were applied and fitted to the experimental data. The models' performance was evaluated by

comparing observed and predicted moisture ratios using the coefficient of determination (R^2) and reduced chi-square (v^2). The analysis revealed that the Page model accurately represented the single layer drying of okra.

Al-Amin, Hossain, and Iqbal 2015 studied to assess the impact of pre-treatments (0.1% KMS, 0.2% KMS, 0.3% KMS, and blanching) and drying methods (mechanical drying and solar drying) on the dehydration and rehydration characteristics of carrots. Both drying methods resulted in dehydrated products with varying dehydration ratio, rehydration ratio, coefficient of reconstitution, and moisture content in both the dehydrated and rehydrated materials. Drying time was influenced by pre-treatments and drying methods. Pre-treatments led to increased drying time, especially for 0.3% KMS, and solar drying required longer drying time for this pre-treatment. Furthermore, pre-treatment, drying methods, and boiling time affected various rehydration properties. The highest rehydration ratio (3.70) and coefficient of reconstitution (0.48) values were obtained for 0.1% KMS pre-treated carrots using mechanical drying and 0.2% KMS pre-treated carrots using solar drying, respectively. Overall, mechanical drying proved to be more effective in terms of dehydration and rehydration properties for all pre-treatments. For example, 0.1% KMS pre-treated carrots had a coefficient of reconstitution of 0.48 when mechanically dried, while the same pre-treatment resulted in a coefficient of reconstitution of 0.45 when subjected to solar drying.

2.2.2 Drying mathematical model

The theory behind mathematical modeling of drying processes is grounded in fundamental heat and mass transfer principles, as well as thermodynamics. These principles serve as the basis for formulating mathematical equations that capture the intricate interactions during moisture evaporation from materials.

Heat and Mass Transfer Mechanisms: Drying mathematical modeling involves quantifying heat transfer (conduction, convection, radiation) and mass transfer (moisture diffusion) mechanisms that propel the drying process. These mechanisms dictate heat supply to the material and moisture movement from interior to surface for evaporation.

Thermodynamic Equilibrium and Psychrometrics: Thermodynamics underpins understanding of equilibrium between material and surroundings.

Psychrometrics, addressing air-water vapor properties, is crucial for analyzing interactions between drying material and medium.

Conservation equations: Energy and mass balance equations are foundational for mathematically describing drying. These equations account for heat and mass transfer rates within the material, interacting with the drying environment.

Empirical and Semi-Empirical Models: Empirical and semi-empirical models, like Page, Henderson-Pabis, and Lewis models, describe drying kinetics from experimental data. These models offer simplified mathematical depictions of drying behavior, aiding drying rate prediction.

Diffusion equations: Diffusion equations (e.g., Fick's second law) describe moisture movement within materials. These equations incorporate material properties and environmental conditions to predict moisture migration during drying.

Boundary and Initial Conditions: The mathematical model requires appropriate boundary and initial conditions, mirroring the physical drying setup. These conditions define starting points and constraints for mathematical equations.

Model Validation and Parameter Estimation: Models are validated by comparing predictions to experimental data. Parameter estimation techniques determine model constants and coefficients fitting experimental outcomes.

The theory underpinning mathematical modeling of drying processes is a multidisciplinary approach, drawing from heat and mass transfer, thermodynamics, and empirical modeling. By integrating these theoretical foundations, researchers can develop precise predictive mathematical models, enriching comprehension and optimization of drying processes for diverse materials and conditions.

Mbegbu et al. 2021 studied on the impact of air temperature on the drying characteristics and kinetics of scent and lemon basil leaves was examined using a vacuum oven dryer at temperatures of 30°C, 40°C, 50°C, 60°C, and 70°C. Appropriate drying models were developed to describe the drying process, which exhibited a falling rate phenomenon for both types of leaves. Six thin-layer drying models, including the Lewis model, Page model, Modified Page model, Logarithmic model, Two-term model, and Midilli model, were fitted to the moisture ratio data for scent and lemon basil leaves. The Logarithmic model demonstrated the highest coefficient of determination (R^2) and the lowest sum of square error (SSE) and root mean square

error (RMSE) values, with values of 0.9998, 0.0002, and 0.0081 for scent leaf and 0.9961, 0.0034, and 0.0222 for lemon basil leaf, respectively. The Two-term model yielded comparable values for scent leaf, while achieving R^2, SSE, and RMSE values of 0.9967, 0.0024, and 0.0185 for lemon basil leaf. These models were found to be the most suitable for all drying temperatures examined. The findings indicated that the optimal drying temperatures for scent and lemon basil leaves were 70°C and 60°C, respectively. Specific energy consumption and effective moisture diffusivity (D_{eff}) were determined at different drying air temperatures. D_{eff} values ranged from 4.76 x 10^{-13} to 1.47 x 10^{-12} m^2/s for scent leaf and from 4.80 x 10^{-13} to 2.06 x 10^{-12} m^2/s for lemon basil leaf, with increasing temperature. By utilizing the Arrhenius equation, the activation energy (E_a) and pre-exponential factor (D_0) were determined as 25.01 kJ/mol and 8.19 x 10^{-9} m^2/s for scent leaf, and 32.35 kJ/mol and 1.49 x 10^{-7} for lemon basil leaves, respectively. Consequently, based on the experimental results, the Logarithmic and Two-term models are recommended as the most suitable models for characterizing the drying kinetics of scent and lemon basil leaves.

Tunde-Akintunde and Ogunlakin 2013 investigated the drying characteristics of both pretreated and untreated pumpkin in a hot-air dryer. The drying process was conducted at air temperatures ranging from 40°C to 80°C, with a constant air velocity of 1.5 m/s. Our observations revealed that the drying occurred during the falling-rate drying period, suggesting that the primary mechanism of moisture movement from the internal regions to the surface of the pumpkin was liquid diffusion. To analyze the experimental drying data, we employed several mathematical models, including the Exponential, General Exponential, Logarithmic, Page, Midilli-Kucuk, and Parabolic models. The suitability of these models was assessed using non-linear regression analysis, considering the statistical validity of the models. Among them, the Parabolic model demonstrated the highest coefficient of determination (R^2) and the lowest values of $\chi 2$ and RMSE. These results indicate that the Parabolic model is the most appropriate for describing the dehydration behavior of pumpkin during the drying process.

Doymaz, Gorel, and Akgun 2004 studied on olive cake, a by-product of olive oil extraction, consists of the pit and pulp of the olive fruit and contains a substantial amount of oil. Although the initial moisture content of olive cake is approximately

44.78% ± 0.5 (wet basis), it possesses a high energy content, allowing for direct burning in bakeries and olive oil mills in Turkey after sun drying. However, when other manufacturing processes such as pomace oil production or bio-oil production utilizing thermal conversion methods are employed, the drying effect becomes significant. Therefore, we investigated the drying behavior of olive cake in a cabinet-type dryer, utilizing heated ambient air within a temperature range of 80-110°C and a constant air velocity of 1.2 m/s. Furthermore, we examined the impact of sample thickness on the drying characteristics, drying time, and energy quality of the dried product. The experimental data was compared to predictions made by the Page model, as well as the Henderson and Pabis model. The results showed good agreement with the Page model. To describe moisture transfer, a diffusion model was employed, and the effective diffusivity at each temperature was determined. The effective diffusivity values ranged from 489.2 to 998.4 μm^2/s. The temperature dependence of the diffusivity coefficient was expressed using an Arrhenius-type relationship, with an activation energy of 26.71 kJ/mol.

Celma et al. 2007 studied the drying characteristics of sludge were examined by subjecting it to hot air at temperatures of 20°C, 40°C, and 80°C, which simulate the range provided by an air solar heater. Air velocities of 1 m/s were used in a laboratory-scale dryer. The sludge had an average moisture content ranging from 2 to approximately 0.7- 0.08 kg water/kg dry matter. Various mathematical models were employed to simulate the drying curves of the sludge, including the Lewis, Page, Modified Page, Henderson and Pabis, Wang and Singh, Logarithmic, Two-term, Two-term exponential, Modified Henderson and Pabis, Midilli, Approximation of diffusion, Verma et al., and Simplified Fick's diffusion models. To assess the models' performance, four statistical parameters were considered: the coefficient of determination squared (r^2), reduced chi-square (v^2), root mean square error (RMSE), and the sum of residuals between observed and predicted moisture ratios. Among the models tested, the Midilli model best represented the drying characteristics of the sludge. The effective diffusivity coefficient for moisture transfer varied from 2.224 x 10^{-10} to 6.993 x 10^{-10} m^2/s over the temperature range studied. The relationship between temperature and the effective diffusivity coefficient was described by an

Arrhenius-type equation. The activation energy for moisture diffusion was determined to be 15.77 kJ/mol.

2.3   Animal feed meal

Animal feed is a vital component of animal husbandry, providing nutrition to domestic animals, especially livestock. There are two primary types of animal feed: fodder and forage. When used in isolation, the term "feed" typically refers to fodder. It is a significant expense for farmers, constituting the main cost of raising animals. To reduce this expense, farms often employ strategies such as growing their own feed, allowing animals to graze, or supplementing expensive feeds with alternatives like food waste, such as spent grain from beer brewing. Animal feed plays a crucial role in animal agriculture, serving as a primary cost for farmers. It has a significant impact on animal well-being, and certain feeding practices can have both positive and negative effects on the environment. During environmental crises, the reliance on expensive manufactured feed can pose economic challenges for farmers and herders.

2.3.1 Livestock Feed Requirements and Composition

Livestock encompasses a variety of animals, including beef cattle, dairy cattle, horses, goats, sheep, and llamas. Their specific feed requirements are not fixed, as they vary based on factors such as age, sex, breed, and environment. However, the basic nutrient requirements for livestock feed must include protein, carbohydrates, vitamins, and minerals (Herdt, 2014). Dairy cattle, for instance, require more energy in their feed compared to other types of cattle. Studies indicate that energy can be derived from different carbohydrate sources, such as non-fiber carbohydrates (NFC) from fermentable feeds, or neutral detergent fiber (NDF) from forage. Feeds with high NDF content are beneficial for rumen health but provide less energy, while the opposite is true for feeds high in NFC. To increase energy concentration in feed, fats are added, especially when NFC content is already high, as excessive NFC can reduce the NDF fraction, impacting rumen digestion. In ruminants, most proteins consumed are broken down by microorganisms in the rumen, and these microorganisms are later digested in the small intestine (Perry, 1995). The N.R.C.N.R.B.C. publication (2000) suggests that crude protein in livestock feed should be less than 7%. Lactating

ruminants, particularly dairy cattle, require higher protein levels, especially for milk synthesis. Essential minerals like calcium, phosphorus, and selenium are also necessary for livestock to maintain growth, reproduction, and bone health (Perry, 1995).

Proper feed proportions of fine and coarse particles are crucial for livestock. Finer particles are theoretically easier to digest in the rumen, but the presence of coarse particles can increase the amount of starch entering the small intestine, enhancing energetic efficiency (Secrist, 2019). Livestock can be fed through grazing on grasslands, either integrated or non-integrated with crop production. Alternatively, landless livestock, often found in stalls or feedlots, are typically fed processed feed containing veterinary drugs, growth hormones, feed additives, or nutraceuticals to improve production (Silbergeld et al., 2008). Grains are a common feed for livestock, either as the main component or as a supplement to forage-based feed. The processing of grains for feed aims to maximize starch availability and increase energy supply.

Hartog and Sijtsma 2013 studied on livestock production that is increasingly impacted by various external factors such as rising demands for animal products, limited feed supplies due to resource competition and trade barriers, concerns about food's health implications, and the effects of production systems on animal welfare and the environment. The optimization of productivity, efficiency, and profitability while considering these constraints is crucial. Animal feed and nutrition play a vital role in the livestock production chain, bridging crop cultivation with animal protein production and processing. It also represents a significant cost in livestock production. Despite advancements, there is still potential for further optimization in animal feed and nutrition. Genetic potential remains underutilized, nutrient utilization is suboptimal, and performance varies greatly among farms and individual animals. Environmental performance can also be enhanced. The emergence of new science and technologies, such as genomics, microsystem and nanotechnology, and information and communication technology (ICT), offer innovative opportunities in animal feed and nutrition. However, consumer and societal acceptance is a critical factor for success. In conclusion, animal feed and nutrition play a crucial role in livestock production. By embracing innovation, it is possible to address challenges, achieve

resource efficiency, ensure the health of both livestock and consumers, foster responsible production systems, and optimize profit along the entire value chain.

2.3.2 The Promising Potential of Cocoa Pod Husk (CPH) in Animal Feed

The potential use of cocoa pod husk (CPH) in animal feed is promising despite its limitations due to theobromine and caffeine content. CPH contains valuable nutrients and compounds, supplementing animal diets with energy and essential elements. Its use contributes to environmental sustainability, reducing waste from cocoa production. In cocoa-growing regions, CPH serves as a cost-effective, locally available feed source, lessening reliance on expensive manufactured feed during certain seasons or crises. Studies suggest CPH inclusion in animal diets can lead to desirable traits in some animals, like darker yolks in hens and larger gizzards in broiler birds. Ruminant animals efficiently digest CPH's fibrous materials, making it suitable as a supplement. However, careful feed formulation and consideration of theobromine content are essential for safe use. Ongoing research aims to optimize CPH use in animal feed, addressing potential challenges.

In conclusion, proper feed intake for livestock varies based on several factors, and their nutrition requirements must include essential nutrients. Different feed sources and processing methods can impact their overall health and productivity, with adjustments aiming to optimize rumen digestion and energy supply. Careful consideration of feed composition and particle sizes contributes to the well-being and performance of livestock, particularly in dairy cattle where milk synthesis is a crucial factor.

Osei et al. 1991 studied on a 10-month trial was conducted to assess the nutritional value of cocoa pod-and-husk (CPH) meal for laying chickens. At 37 weeks of age, 288 AF Bosbek brown egg layers were randomly divided into four groups and fed experimental diets containing 0, 25, 50, or 75 g CPH meal per kg of feed. Each treatment was replicated three times in a completely randomized design, and the chickens had ad libitum access to feed and water. The study measured various production parameters including hen-day egg production, egg weight, yolk color score, shell thickness, and Haugh unit score (a measure of interior quality). Additionally, several hematological variables such as blood hemoglobin, serum total

protein, and cholesterol levels were analyzed. Results showed that only the Haugh unit scores demonstrated a significant positive response ($P < 0.05$) to dietary CPH levels, while the other production parameters were not influenced by the addition of CPH. Similarly, the inclusion of CPH in the diet did not have a significant effect on the hematological variables measured.

Hutjens and Baltz 2000 revealed that cattle fed with ground corn, for example, exhibit significantly better milk performance. Research comparing various corn particle sizes and distribution found that a particle size of 0.5 mm should be used to achieve 80% digestibility during a 16-hour incubation. Investigations on dairy cows feeding on different harvests and processing of corn grain indicated that digestion, metabolism, and heat energy were higher for high moisture corn compared to dry corn. Grinding the corn increased dry matter intake (DMI) and resulted in higher yields of milk, protein, lactose, and non-fat solids (University of Maryland & USDA).

2.4   Theobromine

Theobromine is a naturally occurring compound primarily found in cocoa beans and derived products like chocolate and cocoa powder. It belongs to a class of alkaloids called xanthines, which also includes caffeine and theophylline. Theobromine is renowned for its bitter taste and its ability to stimulate the central nervous system. Theobromine has a chemical formula of $C_7H_8N_4O_2$ and a systematic name of 3,7-dimethylxanthine. The chemical structure of theobromine shown in Figure 2.4 below. Its structure is similar to caffeine and theophylline, although it differs in the arrangement and number of methyl groups. The main natural source of theobromine is cocoa beans, which are utilized in the production of various chocolate products. Other plant sources that contain theobromine include tea leaves, kola nuts, and guarana berries. The amount of theobromine present varies depending on the source, with dark chocolate generally containing higher levels compared to milk chocolate.
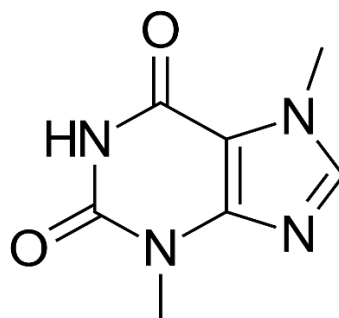
Figure 2.4 The chemical structure of theobromine ($C_7H_8N_4O_2$)

2.4.1 The impact of theobromine on animals

Theobromine acts as a mild stimulant that affects the central nervous system. Its effects are milder than those of caffeine, but it still possesses stimulating properties. Theobromine has been observed to increase heart rate, widen blood vessels, and stimulate the smooth muscles in the bronchi of the lungs. Theobromine undergoes metabolism in the liver through enzymes such as cytochrome P450 1A2. It is primarily excreted from the body through urine after undergoing various metabolic processes. The consumption of theobromine in moderate amounts is generally considered safe for most individuals. It is less likely to cause jitters or insomnia associated with high caffeine intake. However, it can still have some effects on the body, including increased urination, diuresis, and potential gastrointestinal effects such as acid reflux in susceptible individuals. It is important to note that excessive theobromine consumption can be toxic to animals, especially dogs, as their bodies metabolize it more slowly than humans. Apart from being a natural component in chocolate, theobromine has been studied for potential therapeutic applications. It has been investigated for its potential to dilate blood vessels, act as a diuretic, and affect cardiovascular health. Additionally, theobromine has been explored for its potential use as a cough suppressant due to its ability to relax the smooth muscles in the airways. It's worth noting that while theobromine and caffeine share structural and functional similarities, they are distinct compounds. Theobromine is often referred to as a "cousin" of caffeine due to their shared characteristics, but they exhibit different pharmacological profiles and levels of potency.

Eteng and Ettarh 2000 studied the effects of theobromine and a cocoa seed extract on lipid parameters were compared in rats. The rats were orally administered theobromine (700mg/kg) and cocoa extract for four consecutive days, and their serum was collected for lipid analysis. Theobromine led to significant reductions (P<0.01 to P<0.001) in total serum cholesterol, LDL-cholesterol, and triglycerides, while HDL-cholesterol levels were significantly elevated (P<0.001). In contrast, the cocoa seed extract, which contained the same amount of theobromine, caused significant increases (P<0.01 to P<0.001) in all lipid parameters compared to control rats. These findings suggest that the hypercholesterolemic effect observed with the cocoa extract is not attributed to the alkaloid theobromine but may instead be caused by another component of the extract.

Camps-Bossacoma et al. 2018 aimed to investigate the impact of cocoa theobromine on systemic and intestinal immunoglobulin (Ig) concentrations, as well as the effect of cocoa or theobromine feeding on lymphocyte composition in lymphoid tissues. Female Lewis rats at three weeks of age were assigned to three groups: a standard diet group (RF), a 10% cocoa diet group (CC), and a 0.25% theobromine diet group (TB), in two separate experiments lasting 19 days (experiment 1) and 8 days (experiment 2). Serum concentrations of IgG, IgM, IgA, and intestinal secretory IgA (sIgA) were measured. Additionally, lymphocyte populations in the thymus, mesenteric lymph nodes (MLN), and spleen were analyzed at the end of experiment 2. Both CC and TB groups in both experiments exhibited similar serum IgG, IgM, IgA, and intestinal sIgA concentrations, which were lower compared to the RF group (46-98% lower in experiment 1 and 23-91% lower in experiment 2; P < 0.05). Furthermore, in experiment 2, the cocoa and theobromine diets induced similar changes in lymphocyte composition: an increase in CD4-CD8- (+133%) and CD4+CD8- (+53%) proportions in the thymus (P < 0.01), a decrease in the percentage of T-helper (Th) lymphocytes in the MLN (-3%) (P = 0.015), and an increase in the proportion of Th lymphocytes in the spleen (+9%) (P < 0.001) after one week of diet treatment. In conclusion, theobromine present in cocoa plays an immunoregulatory role that affects both systemic and intestinal antibody concentrations and modifies lymphocyte composition in lymphoid tissues of young, healthy Lewis rats. These changes are

primarily observed after just one week of consuming a diet containing 0.25% theobromine.

2.4.2 Methods of reducing theobromine content

Reducing theobromine content in cocoa pod husk (CPH) offers various approaches, including controlled fermentation, roasting, blending with other feed ingredients, genetic selection, post-harvest processing, and chemical treatments. Each method aims to decrease the theobromine levels in CPH, making it safer for animal consumption. To ensure the effectiveness of the chosen method, thorough validation is essential. It's crucial to maintain the nutritional quality of the feed even after theobromine reduction. Additionally, safety measures should be carefully observed throughout the reduction process to ensure that the feed remains suitable and harmless for animals. Implementing these strategies can enhance the potential use of CPH as a valuable ingredient in animal feed formulations, contributing to sustainable and eco-friendly practices in the agricultural industry. Continuous research and advancements in reducing theobromine content in CPH hold promise for optimizing its application as an animal feed resource.

Brunetto et al. 2007 studied a reversed phase HPLC method was developed to analyze theobromine, theophylline, and caffeine in cocoa samples. For sample cleanup, the procedure involves online solid-phase extraction of analytes from cocoa samples into a homemade dry-packed pre-column with ODS-C18, using a column-switching system. Separation was performed on a C18 Nova-Pak column (150 mm × 3.9 mm, 4 μm) with a mobile phase of 20% methanol in water, using isocratic conditions at a flow rate of 1.4 ml/min. The validation of the method demonstrated quantitative recoveries (>95.0%) with coefficients of variation <3.2%, ensuring good precision for data validation. The integration of sample cleanup, analysis, and pre-column reconditioning increased sample throughput to 8 samples/h. The proposed method was successfully applied to analyze cocoa samples of different varieties ("Trinitario," "Forastero," and "Criollo") grown in different seasons and fermented for 3 and 7 days. Results indicated a slight decrease in theobromine and caffeine content with longer fermentation times. Additionally, the theobromine/caffeine ratio was evaluated to establish a correlation with the genotype of the samples.

Júnior et al. 2020 studied to assess the bitter taste of fermented and unfermented Amazonian cocoa samples and their derivatives, an analytical method using square wave voltammetry (SWV) with a boron-doped diamond electrode (BDD) was proposed to determine the concentrations of theobromine (TB) and caffeine (CF), along with other substances like phenolic compounds. Optimal conditions for the SWV technique, including the supporting electrolyte, pH buffer solutions, and parameters, were investigated. Analytical curves were constructed, and the limits of detection and quantification were determined as 0.027 μmol/L and 0.093 μmol/L for CF, and 0.025 μmol/L and 0.085 μmol/L for TB. Repeatability tests showed low relative standard deviation values below 2.51% and 6.50% for intra-day and inter-day analyses, respectively. Interference studies revealed no significant interferences except for high levels of TB in the presence of low CF concentrations, and vice versa. To overcome this, a preparative chromatographic procedure was employed, isolating aliquots of TB and CF for quantification using SWV and high-performance liquid chromatography (HPLC) with photodiode array detectors (PAD) as the reference method. Considering the low CF concentration in the Amazonian cocoa sample, a miniaturized electrochemical cell was developed using 3D printing. The results demonstrated relative errors below 10% and critical values for the F and t tests lower than those tabulated at the 95% confidence level with n = 3. Recoveries ranged from 80% to 115%. Based on these findings, TB and CF contents can be determined with acceptable precision and accuracy in fermented and unfermented Amazonian cocoa samples, using a reduced amount of residues. These analytical tools are valuable for quality control purposes in fermented cocoa and chocolate.

2.5   Antioxidants substances

Antioxidant substances are compounds that can help prevent or reduce damage caused by oxidative stress in the body. Oxidative stress occurs when there is an imbalance between the production of harmful free radicals and the body's ability to neutralize them with antioxidants. Several examples of antioxidant substances include total phenolic content, total flavonoid content, and DPPH scavenging. These are examples of three types of antioxidant substances that were the focus of the study:

2.5.1 Total phenolic content (TPC)

Refers to the overall concentration of phenolic compounds present in a substance or sample. Phenolic compounds are diverse chemical compounds found in plants, known for their antioxidant properties. They play a crucial role in plant defense mechanisms against environmental stresses. A higher total phenolic content is often associated with increased antioxidant activity since phenolic compounds can scavenge free radicals and protect against oxidative stress, which is linked to various chronic diseases. Total phenolic content is expressed as milligrams or grams of gallic acid equivalents (GAE) per unit weight or volume of the sample. Gallic acid is commonly used as a reference compound for calibration in phenolic content analysis.

2.5.2 Total flavonoid content (TFC)

Refers to the overall concentration of flavonoid compounds present in a substance or sample. Flavonoids are a diverse class of plant compounds known for their antioxidant and anti-inflammatory properties. They are widely distributed in fruits, vegetables, grains, herbs, and beverages such as tea and wine. Flavonoids have been extensively studied for their potential health benefits, including antioxidant, anti-inflammatory, anti-cancer, and cardiovascular protective effects. The total flavonoid content is typically expressed as milligrams or grams of a reference compound, such as quercetin or catechin, per unit weight or volume of the sample. These reference compounds are used for calibration purposes to quantify the flavonoid content.

2.5.3 DPPH scavenging (%DPPH)

Refers to the ability of a substance to neutralize or scavenge the free radical DPPH (2,2-diphenyl-1-picrylhydrazyl). The DPPH assay is a widely used method to evaluate the antioxidant activity of compounds or samples. The DPPH assay provides a measure of the percentage of DPPH scavenging activity, which indicates the substance's ability to counteract oxidative stress. The assay involves comparing the absorbance or color change of the test substance with that of a control using a spectrophotometer. A higher percentage of DPPH scavenging activity corresponds to a stronger antioxidant capacity.

These various methods of evaluating antioxidant substances contribute to our understanding of their potential health benefits and play an essential role in assessing the antioxidant properties of compounds or samples.

2.5.4 Literature reviews on antioxidants substances

Anees Ali Jafri et al. 2023 studied to evaluate the antioxidant activities of extracts from various parts of traditional medicinal plants through in vitro testing. The method involved meแบบasuring the sample absorbance at 517 nm using a spectrophotometer to assess the free radical scavenging activity. Methanol and DPPH were utilized as blank and negative controls, respectively. The results revealed that ethanolic extracts of Euphrasiae stricta (E. stricta) and Euphorbia platyphyllos L. (E. platyphyllos L.) exhibited high total phenolic (expressed as gallic acid equivalent, GAE) and flavonoid (expressed as quercetin equivalent, QE) contents, with values of 58.19 GAE μg/mg and 42.44 QE μg/mg for E. stricta, and 46.05 GAE μg/mg and 43.39 QE μg/mg for E. platyphyllos L., respectively. Epimedium brevicomum Maxim. (E. brevicomum Maxim.) also showed significant phenolic (51.93 GAE μg/mg) and flavonoid (39.21 QE μg/mg) contents. The presence of phenolic and flavonoid compounds in these plants, along with their hydroxyl groups, contributes to their free radical scavenging abilities. The highest scavenging activity was observed in E. stricta (IC50 = 38.972 μg/mL), E. platyphyllos L. (IC50 = 40.817 μg/mL), and E. brevicomum Maxim. (IC50 = 46.265 μg/mL) for both their ethanolic and methanolic extracts, surpassing the scavenging activity of ascorbic acid (IC50 = 37.337 μg/mL). In conclusion, these plants exhibit potent antioxidant properties that can be beneficial in treating and preventing various degenerative diseases associated with oxidative stress, including cancer, cardiovascular diseases, inflammation, atherosclerosis, dementia, diabetes, asthma, and eye degenerative diseases.

Hussain et al. 2022 studied to assess the total phenolics, flavonoids, and antioxidant activity of agricultural waste while also examining their potential for controlling pesticide residues (diazinon and parathion) at a laboratory scale. Dried-milled fruit wastes, including orange and banana peels, as well as date stones, were utilized at two concentrations (3 and 9 g/30 mL deionized water). The total phenolic and flavonoid contents and antioxidant activity were measured in the fruit wastes.

Fourier transmitted infrared (FTIR) spectra were analyzed to identify functional groups present before and after pesticide residue removal. Gas Chromatography/Mass spectrometry (GC/MS) was employed to determine the ability of fruit wastes to eliminate pesticide residues. The results showed that date stones had higher total phenolic content compared to orange and banana peels. However, orange peels exhibited higher total flavonoid content than date stones and banana peels. Banana peels displayed the highest antioxidant activity, followed by orange peels and date stones. Interestingly, there was no correlation observed between total phenolic content, total flavonoid content, and antioxidant activity. Regarding pesticide residue removal, date stones at a concentration of 9 g effectively reduced diazinon by 81.18%, while banana peels (63.86%) and orange peels (43.42%) also demonstrated significant reduction capabilities. For parathion, banana peels at a concentration of 9 g exhibited a reduction rate of 50.34%, followed by orange peels (45.28%) and date stones (39.52%). This study highlights the effectiveness of agricultural waste in adsorbing diazinon from water, indicating their environmentally safe potential.

Cimrin et al. 2019 studied the effects of the supplementation of natural and synthetic antioxidant additives in layer diets on egg weight loss, yolk lipid peroxidation (TBARS values) and fatty acid composition of eggs stored at different temperatures and duration were evaluated. In total, 112 48-weeks-old Bovans White layers were randomly allotted to four dietary treatments with four replicates of seven birds each. The treatments consisted of a control diet, containing no additives, and diets with the inclusion of 200 mg synthetic vitamin E/kg, 1000 mg thyme extract/kg and 1000 mg rosemary extract/kg. Dietary treatments did not influence ($p > 0.05$) relative weight loss of eggs stored for 14, 28, and 56 days, except for those from rosemary-fed hens stored at room temperature on d 42, which were significantly lighter than the eggs from vitamin E-and thyme-fed hens ($p < 0.001$). Relative egg weight loss was significantly higher ($p < 0.001$) when stored at room temperature than under refrigeration, independently of storage time. In eggs stored at room temperature, yolk TBARS values were significantly lower ($p < 0.001$) in the eggs of vitamin E-fed hens, whereas no influence ($p > 0.05$) of dietary treatment on yolk TBARS values were detected in refrigerated eggs. The inclusion of the synthetic and both natural antioxidants in layer diets significantly reduced stearic acid (C18: 0) level in the egg

yolk. In addition, only natural antioxidants significantly increased yolk levels of palmitoleic acid (C16: 1) and vaccenic acid (C18: 1n7). The results of the present study showed that adequate storage temperature was more effective in improving egg shelf life than feeding layers synthetic or natural antioxidant additives. However, the positive effects of the evaluated natural antioxidants on yolk fatty acid composition suggest their supplementation to layer diets may provide health benefits to the consumer.

Hu et al. 2017a studied to enhance the functional properties and taste of germinated red rice, this study examined the variations in phytochemicals and physicochemical properties at different parboiling durations (2, 5, 10, and 15 minutes). Germinated red rice parboiled for 5 and 15 minutes exhibited higher total free phenolic content and antioxidant activity compared to non-parboiled rice. The levels of free p-coumaric acid increased from 0.20 to 0.67 mg/100g as the parboiling time extended from 5 to 15 minutes. Bound vanillic acid (0.17-0.27 mg/100g) and p-coumaric acid (6.56-8.59 mg/100g) showed higher concentrations at 0, 2, or 5 minutes of parboiling. However, after 15 minutes of parboiling, the color difference (ΔE) increased from 0.58 to 9.09, the heat enthalpy (ΔH) decreased from 4.69 to 1.94 J/g, and the internal structure of the rice was compromised. Overall, a parboiling duration of less than 5 minutes was deemed suitable for enhancing the quality of germinated red rice.

Utami et al. 2016a studied to assess the impact of cocoa bean fermentation on the total phenolic content and antioxidant activity of cocoa bean shell (CBS). Cocoa beans underwent spontaneous fermentation for different durations (24, 48, 60, 72, 96, and 120 hours) in a fermentation box. Subsequently, the CBS was separated from the cocoa beans and extracted using a mixture of acetone and water (70:30 v/v). The total phenolic content was determined using the Folin-Ciocalteu method, while the antioxidant activity was measured using the 2,2-diphenyl-1-picrylhydrazyl (DPPH) method. Additionally, Fourier Transform Infrared Spectroscopy (FTIR) analysis was conducted to examine the functional groups present in the samples. The results revealed that CBS obtained from partially fermented cocoa beans (24 hours) exhibited the highest phenolic content. The antioxidant activity was also highest (88.67±1.12%) in CBS derived from partially fermented cocoa beans (24 hours), whereas the lowest activity (44.60±2.48%) was observed in CBS obtained from cocoa beans fermented

for 120 hours. There was a strong correlation between the phenolic content and antioxidant activity. FTIR analysis indicated that CBS from 24 hours of fermentation displayed a greater variety of functional groups compared to the other samples. In conclusion, cocoa bean fermentation influenced both the total phenolic content and antioxidant activity of CBS, along with causing shifts in the functional groups. These findings emphasize that CBS serves as a valuable source of antioxidants and phenolic compounds. Further investigation should focus on determining the specific phenolic compounds in CBS and understanding their mechanisms of action.

2.6   Total Crude Protein (TCP) content

Total crude protein content (TCP) is the quantitative measurement of the overall protein content within a substance or sample. This parameter is determined through various analytical methods in fields such as food science, agriculture, animal nutrition, and biochemistry. It serves as a crucial factor for assessing nutritional value and quality in different products. Total crude protein content signifies the combined amount of protein present in a sample, encompassing both true protein and non-protein nitrogenous compounds. It is expressed as a percentage of the sample's total weight.

2.6.1 Significance and applications of TCP content

While total crude protein content provides a valuable estimate of protein quantity, it does not provide information about the specific types or quality of proteins present in a sample. A representation of the 3D structure of the protein myoglobin showing turquoise α-helices. The 3D structure of total crude protein content was shown in Figure 2.5 below showcasing α-helices colored in turquoise. This protein holds significance as it was the first to have its structure deciphered using X-ray crystallography. Located towards the right-center among the coiled α-helices, a prosthetic group known as a heme group is visible in gray. Additionally, the image illustrates an oxygen molecule (colored red) bound to the heme group.
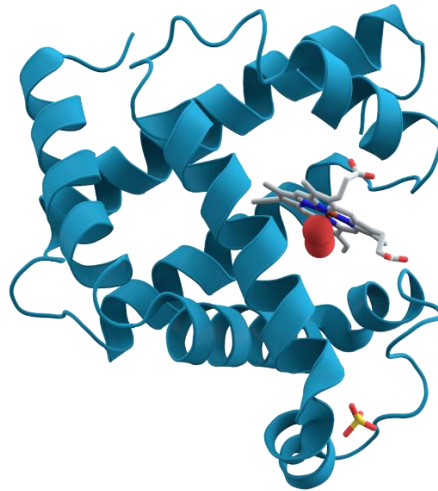
Figure 2.5 The 3D structure of the protein myoglobin.

Total crude protein content plays a vital role in assessing the nutritional composition and value of various substances. In the context of animal feed and agriculture, it helps evaluate the suitability of feed ingredients and assess the protein requirements of livestock. In the food industry, it assists in labeling and quality control, enabling accurate estimation of protein content in products such as grains, pulses, meat, dairy, and processed foods.

Total crude protein content is widely utilized in various domains. In agriculture, it aids in formulating balanced animal diets and determining the nutritional adequacy of feed ingredients. In food science, it enables quality assessment, label declaration, and protein fortification strategies. Additionally, it serves as a reference for evaluating protein-rich products and monitoring protein levels during processing and storage.

Gervasi et al. 2018 investigations are underway to explore useful and innovative recycling methods to address the significant issue of food waste, which constitutes the largest portion of the waste stream. This is crucial for the protection and preservation of public health. One promising practice involves converting food waste into valuable products. This study focused on the conversion of food waste collected from the distribution sector and citrus industries into value-added products through fermentation processes. The objective was to produce single-cell protein (SCP) using Saccharomyces cerevisiae as a fermentation substrate. To achieve this, a primary fermentation test was conducted in a 25-liter bioreactor. By utilizing food waste, we

not only contribute to reducing environmental pollution but also obtain valuable products, such as a protein source for animal feed.

2.6.2 Strategies for enhancing TCP content in CPH

To increase total crude protein content in substances like animal feed or food products, various methods can be used, depending on the application and desired outcome. Common approaches include incorporating protein-rich ingredients (soybean meal, fishmeal, legumes, nuts, seeds, or protein isolates) to boost protein content. Using protein concentrates or isolates derived from plants and animals can also fortify products with higher protein content. Enzymatic hydrolysis breaks down proteins into smaller peptides and amino acids, increasing protein content and digestibility.

Protein fortification with additives or concentrates enhances nutritional value without altering the original formulation. Selective breeding and genetic improvement in agriculture and animal husbandry can lead to crops and livestock with higher protein content. Fertilization and agronomic practices in crop production boost plant growth and protein content. Proper pre- and post-harvest management preserves protein content in crops and food products. Utilizing fermentation or bioprocessing elevates protein content in certain food products and feed ingredients.

Consider specific requirements and constraints for the target application when implementing methods. Assess nutritional quality, digestibility, and anti-nutritional factors for overall efficacy and safety.

Adeoye et al. 2021 studied on a feeding trial replaced fish meal (FM) with bacterial protein (BP) in African catfish diets. Four diets with equal nitrogen and lipid content (369 g kg^{-1} and 142 g kg^{-1}, respectively) were used. FM protein was replaced at different levels (0%, 30%, 60%, and 100%) with corresponding BP inclusion levels (0, 27.90, 55.70, and 93.00 g kg^{-1}). Catfish (n = 20) in three tanks were fed these diets for 56 days. Results showed that catfish fed the 30% BP diet had superior performance ($P < 0.05$) compared to the control diet (100% FM), exhibiting higher mean weight gain (MWG), percentage weight gain (PWG), specific growth rate (SGR), and metabolic growth rate (MGR). No significant differences in growth response (MWG, PWG, SGR, and MGR) were observed between diets with 60% and 100% BP and the control diet. Catfish fed the 30% BP diet had higher whole-body protein (+8%) and

lipid (+12%) contents than those without BP inclusion (P < 0.05). The replacement of FM with BP did not significantly affect catfish hematological status (P > 0.05). Histological analysis of the catfish mid-intestine showed intact epithelial barriers with extensive mucosal folds into the lumen. The intestinal perimeter ratio of fish fed the 30% BP diet was higher (+32%) than the control group (P < 0.05), but similar to the 100% BP-fed diet (P > 0.05). Measures of liver health, including serum aspartate transaminase, alanine transaminase, alkaline phosphatase activities, and hepatocyte density, remained statistically unchanged across dietary groups (P > 0.05). Overall, the results suggest that BP can be a complete or partial replacement for FM in African catfish (C. gariepinus) diets, supporting growth performance, haemato-biochemistry, intestinal integrity, and liver functionality.

Najari et al. 2022 aimed to valorize almond hulls through a zero-waste approach, promoting sustainable agricultural development and the production of valuable compounds. The study focused on extracting four products: pectin (AHP), phenolic compounds (AHPC), pullulan (PUL), and single-cell protein (SCP). Acidic extraction factors were optimized using a Box-Behnken design to simultaneously extract AHP and AHPC. Results indicated that the highest yields of AHP (26.32% w/w) and AHPC (6.97% w/w) were obtained at an optimum point of 90°C, pH 1.4, 58.65 minutes, and a liquid-to-solid ratio (LSR) of 20.13 v/w. The solid residues remaining after AHP and AHPC extraction (PESR) were then subjected to cellulase enzyme treatment and ultrasound to facilitate simultaneous microbial production of PUL (34.29–24.56 g/L) and SCP-containing biomass (19.31–13.44% w/w). Analysis revealed that AHP had low methylation (26.40%), high galacturonic acid content (67.88%), and a large molecular weight (595.299 kDa). Structural investigations confirmed the presence of chemical structures of AHP and PUL in the formed supernatants. Additionally, AHPC exhibited significant antioxidant activity compared to ascorbic acid (ASC) and BHA.

Khan et al. 2023 studied on current food and feed production practices in agriculture generate nitrogen-rich waste streams, contributing to environmental pollution. To promote a circular economy, it is essential to convert nitrogen from agricultural waste into valuable products. Agricultural waste contains nitrogen in both water-soluble and solid forms. While microalgae can utilize water-soluble nitrogen to produce protein-rich biomass, pretreatment steps are often required for agricultural

wastes to make nitrogen and other elements available for microalgae consumption. Apart from nitrogen recovery, certain microalgae can also produce valuable metabolites (e.g., pigments, polyunsaturated fatty acids) using waste sources. This review examines recent advancements in cultivating microalgae using agricultural waste to produce protein-rich biomass and other valuable metabolites for food and feed applications. Finally, the challenges and prospects of microalgal nitrogen recovery from various agricultural wastes are briefly discussed.

2.7   Fermentation processes

Fermentation is a metabolic process in which microorganisms, such as bacteria, yeast, or fungi, convert organic compounds into simpler substances, typically in the absence of oxygen. It is a natural and extensively utilized process across various industries, including food and beverage production, pharmaceuticals, biofuel production, and biotechnology. The fermentation process can be classified into two main types:

2.7.1 Submerged fermentation (SmF)

SmF referred to as Liquid Fermentation or Submerged Culture, involves the cultivation and growth of microorganisms in a liquid medium. In this process, the microorganisms are submerged in the liquid, and essential nutrients and oxygen are supplied to facilitate their growth and metabolic activities. Submerged fermentation is widely employed in large-scale production of diverse products, including enzymes, antibiotics, organic acids, and biofuels. The liquid medium provides an optimal environment for the microorganisms to thrive and produce the desired substances.

Ouattara and Niamké 2021 studied the inconsistent quality of cocoa produced by farmers remains a persistent issue in the value chain, largely influenced by microbial activities. To address this, we conducted an analysis of cocoa microbiota from all twelve producing regions in Cote d'Ivoire and created a geographical distribution map of the isolated microbiota. Through ribosomal gene sequencing, we identified microbial species, characterized strains using RFLP, and further investigated their techno-functional capacities. The results revealed a limited diversity of lactic acid bacteria (LAB) and acetic acid bacteria (AAB) with 10 and 5 strains, respectively.

Dominant LAB and AAB strains, including Lactobacillus plantarum 1A, Acetobacter pasteurianus 1A, Acetobacter okinawensis 2A, and Acetobacter tropicalis 3A, were present in all regions, indicating a relatively stable acid microbiota. However, variations in their functional performance, such as acidification capability, were observed, with stronger strains found in the Nawa and Haut-Sassandra regions and weaker strains in the Indenie-Djuablin and San Pedro regions. This distribution seemed to be random. Additionally, a diverse and complex population of yeasts was identified, encompassing 22 species and 45 strains, indicating intraspecific heterogeneity. Strains exhibited regional differences, contributing to a variable yeasts microbiota across the regions. Furthermore, functional capacities, such as pectinolytic activity, varied among strains. For example, Pichia kudriazevii strain 2K from Gboklè displayed weaker pectinolytic capability, while Pichia kudriazevii strain 2A from Loh-Djiboua exhibited stronger activity. The quality of fermented cocoa beans also demonstrated variability across the regions. The significant variation in yeast strains among different regions may be a primary microbial factor contributing to the observed differences in fermented cocoa quality.

2.7.2 Solid state fermentation (SsF)

SsF entails the growth of microorganisms on solid substrates with limited moisture content. Microorganisms utilize the solid substrate as a source of nutrients for their growth and metabolism. Common solid substrates utilized in Solid-State Fermentation include agricultural residues, cereal grains, sawdust, and other lignocellulosic materials. This type of fermentation finds applications in the production of enzymes, organic acids, bioactive compounds, and animal feed. Solid-State Fermentation offers several advantages, including reduced energy and water requirements, higher product yields, and the utilization of cost-effective agricultural waste materials.

Both SmF and SsF are significant fermentation techniques utilized in different industries. The choice of fermentation type depends on various factors, such as the specific microorganisms involved, the nature of the substrate, and the desired end products. These fermentation processes play a crucial role in meeting the demands of various sectors and contribute to the production of a wide range of valuable substances.

de Oliveira et al. 2022 aimed to utilize cocoa pod husks (CPHs) as a novel substrate/support for citric acid (CA) production through solid-state fermentation (SSF) using Aspergillus niger strains. CPHs, which currently lack a proper final destination, possess favorable characteristics that make them suitable as the sole substrate for CA production in SSF. The CPHs were partially characterized, revealing an interesting composition and potential for fungal growth. A mutant strain of A. niger, B6 - CCT 7717, was selected based on its exceptional capacity for CA production. The peak CA production of 978.52 g/kg of dry CPHs was achieved at 72 hours, with a yield of 88.70% (dry CPHs) and a productivity of 13.59 g/kg/h. These results surpass the highest reported rates of CA production, demonstrating promising prospects for this process.

Chebaibi et al. 2019b studied to investigate the bioconversion of olive cake (OC) generated by Moroccan olive oil industries. The goal is to enhance its nutritional value through solid-state fermentation using selected filamentous fungi. The resulting OC can then be utilized as feed for ruminants. Four fungi (Beauveria bassiana, Fusarium flocciferum, Rhizodiscina cf. lignyota, and Aspergillus niger) were cultured on OC for 15 days. Chemical composition and enzyme activities were analyzed. The results demonstrate a significant increase in protein content of treated OC, reaching up to 94%. There were also notable reductions ($P < 0.05$) in phenolic compounds, including total phenolic content, total flavonoids content, and total condensed tannins, with decreases of up to 43%, 70%, and 42%, respectively. RP-HPLC analysis of fermented OC confirmed the degradation of individual phenolic compounds by the fungal strains. These findings highlight the efficiency of F. flocciferum and Rhizodiscina cf. lignyota in producing enzymes that enhance the nutritional value of this by-product.

2.7.3 Fermentation of CPH

The fermentation process of CPH in a biodigester, specific groups of microorganisms play a vital role in breaking down the organic matter. These microorganisms are responsible for the conversion of complex compounds, including proteins, carbohydrates, and fats, into simpler substances such as methane and carbon dioxide. The production of biogas during fermentation is a result of the metabolic activity of these microorganisms.

The fermentation of cocoa pod husk (CPH) holds potential to enhance the overall nutritional value and utilization of this biomass feedstock. Throughout the fermentation process, microorganisms break down the organic matter in CPH, including proteins, resulting in the production of simpler compounds like methane, carbon dioxide, and other trace gases. Furthermore, the residual material known as digestate, which remains after biogas production, may contain higher concentrations of nutrients, including proteins, compared to the original CPH. This nutrient-rich digestate can be utilized as a valuable raw material in animal feed production, thus contributing to cost reduction in this area. Consequently, the fermentation of CPH represents a valuable approach in both waste reduction and nutrient recycling within agricultural practices.

Brito et al. 2000a studied on cocoa seeds and pulp underwent fermentation for 144 hours, followed by natural drying. The tegument was removed, and the cotyledons were broken into nibs, which were then roasted at 150°C for 30 minutes. Samples were prepared for chemical and microscopic analysis, including non-fermented material, material fermented for 24, 48, and 72 hours, material fermented for 144 hours and then dried, and the roasted nibs. Light microscopy revealed the presence of anionic and cationic residues, as well as neutral sugars. During fermentation, there was a decrease in phenolic compounds and a reduction in the number of protein bodies in the cytoplasm. The cell wall exhibited decreased anionic residues and a loss of crystallinity, with the most significant changes observed after 72 hours. Drying and roasting led to an increase in damaged cells and a decrease in cytoplasmic material. The chemical analyses generally supported the findings from microscopy. The concentration of amino-terminal groups and total free amino acids increased during fermentation (up to 72 hours) but returned to initial levels after roasting. The main chemical changes were associated with reducing sugars, free amino acids, proteins, and phenols. Principal Component Analysis (PCA) was suggested as a useful tool for comparing different samples. Microscopic analysis demonstrated the degradation of protein and phenolic bodies, as well as cellular damage during the roasting process.

Hernández-Mendoza et al. 2021 presented the optimized processes of alkaline pretreatment and enzymatic hydrolysis for the production of bioethanol from cocoa pod husk (CPH). Central Composite Design (CCD) was used to assess the impact of

NaOH concentration, residence time, and temperature during alkaline pretreatments. Structural characteristics of the solid fraction were analyzed using SEM and XRD techniques. Enzymatic hydrolysis experiments were conducted to optimize enzyme (Cellic Ctec2, Novozyme) and solid loadings. The resulting hydrolysate was subjected to fermentation using Saccharomyces cerevisiae Y2034 yeast. The findings indicated that the optimal alkaline pretreatment condition was achieved at 5% (w/v) NaOH concentration for 30 minutes at 120°C. This pretreatment increased the cellulose content of CPH from $27.68 \pm 0.15\%$ (untreated) to $57 \pm 0.25\%$. SEM analysis revealed changes in porosity and biomass structure, while XRD analysis demonstrated increased crystallinity. Enzymatic hydrolysis was optimized with 10 FPU/g substrate and a solid loading of 10% (w/v), resulting in yields of 98.75% and generating 66.80 g/L of reducing sugars. During fermentation, 80.74% of the reducing sugars were consumed, leading to the production of 18.06 g/L of ethanol within 24 hours, corresponding to a theoretical yield of 51.45%. These results highlight the potential of utilizing cocoa pod husk as a raw material for bioethanol production.

Muharja et al. 2023 aimed to optimize the sequential processes for the valorization of cocoa pod husk (CPH) into biobutanol, various treatments were investigated, including depectination, delignification, enzymatic hydrolysis, and fermentation. The addition of surfactants, namely Tween 80, Polyethylene Glycol (PEG) 6000, and Sodium Dodecyl Sulfate (SDS), was explored to improve enzymatic hydrolysis performance. L-cysteine was also used to support fermentation by Clostridium saccharoperbutylacetonicum N1-4. The optimal cellulase activity was achieved at 0.25 FPU/g. The most effective strategy, involving depectination, microwave-assisted delignification, and the addition of 2.5 g/L PEG 6000, resulted in the highest sugar concentration of 9.24 g/L. Furthermore, by utilizing immobilized cells and supplementing with L-cysteine, the highest concentrations of butanol (20.4 g/L) and acetone-butanol-ethanol (ABE) (54.4 g/L) were obtained. Extractive fermentation, combined with immobilized cells and L-cysteine supplementation, enhanced ABE production.

2.8   Statistical analysis

Design of Experiment (DOE) is a systematic approach used to plan and conduct experiments to gather reliable and meaningful data for analysis. When combined with Response Surface Methodology (RSM), DOE becomes a powerful tool for optimizing processes and understanding the relationship between variables and responses.

In DOE with RSM, a series of carefully planned experiments are conducted to gather data on the response variable of interest while systematically varying the input variables. RSM provides a mathematical framework for analyzing experimental data and developing predictive models that describe the relationship between the input variables and the response variable. By using RSM in conjunction with DOE, the optimal values of the input variables can be determined to achieve the desired response. The key steps involved in DOE with RSM include: Defining the objectives: Clearly define the research or process optimization objectives and identify the response variable that is to be optimized. Identifying the input variables: Determine the variables that may potentially affect the response variable and select the appropriate range and levels for each variable. Designing the experimental plan: Use statistical principles to design an experimental plan that specifies the combinations of input variable levels to be tested. Commonly used designs include factorial designs, central composite designs, and Box-Behnken designs. Conducting the experiments: Perform the experiments according to the planned design, recording the response variable for each combination of input variables. Analyzing the data: Use statistical techniques, such as regression analysis, to analyze the data obtained from the experiments. Fit a response surface model that describes the relationship between the input variables and the response variable. Optimizing the process: Use the response surface model to determine the optimal values of the input variables that maximize or minimize the response variable. Optimization techniques, such as numerical optimization or graphical methods, can be applied. Verifying and validating the results: Verify the optimized conditions through further experimentation and validate the model by testing its predictions against new data.

The combination of Design of Experiment and Response Surface Methodology allows for efficient exploration of the input variable space, identification of important variables, and optimization of the response variable. This approach has been widely

used in various industries, including manufacturing, engineering, chemistry, and pharmaceuticals, to improve processes, reduce costs, and enhance product quality.

2.8.1 Face-Centered Central Composite Design (FCCD)

It is a type of experimental design commonly used in response surface methodology (RSM). FCCD is based on a combination of factorial and central composite designs. It involves systematically varying the levels of multiple factors or variables to determine their individual and interactive effects on a response or outcome of interest. The design consists of a factorial design at the center, which allows for estimating the main effects of the factors, and additional star points that enable the estimation of curvature or quadratic effects. The star points are located at a distance called the alpha level from the center. The number of star points depends on the number of factors being studied. The main advantage of FCCD is that it allows for efficient exploration of the response surface, providing valuable information about the relationship between the factors and the response. By fitting a regression model to the data collected from the design, researchers can obtain mathematical equations that describe the relationship between the factors and the response and use these equations to optimize the process or system being studied. FCCD is widely used in various fields, including engineering, chemistry, and product development. It helps researchers efficiently study and optimize complex systems by systematically varying the factors of interest and evaluating their effects on the response.

Roy et al. 2023b studied on a comparison that was made between two statistical response surface modeling methods, Face Centered-Central Composite Designs (FCCD-RSM) and Box-Behnken Designs (BBD-RSM), to determine the optimal operating conditions for the extraction of turmeric oil from grated turmeric rhizomes using supercritical carbon dioxide extraction (SCO2E) with a specially designed annular extractor bed. The effects of extraction pressure, temperature, and particle size were investigated within specific ranges. The extraction pressure options were 21.6 MPa, 24.55 MPa, or 27.5 MPa, the extraction temperature options were 40°C, 50°C, or 60°C, and the particle sizes were 0.3 mm, 0.6 mm, or 0.9 mm. The yield of turmeric oil ranged from 1.84 wt% to 4.45 wt% for different combinations of operating parameters using both FCCD-RSM and BBD-RSM. Both methods proved effective in

building the experimental design and optimizing the process by fitting the experimental data into quadratic models within the design range. FCCD-RSM optimization resulted in the following optimal conditions: extraction pressure of 26.859 MPa, extraction temperature of 59.886°C, and particle size of 0.301 mm, with a slightly higher yield of 4.452%. BBD-RSM optimization yielded slightly different optimal conditions: extraction pressure of 27.325 MPa, extraction temperature of 58.417°C, and particle size of 0.31 mm, with a yield of 4.403%. Considering the time, labor, and cost involved in conducting all the experiments for three factors-three levels optimization, BBD-RSM is proposed as a suitable alternative method for experimental design in SCO2E studies of turmeric oil alongside the more widely accepted FCCD-RSM method.

2.8.2 Response Surface Methodology (RSM)

Response Surface Methodology (RSM) is a statistical approach that optimizes processes by examining the relationship between input variables and the desired response. It involves designing experiments to understand this relationship and identify the optimal combination of input variables for achieving the desired performance.

The main goal of RSM is to create a mathematical model that represents the response in terms of the input variables. By analyzing experimental data and fitting a regression model, RSM enables predictions of the response across a broader range of input variable combinations than those tested directly. This allows for the determination of the optimal conditions that lead to the desired outcome. RSM commonly employs design methodologies like Central Composite Design (CCD), Box-Behnken Design (BBD), or other suitable designs. These designs aid in selecting specific combinations of input variable levels to be tested, considering both factorial and axial points. The data collected from these experiments are then used to develop a response surface model and optimize the process.

Through the analysis of the response surface model, RSM provides insights into the main effects and interactions among the input variables. This helps identify the key factors that significantly influence the response. By considering these factors,

RSM guides the determination of optimal conditions that maximize the desired response or minimize process variability.

Rachmawaty et al. 2019 studied the initial screening for chitinase production by Trichoderma virens involved a 2-level factorial design to determine the physical factors involved. Incubation time, temperature, moisture substrate, pH, inoculum size, and ammonium sulfate concentration were selected as model factors. The results of the factorial design experiment revealed that all three independent variables had a significant effect on chitinase production. To optimize the physical factors, a Central Composite Design was employed, and a response surface was generated based on the derived model. Using Design Expert® Software, Version 6.0.4, an experimental design was created with three variables: incubation time, temperature, and moisture substrate. This design consisted of 20 experiments, including 6 replicates at center points. The optimal values determined were a sixth-day incubation time, a temperature of 27.8°C, and a moisture substrate of 54%, with a predicted chitinase activity of 0.48738 U/g of dry substrate. These predicted parameters were then tested in the laboratory, and the final chitinase activity obtained was 0.48864 U/g of dry substrate, which closely matched the predicted value. The obtained chitinase production value of 0.48738 U/g of IDS was 1.2-fold higher than that achieved using the 2-level factorial design (0.261 U/gds).

Eryasar-Orer and Karasu-Yalcin 2019 studied the optimization of xylitol production by Candida tropicalis M_2 was carried out using chestnut shell hemicellulosic hydrolysate. The independent variables selected were the initial xylose concentration, the initial concentration of ammonium chloride (chosen as the nitrogen source), and the shaking rate. Response surface methodology, specifically central composite design, was employed to model the effects of these independent variables on various parameters: maximum xylitol concentration (Y_1), xylitol yield (Y_2), maximum xylitol production rate (Y_3), percentage of substrate conversion (Y_4), and specific product formation rate (Y_5). A quadratic model was used to describe the variations of the responses with the independent variables, except for Y_4. The analysis of variance (ANOVA) results indicated that the initial concentration of ammonium chloride had the most significant impact. The linear effect of the initial xylose concentration was found to be significant only for Y_1. The shaking rate had a highly

significant effect on both Y_1 and Y_4. Through numeric optimization, the following conditions were predicted as the optimum: an initial xylose concentration of 80 g/L, an initial ammonium chloride concentration of 3.761 g/L, and a shaking rate of 80 strokes/min. Under these optimum conditions, the values obtained for Y_1, Y_2, Y_3, Y_4, and Y_5 were 24.50 g/L, 31.517%, 0.497 g/L.h, 97.35%, and 0.06 g/L.h.N, respectively.

Mehmood et al. 2018b studied Response Surface Methodology (RSM), using Central Composite Rotatable Design (CCRD), was employed to optimize the trans-esterification process of Eruca sativa oil into methyl esters (EOMEs). Four reaction parameters, namely reaction temperature, catalyst concentration, reaction time, and methanol-to-oil molar ratio, were evaluated to achieve a high yield. A 24 full factorial CCRD with five levels for each parameter resulted in 30 experiments. The molar ratio of methanol to oil and the catalyst concentration were identified as the most significant factors ($P < 0.5$) affecting EOME yield. A strong linear relationship ($R^2 = 0.97$) was observed between the observed and predicted values. Through multiple regression analysis, a quadratic polynomial equation was derived for methyl ester yield (MEY). The quadratic terms of the molar ratio and catalyst concentration had a significant impact on the yield. The interaction terms between the molar ratio, catalyst concentration, and reaction time positively influenced MEY ($P < 0.05$). The optimal reaction conditions for transesterification were determined as follows: catalyst concentration of 0.8%, reaction temperature of 65°C, methanol-to-oil ratio of 6:1, and reaction time of 120 minutes. Under these conditions, a MEY of 95.88% for Eruca oil was achieved. RSM proved to be a suitable technique for optimizing the transesterification process, and the produced fuel properties complied with the standards of EN 14214 and ASTM D6751.

Ali et al. 2023 studied on the use of pumice stone (PS) as a lightweight aggregate to replace natural coarse aggregates in concrete. The aim is to assess the physical and mechanical properties of the concrete with varying percentages of PS. Response surface methodology (RSM) is employed to design experiments and prepare concrete mixtures with different PS ratios. Fresh properties, such as workability, are evaluated using slump and compaction factor tests, while hardened concrete properties are determined through compressive strength (CS), flexural strength (FS), and split tensile strength (STS) tests. The experimental, optimization, and validation results indicate

that up to 30% replacement of PS in lightweight aggregate concrete is feasible for curing periods of 7 to 56 days, provided the CS exceeds 15 MPa, STS is between 7% and 12% of the CS, and FS ranges from 9% to 11% of the CS. The optimum CS for this study falls within the range of 17 to 20 MPa, with STS between 9.39% and 10.54% of the CS, and FS ranging from 17.49% to 21.12% of the CS. A quadratic model is proposed, and the RSM analysis reveals a coefficient of determination (R^2) above 0.99 (99%) for all three responses, indicating the model's high importance. The R^2 and adjusted R^2 values show negligible differences, and the P-Values for CS, STS, and FS are below 0.05 (<0.0001), demonstrating the model's strong relevance. RSM is utilized to enhance and validate the model through additional laboratory trials.

2.8.3 Analysis of variance (ANOVA)

ANOVA, or Analysis of Variance, is a statistical technique that compares means of two or more groups to determine if there are significant differences between them. It assesses variation between groups and within groups to identify meaningful differences in means. The main goal of ANOVA is to determine if there is evidence supporting the hypothesis that the means of compared groups are unequal. It helps identify significant differences and provides insights into specific group variations.

ANOVA partitions total data variation into two components: between-group variation, reflecting differences among group means, and within-group variation, representing variability within each group. By comparing the magnitudes of these components, ANOVA determines if observed mean differences are statistically significant. Common ANOVA designs include One-Way ANOVA: Compares means of groups with one independent variable and multiple levels. Two-Way ANOVA: Analyzes two independent variables to examine main effects and interaction effects. Repeated Measures ANOVA: Evaluates within-subject differences by measuring subjects repeatedly under different conditions.

ANOVA output includes an F-statistic, comparing between-group and within-group variability. A p-value is calculated based on the F-statistic, representing the probability of chance differences. If the p-value is below a predetermined significance level (e.g., 0.05), significant differences among groups are concluded. ANOVA finds applications in experimental research, clinical trials, social sciences, and

manufacturing quality control. It is a robust statistical method for comparing means and detecting group differences, aiding researchers in making valid conclusions and informed decisions.

The examination of the Design of Experiment (DOE) employing Response Surface Methodology (RSM) for this study was conducted utilizing Design-Expert® version 13 for Windows, as illustrated in Figure 2.6 below.
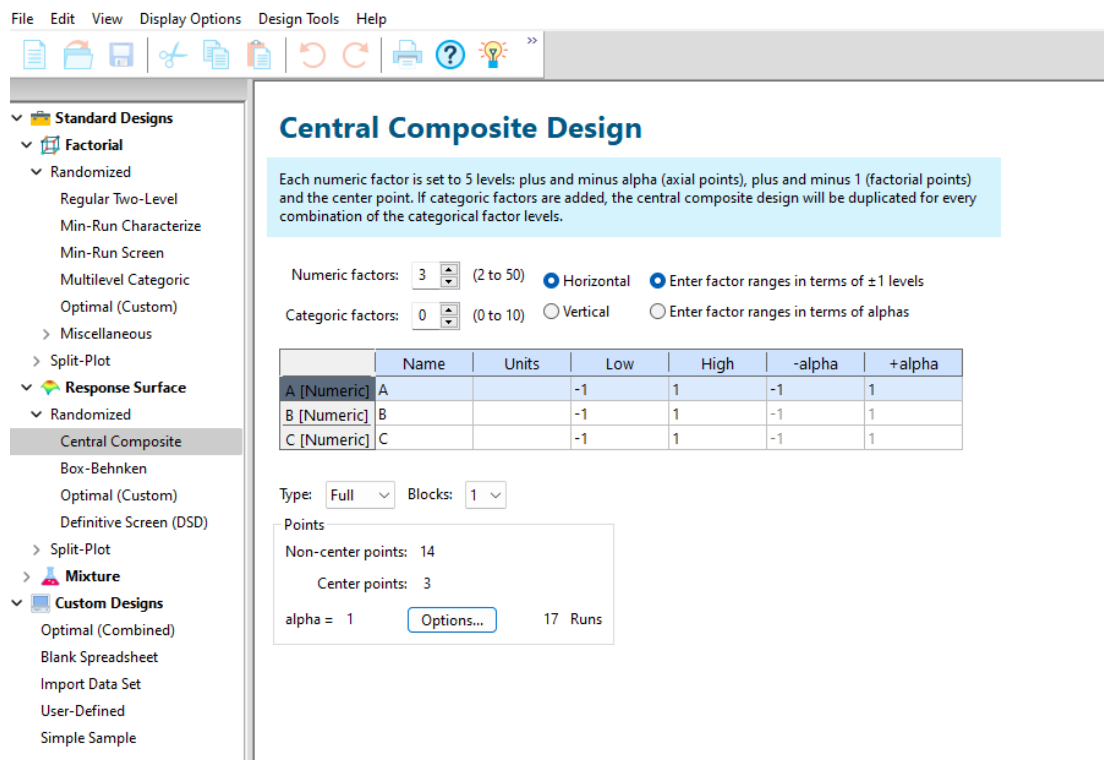
Figure 2.6 Design-expert ® version 13 interface for statistical analysis.

Mohammed Raffic et al. 2023 studied on statistical examination, ANOVA is a crucial tool, especially with numerous results. It investigates how various parameters (e.g., electrolyte concentrations, types, heat treatments, pre-treatment) affect corrosion behavior in engineering materials. A one-way ANOVA shows the impact of one parameter, while two-way or three-way ANOVA reveals synergistic effects of multiple parameters. This study explores how heat treatment type, temperature, cooling, and hardness variations influence corrosion in the 7021 Al alloy under Red Sea-like conditions. Remarkably, artificial aging significantly affects its corrosion behavior.

L et al. 2023 studied on light-transmitting concrete utilizes optical fibers for impressive light transmission. While natural light is preferred, artificial light is crucial in urban areas to reduce carbon emissions. Understanding the mechanical properties and light distribution is vital for its application. Studies on Light-Transmitting Concrete reveal its potential to decrease reliance on artificial lighting. Compressive strengths are initially lower but catch up at 28 days. Light transmission depends on optical fibers, with curing age having minimal impact. ANOVA is used to optimize compressive strength and light transmission, assessing variability among tests and instances.

CHAPTER 3

MATERIAL AND METHODOLOGY

3.1 Material

Cocoa mature fruits [Pa_7+Na_{32}] were obtained from Tah-Sala in Nakhon Si Thammarat Province, Southern Thailand. The fruits were washed with tap water, and the seeds were removed to obtain cocoa pod husk (CPH). The CPH was ground to a small size using a commercial grinder machine and then kept in a vacuum bag. It was stored in a freezer at 0°C until use.

3.2 Reagents and microorganisms

The chemical reagents used in this research were of analytical grade. Standard theobromine (purity 98.5%), absolute ethanol, acetonitrile, phosphoric acid, quercetin, DPPH, gallic acid, sodium carbonate, Folin-Ciocalteu reagent, and NaOH (98%) were purchased from Sigma-Aldrich Pte Ltd. (Nucleos, Singapore). The Aspergillus. N GH1 strain sourced from the collection of the Department of Food Research at the Universidad Autonoma de Coahuila (UAdeC). The fungal strains were cryo-preserved at a temperature of -50 °C and employed for the research.

3.3 Part I: Drying kinetics and mathematical modeling of moisture diffusivity in CPH.

3.3.1 Sample preparation

The CPH was defrosted at ambient temperature to allow equilibration before the experiment. Initial moisture content was determined according to the AOAC (2000) standard by placing 20-30 g of CPH in an aluminum container in a convection dryer at 105°C for 5-6 h. The sample was weighed with a 4 decimal digital weighing scale (Analytical Balance ME204T/00) at time intervals of 30 min. The drying process continued until the sample weight changed by only ± 0.0005 g. The experiments were triplicated to obtain average moisture content and minimize error.

3.3.2 Drying oven with HX-711 load cell sensor

An oven chamber with a volume of 0.1215 m^3 shown in Figure 3.1 was used to study CPH drying behavior. A single perforated tray, 0.045 m^2 surface area, was hung with the load cell sensor (SN-LC-2KG). A strain gauge load cell with a 24-bit analog to digital converter (HX-711) and a 400ms response time was installed on the top of the oven to track sample weight loss on the perforated tray during the drying process. The load cell capacity was 0-2000 g with an accuracy of ±0.05%.
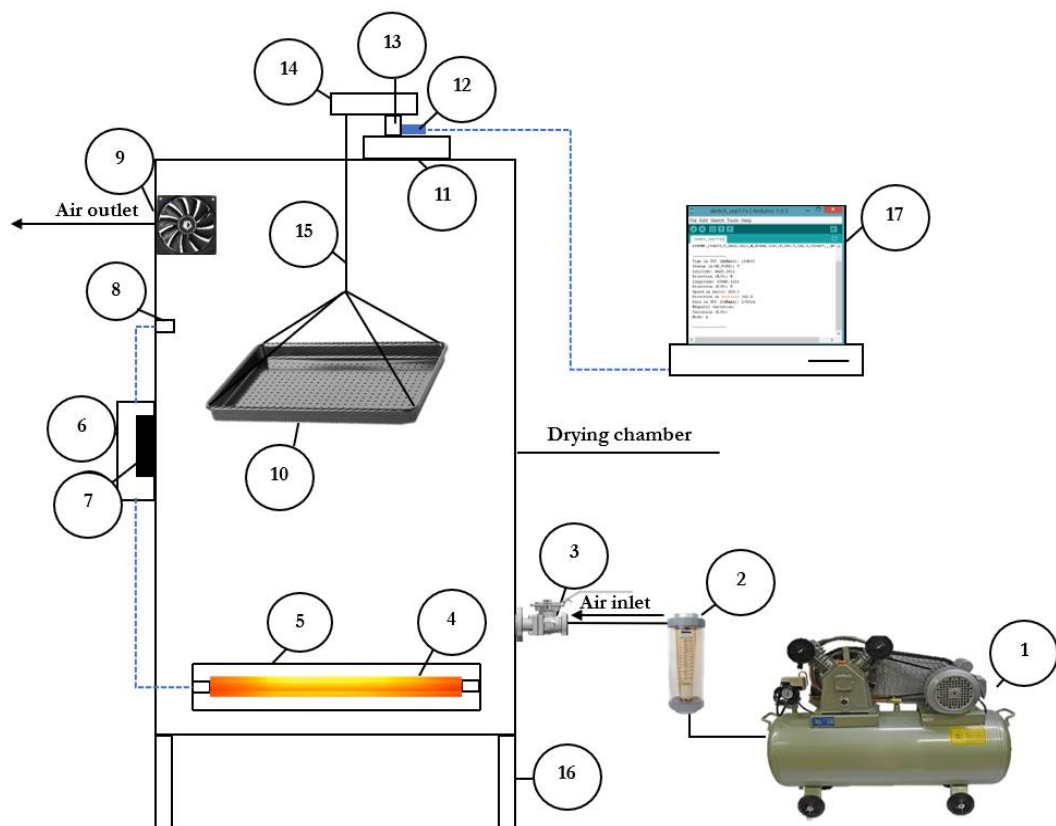
(1) Air compressor, (2) Rotameter, (3) Gas ball valve, (4) Infrared heater,
(5) Heater clamp, (6) Control panel, (7) Digital screen, (8) Thermocouple,
(9) Suction fan, (10) Single perforated tray, (11) Load cell base, (12) Load cell
module (HX-711), (13) Load cell sensor, (14) Acrylic support plate, (15) Steel wire,
(16) Chamber base, (17) Laptop.

Figure 3.1 Experimental set-up

A 300-watt infrared heater was installed as a heat generator inside the oven. The temperature inside the chamber was controlled by a control box that consisted of a type-K thermocouple and a digital screen.

Airflow inside the oven was mobilized by an air compressor with a flow rate of 3 L/min. A 6-watt electrical fan was installed on the top of the lab oven to improve air circulation inside the oven. Fresh air from the air compressor was pumped into the bottom of the oven and immediately heated by the heater.

Hot air flowed from the bottom to the top and was drawn out of the lab oven by the electric fan. Samples utilized in each experimental condition weighed 200±2 g. The temperature in each drying process was set in the range 50-70°C with 1°C of temperature increment. For a steady-state system, the oven was warmed for about half an hour before the experiment started. The reduced weight of the sample was real-time tracked by the load cell sensor and monitored by Arduino IDE. The load cell sensor was recalibrated before starting each experiment to avoid numerical errors.

3.3.3 Experimental procedure

Drying experiments were performed at 50, 60 and 70°C in the convective dryer attached to the load cell sensor. The perforated tray was weighed with a digital balance and used as a reference for load cell sensor calibration. Two hundred grams of square pieces of CPH with a thickness of 10 mm and an initial moisture content of 540.03% (dry basis, DB) were uniformly separated in the perforated tray while hanging with the load cell sensor. The time interval was tracked by the load cell sensor and monitored by Arduino IDE at 15 min intervals to observe the reduction in CPH weight. The CPH drying process in each set was carried out until moisture content was approximately reduced to 169% (dry basis, DB). The experiment was performed in triplicate for each run.

3.3.4 Drying mathematical modeling

Empirical equations have been widely employed to describe and support the drying kinetics of agricultural products, particularly under the assumption of thin layer drying. The reduction of moisture content during the drying process serves as the primary data, which allows for expressing the drying rate as a function of time. The

integral term of the drying rate can be represented using critical time, enabling the determination of the optimal time for the drying process. Empirical models play a crucial role in achieving this objective. Additionally, empirical models are utilized to elucidate the heat transfer phenomenon that occurs when hot air is employed for drying materials. These models provide insights into the drying rate, enabling a better understanding of the heat perforation process. To describe the drying kinetics of thin layer CPH through empirical equations, several assumptions need to be considered:

    i.   The empirical equations or drying models should involve no more than two parameters for fitting the raw data.

    ii.   The drying models should yield an expression for the drying rate as a function of time.

    iii.   An empirical equation should provide an expression for the drying time as a function of moisture content.

Furthermore, expressing the moisture content in terms of the moisture ratio (MR) on a dry basis (db) facilitates easy observation of the drying process. Based on these assumptions, the first assumption (i), the moisture ratio (MR) at any given time (t), can be determined using the expression in equation (3.1).

By following these assumptions and utilizing empirical equations, researchers can gain valuable insights into the drying kinetics of thin layer agricultural products. This knowledge contributes to optimizing the drying process and enhancing overall efficiency.

$$MR = MR_{eq} + (MR_i - MR_{eq})f(t, a, b), \quad (3.1)$$

where a term of (t, a, b) is a function, it should include 1 or 2 fitting parameters (a and b), and this function should be satisfied with the assumptions. To simplify the equation (3.2), equation (3.1) can be expressed as the dimensionless moisture content at any time t as follows equations (3.2, and 3.3):

$$MR = f(t, a, b) \qquad (3.2)$$

$$MR = \frac{M_t}{M_0} \qquad\qquad\qquad (3.3)$$

Thus, the term of M_t, and M_0 can be written as follows equation (3.4):

$$MR = \frac{M_t - M_{eq}}{M_i - M_{eq}} \qquad\qquad\qquad (3.4)$$

where MR is a final moisture content, M_t, M_{eq}, and M_i are any time (t), equilibrium, and initial moisture content, respectively. The selected mathematical model for this study were shown in Table 3.1 below.

Table 3.1 The selected mathematical models for thin layer drying of CPH.

Model no	Model name	Model equation	Reference
1	Lewis	$MR = \exp(-kt)$	(Bruce, 1985)
2	Page	$MR = \exp(-kt^n)$	(Page, 1949)
3	Modified Page-I	$MR = \exp[(-kt)^n]$	(White et al., 1979)
4	Henderson and Pabis	$MR = a\exp(-kt)$	Henderson and Pabis (1961)
5	Wang and Singh	$MR = 1 + at + bt^2$	Wang and Singh (1978)
6	Logarithmic	$MR = a\exp(-kt) + c$	(Togrul and Pehlivan, 2002)
7	Two term	$MR = a\exp(-k_1 t) + b\exp(-k_2 t)$	(Henderson, 1974)
8	Two term exponential	$MR = a\exp(-kt) + (1 - a)\exp(-kat)$	(Sharaf-Eldeen et al., 1980)
9	Modified Henderson and Pabis	$MR = a\exp(-kt) + b\exp(-gt) + c\exp(-ht)$	(Karathanos, 1999)
10	Midilli et al.	$MR = a\exp(-kt^n) + bt$	(Midilli et al., 2002)
11	Approximation of diffusion	$MR = a\exp(-kt) + (1 - a)\exp(-kbt)$	(Yaldiz et al., 2001)
12	Verma et al.	$MR = a\exp(-kt) + (1 - a)\exp(-gt)$	(Hutjens and Baltz, 2000)

3.3.5 Calculation of activation energy

The Arrhenius-type equation is applicable in describing the temperature dependency of drying rate or moisture content reduction. Although originally developed for chemical reactions, it can be adapted for drying kinetics. The effective diffusivity is also dependent on the temperature, and can described by an Arrhenius-type relationship equation as follows equation (3.5):

$$D_{eff} = D_0 \exp\left(-\frac{E_a}{RT}\right) \qquad (3.5)$$

where D_0 is the pre-exponential factor of the Arrhenius equation (m^2/s), Ea is the activation energy (kJ/mol), R is the universal gas constant (kJ/mol K) and T is the absolute temperature (K). Equation (3.5) can be simplified by plotting ln De versus the reciprocal of the absolute temperature (Ta). The linearity of equation (3.5) is shown in equation (3.6). The slope obtained from the plot represents the activation energy in the Arrhenius equation.

$$\ln D_{eff} = \ln D_0 - \frac{E_a}{RT} \qquad (3.6)$$

3.3.6 Specific energy consumption (SEC)

Specific energy consumption is a widely employed metric in diverse fields, encompassing engineering, industry, and energy management. It serves as a means to precisely quantify the energy demanded for executing a particular task or generating a unit of output. Typically, it is articulated as energy expended per unit of a specific metric, encompassing energy per unit of production, energy per unit of time, or energy per unit of distance, depending on the application and context.

The specific energy consumption (SEC) equation is represented in equation (3.7) below.

$$SEC = \frac{\text{Total electrical power supplied in drying } (P_{total})}{\text{Amount of water removed during drying}}, \frac{kWh}{kg} \quad (3.7)$$

where P_{total} is a total electric power that is supplied in the drying process, this term can be expressed as equation (3.8) below.

$$P_{total} = P_{heater} + P_{fan} + P_{sensor} + P_{control\ system} + P_{compressor} \text{ , [kW x 3,600s]} \qquad (3.8)$$

where P_{heater} is the electric power supplied to the heater, P_{fan} is the electric supplied to the fan for air ventilation, P_{sensor} is the electric supplied to the sensor which used to track the reduction of moisture content during the drying process, $P_{control\ box}$ is the electric power supplied to the control gadgets which used to adjust the heater to set point, $P_{compressor}$ is the electric supplied to the compressor to generate air flow through the system.

3.3.7 Correlation coefficients and error analyses

Many statistical parameters have been used to evaluate the appropriate model for describing the drying mechanism including the correlation coefficient (R^2). This parameter is the primary criterion used as a tool to support the appropriate selection, while reduced chi-square (χ^2) and root mean square error (RMSE) values are also considered. The goodness of fit mathematical model of the result gives higher R^2 but lower χ^2 and RMSE are preferred. As shown in equation (3.9), the reduced chi-square (χ^2) obtained from calculating the mean square deviations between the calculated value and the experiment value was also considered. The reduced chi-square (χ^2) can be calculated as follows:

$$\chi^2 = \frac{\Sigma_{i=1}^{N} \left(MR_{exp,i} - MR_{pre,i}\right)^2}{(N-n)} \qquad (3.9)$$

The root mean square error (RMSE) is shown in equation (3.10):

$$RMSE = \sqrt{\frac{1}{N} \Sigma_{i=1}^{N} \left(MR_{exp,i} - MR_{pre,i}\right)^2} \qquad (3.10)$$

where $MR_{exp,i}$ is the moisture content obtained from the number of experiments, $MR_{pre,i}$ is the calculated result as predicted moisture content, N is the number of data points and *n* is the number of constants used to fit the selected model and the MR can be calculated according to equation (3.11) below:

$$MR = \frac{8}{\pi^2} \sum_{n=0}^{\infty} \frac{1}{(2n+1)^2} \exp\left(-\frac{(2n+1)^2 \pi^2 D_{eff} t}{4L_0^2}\right) \qquad (3.11)$$

where D_{eff} is the effective diffusivity (m^2/s) and L_0 is the half thickness of slab object (m). For an extended drying period, the first term of equation (3.11) can be simplified to the logarithmic term, as shown in equation (3.12):

$$\ln MR = \ln \frac{8}{\pi^2} - \frac{\pi^2 D_{eff} t}{4L_0^2} \qquad (3.12)$$

The determination of diffusivity can be obtained by plotting experimental data from the drying process in terms of the natural logarithm of MR as a function of unit time (t) in equation (3.12). A slope obtained from this plot is shown in equation (3.13) as follows:

$$Slope = \frac{\pi^2 D_{eff}}{4L_0^2} \qquad (3.13)$$

The summary process for Part I, which focuses on the drying characteristics of CPH, is depicted in Figure 3.2 below.
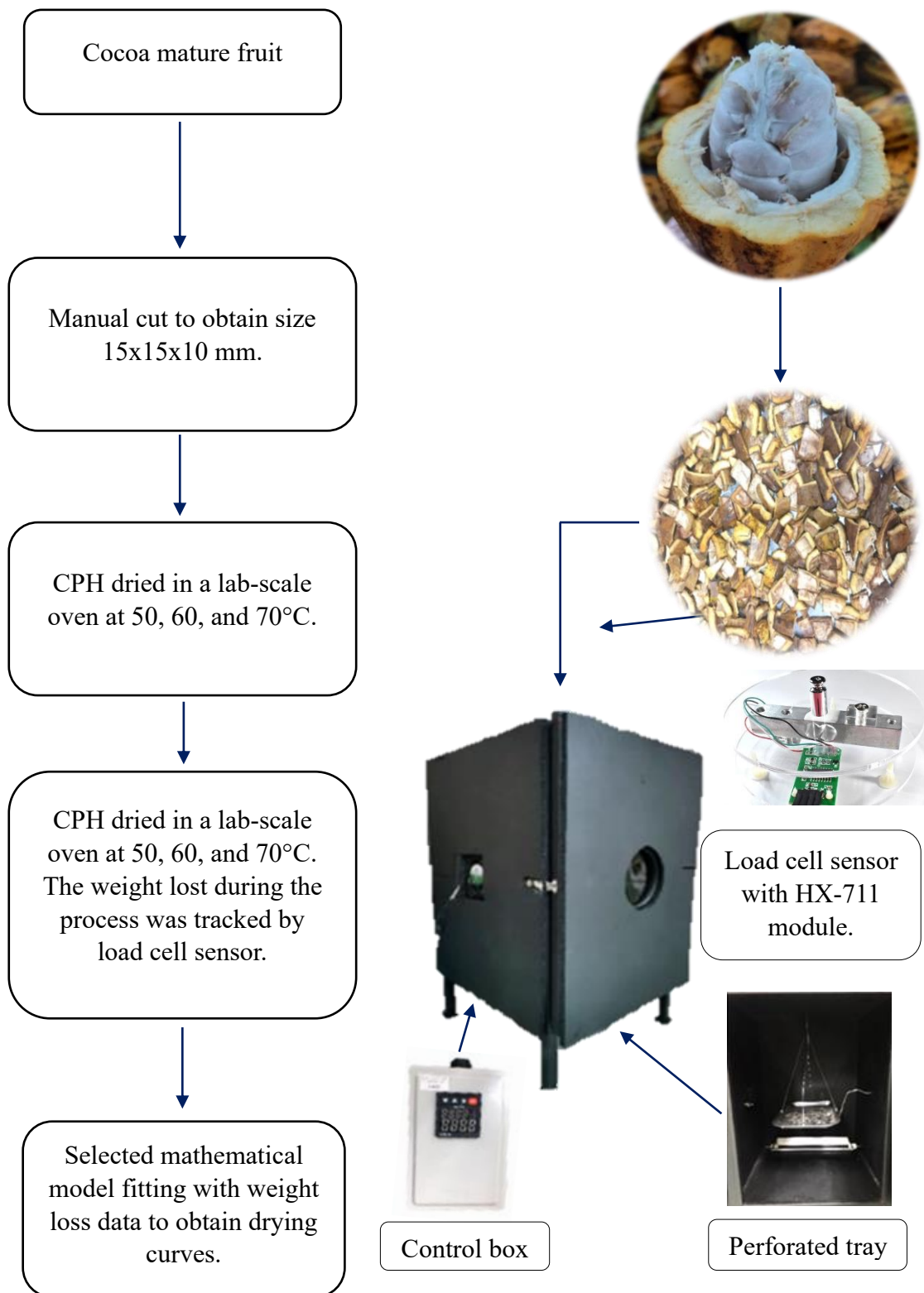
Figure 3.2 The summary process for part I.

3.4 Part II: Fermentation of Cocoa Pod Husk for Theobromine reduction, antioxidant enhancement, and total crude protein increase using RSM

3.4.1 Theobromine in CPH reduction

Fifty grams of fresh CPH were fermented in a 1,000 ml Duran's bottle to remove theobromine content. The experimental conditions, including an 8 L/S ratio, 4% molasses for promoting microorganism growth, and 1-4% alkali substance to break down complex compounds, were performed as shown in Table 3.2. Petri dish reactors were prepared with 10.42 g of the sample and 11.58 mL of Czapek Dox mineral medium, inoculated with 2×10^7 spores per gram of substrate. The reactors were then incubated at 30°C. For the alkali fermented condition, solid NaOH (98% purity) was added to the reactor according to the design table, and each reactor was shaken to ensure thorough mixing. The fermentation procedure was carried out at room temperature for 7 days.

Table 3.2 Conditions of fermentation for theobromine reduction.

Bottle No.	Conditions		
	NaOH (w/v)	4% of molasses (w/w)	Water added
1	-	-	-
2	-	-	/
3	-	/	/
4	1%	-	/
5	2%	-	/
6	4%	-	/

3.4.2 The increasing of crude protein in CPH

Response Surface Methodology (RSM) design of experiments (DOE) was employed to examine the effect of fermentation conditions on the increase in TCP content. Fermentation time (X_1), percentage of additional molasses (X_2), and the ratio of additional water to CPH (X_3) were the parameters of interest in this study. The alpha coefficient value (α) was set to face the center, resulting in 17 experimental runs

obtained from the DOE. The effects of these three independent variables were represented as '-1' (low level), '0' (normal level), and '1' (high level), as shown in Table 3.3. The axial or star points in the FCCD variables were statistically examined. Multiple regressions were used to fit a quadratic polynomial model to the experimental design data, as shown in Eq (3.14).

$$Y = b_0 + \sum_{i=1}^{i=3} b_i X_i + \sum_{i=1}^{i=3} b_{ii} X_i^2 + \sum_{i=1}^{i=2} \sum_{j=i+1}^{j=3} b_{ij} X_i X_j \quad (3.14)$$

Where Y is the predicted crude protein content and b_0, b_i, b_{ii}, and b_{ij} are the regression coefficients for the model intercept, linear quadratic, and interaction terms, respectively. The independent variables in the model were fermentation time (X_1), percentage of molasses (X_2), and liquid-to-solid ratio (L/S) (X_3).

Table 3.3 Three independent variables and their CCD levels.

Variables	level		
	-1	**0**	**1**
X_1: Fermentation time (days.)	7	14	21
X_2: molasses (%)	0	5	10
X_3: L/S ratio (mL/g)	0	7.5	15

The FCCD design was carried out using Design-Expert® software for Windows, version 13. The acceptability of the model was assessed based on the correlation coefficient (R^2), adjusted correlation coefficient (R^2_{adj}), and the lack-of-fit test. Regression analysis and three-dimensional (3D) response surface plots were utilized to determine the optimal condition for protein content. The study conditions from FCCD design are shown in Table 3.4 below, and the first days of each fermentation conditions are show in Figure 3.3 below.

Table 3.4 The study conditions of independent parameters obtained from FCCD.

#Exp	X_1: Fermentation time (days)	X_2: Molasses (%)	X_3: L/S ratio (ml/g)
1	21	10	15
2	21	5	7.5
3	14	5	0
4	14	5	7.5
5	14	0	7.5
6	14	5	7.5
7	7	0	15
8	7	0	0
9	21	0	0
10	14	5	15
11	7	5	7.5
12	21	0	15
13	7	10	0
14	14	5	7.5
15	21	10	0
16	14	10	7.5
17	7	10	15
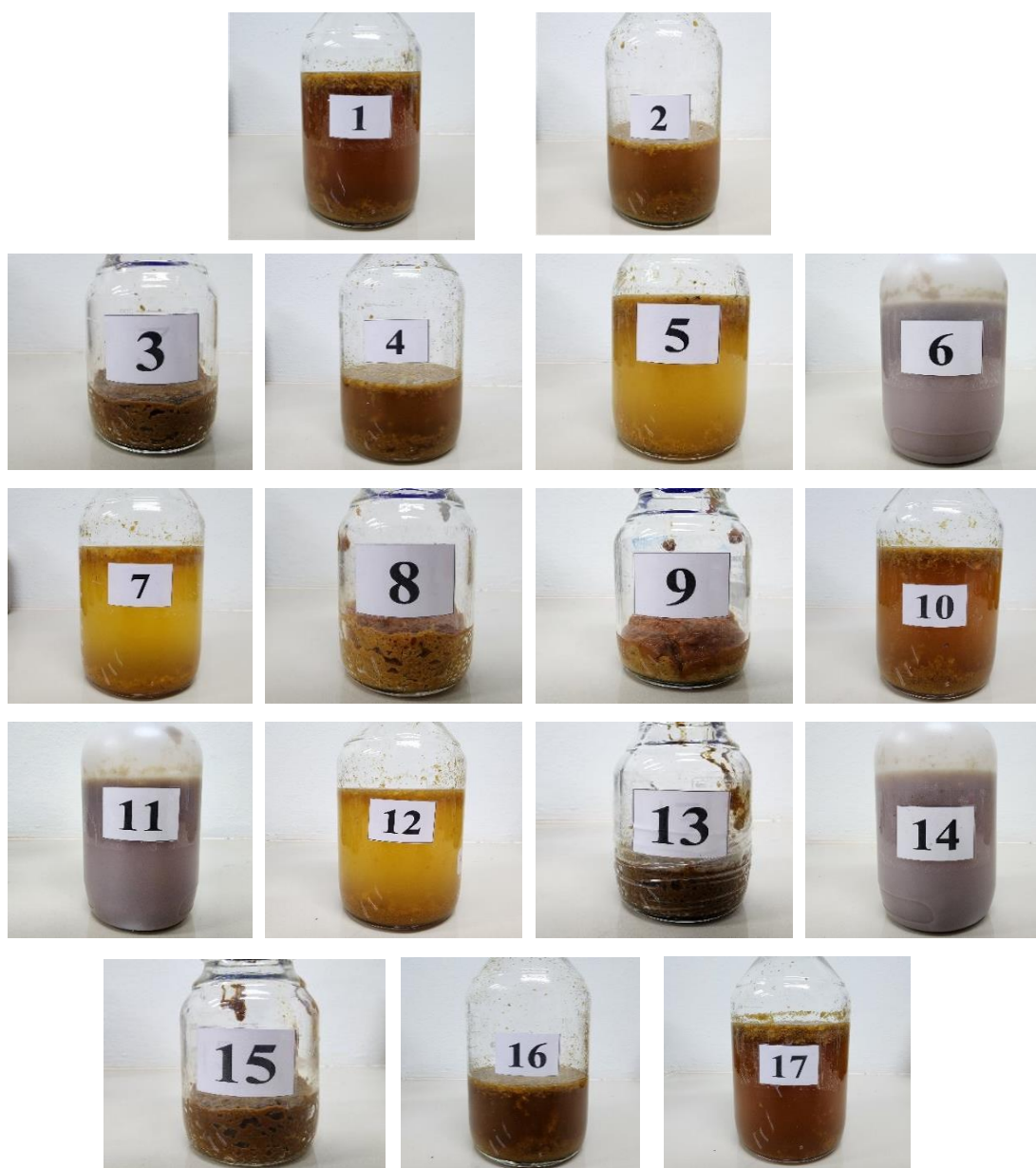
Figure 3.3 First day of fermentation unit of independent parameters from FCCD.

3.4.3 CPH extracts preparation

For the analysis of the fermentation results, CPH from the fermented samples was extracted using ethanol through ultrasonic-assisted extraction. The fermented CPH samples were dried in a convective oven, and accurately weighed amounts of 1.5 g were added to 250 ml Erlenmeyer flasks. Each flask was then filled with 45 ml of 55% ethanol and placed in an ultrasonic bath at 50°C for 60 minutes. Subsequently,

the samples were centrifuged for 10 minutes at 6,000 rpm at room temperature. The resulting supernatants, which contained the extract solutions, were collected in individual vials and stored at 0°C until they were used for the determination of theobromine content and antioxidant properties.

3.4.4 Determination of Theobromine content

The theobromine content in the CPH extracts was analyzed by an Agilent 1200 HPLC system based on the modified method of Nguyen et al. (2019). In summary, the theobromine standard (100 µg/mL in methanol) and extract solutions were filtered through 0.45 µm nylon membranes, and 50 µL of the samples were injected using an auto-injection system. A calibration curve for the standard theobromine was created, ranging from 0 to 400 mg/L, using a C_{18} column (Hypersil ODS, 5 µm, 4.0 x 250 mm cartridge). The column oven maintained the temperature at 35°C during operation. Isocratic elution was performed using a mobile phase consisting of distilled water (A) and pure acetonitrile (B) in a ratio of 80:20, with a flow rate of 1 mL/min. An Agilent Multi λ fluorescence detector (EX:330, EM:440 nm) was set to detect the theobromine compound content in the extracts at 274 nm. The theobromine content in the extracts was quantified in mg/100 g dry mass using the Eq (3.15) below:

$$\text{Theobromine content} = \frac{A \times B}{C} \qquad (3.15)$$

Where A = Peak area of sample/slope of calibration curve, B = weight of extract obtained per 100g of dry mass, C = weight of extract diluted in 55% ethanol before HPLC analysis.

3.4.5 Total phenolic content determination

The total phenolic content (TPC) of the sample was determined using the Folin-Ciocalteu method (Singleton et al., 1999a). The Folin-Ciocalteu reagent was diluted at a ratio of 1:10 with pure distilled water. Sodium carbonate with a purity of 99.5%, weighing 57.5 g, was diluted with distilled water to a final volume of 500 ml. In a test tube, 0.1 ml of CPH extract sample was added to 5 ml of Folin-Ciocalteu reagent,

followed by the addition of 3.5 ml of the sodium carbonate solution. The mixture was incubated in a water bath at 40°C for 1 hour. Subsequently, the samples were measured using a UV-vis spectrophotometer at a wavelength of 738 nm. Gallic acid, at concentrations ranging from 0.05 to 0.5 mg/ml, was used as the standard to generate a standard curve. The results were expressed as milligrams of gallic acid equivalents (GAE) per 100 grams of sample dry mass (d.m.).

3.4.6 Determination total flavonoid content

The total flavonoid content in each sample was determined using a modified method based on the method of Hu et al. (2017b). In a screw-capped tube, 1 mL of CPH extract solutions was diluted to 10 mL with 55% ethanol. Then, 0.5 mL of each sample extract was added, followed by the addition of 0.1 mL of 5% $NaNO_2$ solution. Next, 1 mL of 10% $AlCl_3$ solution was added to the tube. Finally, 1.0 mL of 1M NaOH solution and 3 mL of distilled water were added to the tube. The flavonoid content in each extract sample was determined using a UV-Vis spectrophotometer at a wavelength of 510 nm. The experiment was conducted in triplicate, and no sample was utilized as a blank. The results were reported as milligrams of quercetin equivalent (QE) per 100 grams of dry mass (d.m.), with quercetin used as the standard to generate a calibration curve.

3.4.7 Determination of %DPPH scavenging activity

The DPPH radical scavenging activity of the extract samples was examined and adapted following the method of Thabti et al. (2011). Firstly, 3.0 mL of DPPH solution (200 mM DPPH in 95% ethanol) was thoroughly mixed with 1.0 mL of extract solution at concentrations of 333, 666, and 1332 µg/mL in a screw-capped tube. The absorbance was measured at 517 nm using a UV-Vis spectrophotometer. The DPPH scavenging activity (%) was calculated according to Eq (3.16) below:

$$\text{Scavenging DPPH\%} = \frac{A_{control} - A_{sample}}{A_{control}} \times 100\% \qquad (3.16)$$

Where, $A_{control}$ = Light absorption value of the DPPH solution, and A_{sample} = Light absorbance value of the extract mixed with DPPH solution.

3.4.8 Determination of TCP content

The TCP content of each sample was determined using the modified Kjeldahl method (Jacobs, 1960). 2 g of dried CPH samples were placed in a Kjeldahl flask for the digestion procedure. To the flask, 20 ml of sulfuric acid and 2 g of Kjeldahl catalyst were added. The flasks were then placed in a block heater at 420°C for 3 hours. The resulting solutions were diluted by adding 30 ml of distilled water, followed by the addition of 30 ml of 40% sodium hydroxide (w/v). The flasks were placed on the heater blocks and connected to a condenser for distillation. The distillates were collected using 30 ml of 4% boric acid and analyzed by titration with 0.1 N HCl as a titrant. The total nitrogen content of CPH from the Kjeldahl method was calculated according to Eq (3.17) below:

$$N\% = \frac{V_1 \times n_1 \times F_1 \times M_w}{w_s \times 10} \qquad (3.17)$$

Where, V_1 is volume of HCL used in the titration (ml), n_1 is normality of HCL, F_1 is acid factor, and M_w is molecular weight of nitrogen. To calculate the TCP content the Eq (3.18) below was used.

$$\text{Total Crude Protein content } \% = N\% \times \text{Factor} \times F_2 \qquad (3.18)$$

Where, Factor value of 6.25 was used for food and feed, and F_2 is dilute factor in the dilution.

3.4.9 Statistical Analysis

All experiments were performed in triplicate. The data were presented as mean ± standard deviation, with statistical analysis conducted using Design-Expert® software (version-13). One-way ANOVA was used to analyze results, with a significance level set at less than 5% ($p \leq 0.05$).

The summary processes for Part II are depicted in terms of block diagrams, as illustrated in Figure 3.4 below.
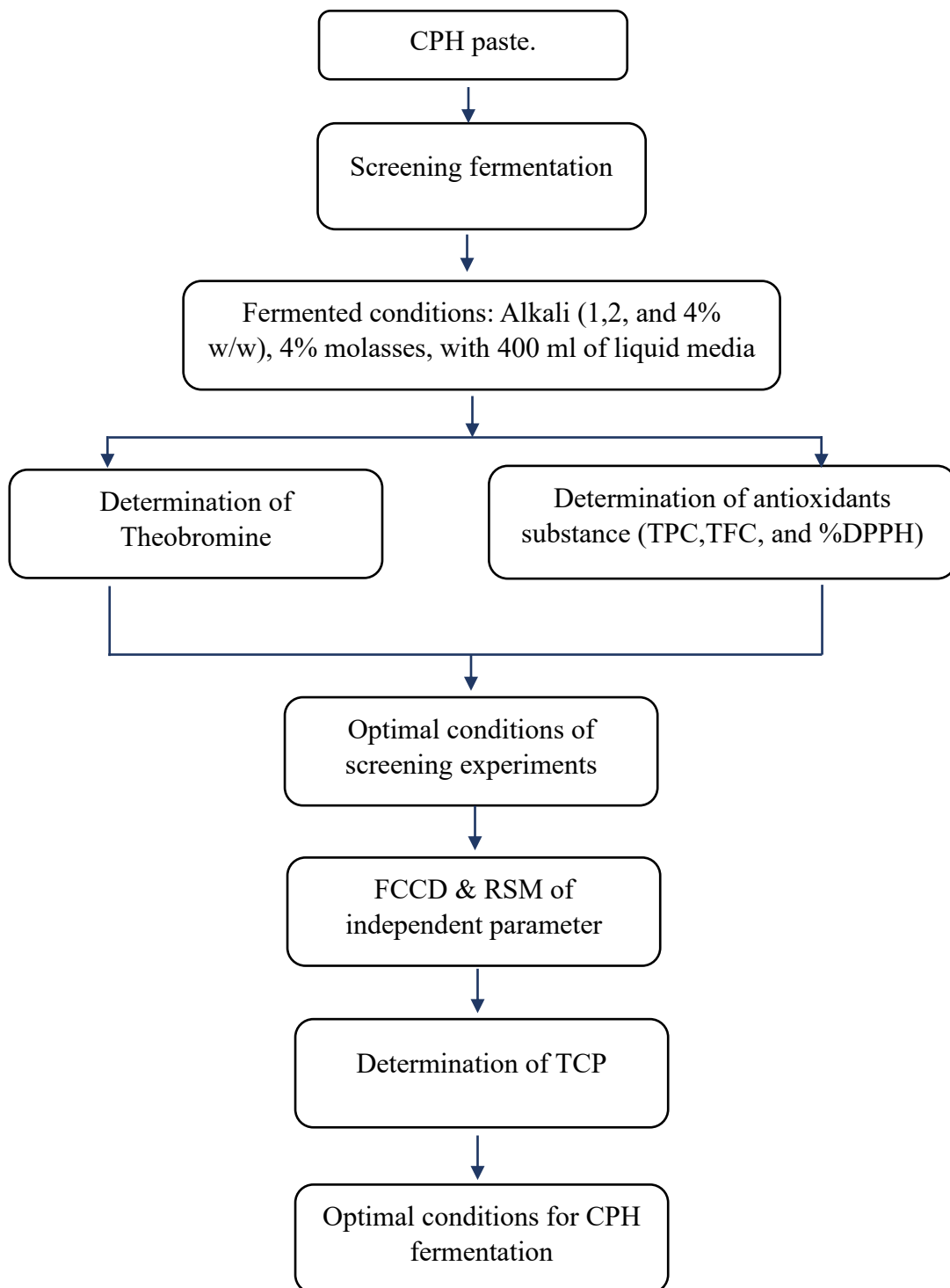
Figure 3.4 Summary process of part II.

CHAPTER 4

RESULT AND DISCUSSION

Part I: Drying kinetics and mathematical modeling of moisture diffusivity in CPH

In Part I, the study was aimed at investigating the drying characteristics of CPH. The research was designed to gather drying data of CPH under specific conditions, with a particular emphasis on identifying an appropriate model to describe its drying behavior. The drying outcomes were acquired through experiments, during which real-time data were collected using a load cell sensor in conjunction with an HX-711 module. The resulting data were subsequently analyzed.

4.1 Drying curves

CPH contained an initial moisture content of 5.40 ± 0.05 kg$_{water}$/kg$_{dry\ matter}$ (84.16% wet basis) and thickness of 10 mm as a thin layer. CPH was dried at 50, 60 and 70°C in a convective dryer attached to a load cell sensor. The CPH equilibrium moisture content was 1.67 ± 0.01 kg$_{water}$/kg$_{dry\ matter}$, while the weight did not change. Moisture content decreased continually as drying time increased. Drying times that reached equilibrium moisture content for CPH samples were 555, 465 and 360 min at 50, 60 and 70°C, respectively. This result concurred with Wang et al. (2007) who studied drying temperature range of 75-105°C for apple pomace and Tunde-Akintunde et al. (2011) who studied drying temperature range of 40-80°C for pumpkin. A constant rate period of the drying process did not appear but falling rate period occurred throughout the drying process. This phenomenon was induced by the mechanism of liquid and/or vapor diffusion and caused moisture movement in the CPH samples (Celma et al., 2007). Accelerating the rate of moisture evacuation from the surface by increasing heat transfer between CPH materials and dried air caused an increase in moisture diffusion from the inner layer to the surface of materials. Experimental results revealed that operating temperature was the most important factor that influenced drying time. The drying rate (DR) can be expressed as the amount of evaporated moisture over time (g$_{water}$/g$_{dry\ matter}$ x min). Figure 4.1 (a) shows the variation of drying

rate versus drying time and Figure 4.1 (b) shows moisture content (% dry basis) of the CPH samples at 50, 60 and 70°C at 3 L/min, respectively. After the initial period of the drying process, the drying rate reached its maximum value. Afterward, the CPH samples dried during the falling rate period. Initial values of drying rate increased when the operating temperature increased. An increase in temperature from 50°C to 70°C caused the maximum drying rate of 77% from 0.42 to 0.64 $g_{water}/g_{dry\ matter}$ x min. Moisture evaporation initially occurred on the surface of the CPH samples, but this phenomenon became less important as drying time increased. Moisture diffusion from the inner layers of CPH samples progressively increased. Our experimental results concurred with other studies related to the drying process of agricultural and vegetable products: (Barroca and Guiné, 2012) for quince, (Omolola et al., 2015) for banana, (Tunde-Akintunde and Ogunlakin, 2013) for pumpkin, (Faal et al., 2015) for apricot, (Valadez-Carmona et al., 2017) and (Midilli et al., 2002) for mushroom, pistachio, and pollen.

(a)

(b)
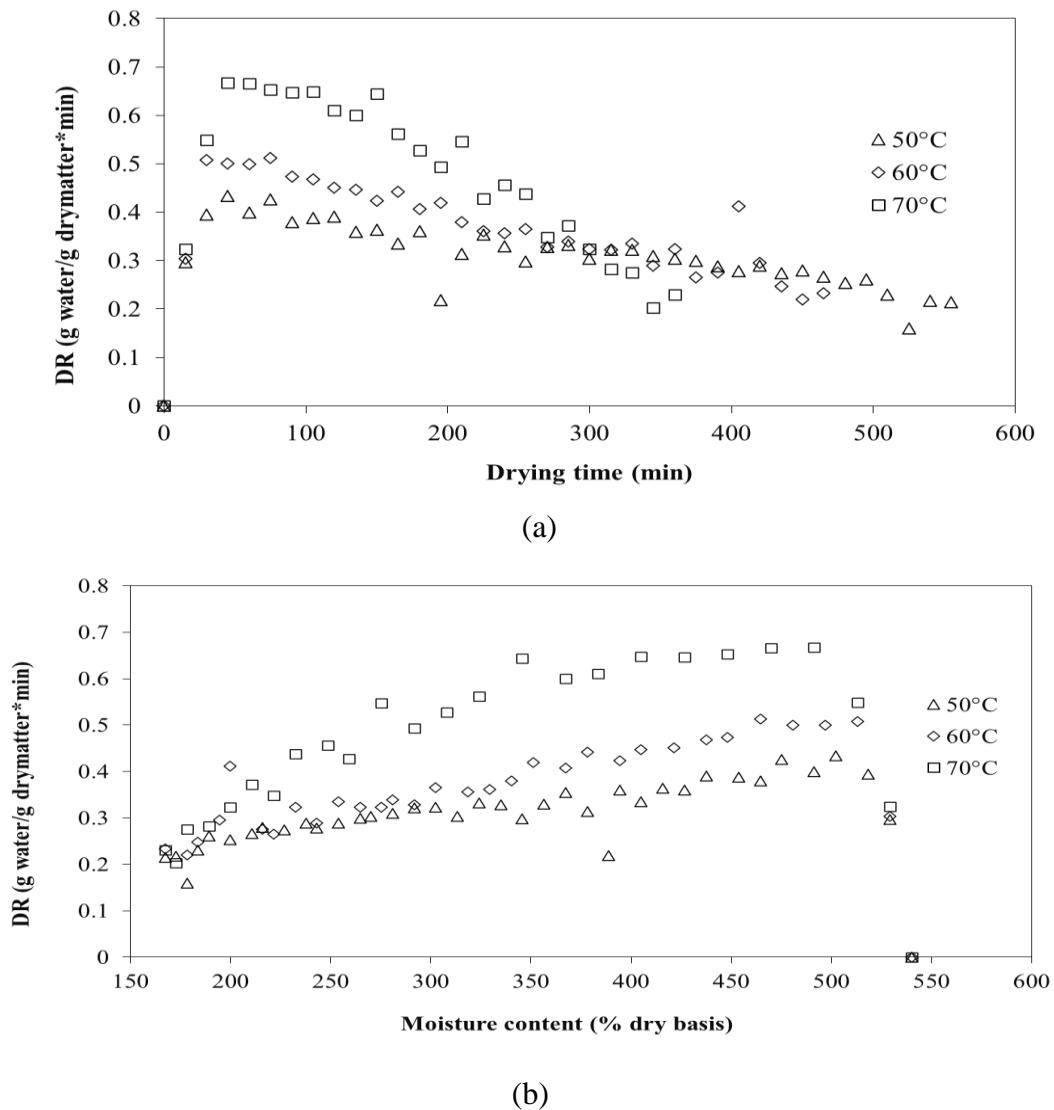
Figure 4.1 Variation of drying rate with **(a)** drying time and **(b)** moisture content of CPH.

4.2 Fitting the mathematical models

Curve fitting in MATLAB software was used to plot the experimental moisture ratio (MR) data from the drying process in each condition as a function of time. Twelve semi-theoretical models that have been widely used in literature to explain the kinetics of the drying process were selected. Non-linear regression techniques were used to attain the values of constants in each model. The goodness of fit was evaluated by calculating parameters including the coefficient of determination (R^2), the reduced chi-

square (χ^2), root mean square error (RMSE) and the sum of square errors (SSE). The calculated statistical parameters at 50, 60, and 70°C of operating temperature are shown in Table 4.1, 4.2, and 4.3 respectively. Results demonstrated that the Midilli model provided the best statistical values, with an R^2 of over 0.999 for all operating temperatures, while magnitudes of χ^2 and RMSE were lowest compared with the other models; between 1.2257 x 10^{-5} and 1.8923 x 10^{-5} for χ^2 and between 0.003441 and 0.004302 for RMSE. The SSE of this model presented values between 0.00140 and 0.00337, indicating that the Midilli model offered the best approximation for the experimental data.

Table 4.1 Curve fitting boundary of the semi-theoretical thin layer models for CPH at 50°C of operating temperature.

Model no	Model constants	R^2	χ^2	RMSE	SSE
	50°C				
1	k =0.001918	0.9889	4.6682×10^{-4}	0.02155	0.08590
2	k =0.0007266, n =1.166	0.9983	7.0210×10^{-5}	0.00833	0.01278
3	k=0.002038, n=1.166	0.9983	7.0210×10^{-5}	0.00833	0.01278
4	a=1.036, k=0.002035	0.9937	2.6832×10^{-4}	0.01629	0.04883
5	a=-0.001587, b=5.849 x 10^{-7}	0.9995	2.0002×10^{-5}	0.00445	0.00364
6	a=1.701, c=-0.6975, k=0.0009644	0.9996	1.9174×10^{-5}	0.00434	0.00345
7	a=0.04432, b=0.9544, k_1=0.001867, k_2=0.001917	0.9989	4.5941×10^{-5}	0.00670	0.00818
8	a=0.9987, k=0.001918	0.9889	4.7195×10^{-4}	0.02161	0.08590
9	a=0.9981, b=0.0325, c=1.136 x 10^{-6}, g=0.002015, h=4.535, k=0.002019	0.9934	2.8475×10^{-4}	0.01659	0.04955
10	a=1.008, b=-0.0003868, k=0.001528, n=0.9645	0.9996	1.8923×10^{-5}	0.00430	0.00337
11	a=-4.095, b=0.878, k=0.003718	0.9989	4.7271×10^{-5}	0.00682	0.00851
12	a=0.03899, g=0.001918, k=0.001917	0.9888	4.7720×10^{-4}	0.02167	0.08590

Table 4.2 Curve fitting boundary of the semi-theoretical thin layer models for CPH at 60°C of operating temperature.

Model no	Model constants	R^2	χ^2	RMSE	SSE
	60°C				
1	k=0.002303	0.9929	3.0379 x 10-4	0.01737	0.04800
2	k=0.001078, n=1.134	0.9994	2.6634 x 10-5	0.00513	0.00415
3	k=0.002415, n=1.134	0.9994	2.6634 x 10-5	0.00513	0.00415
4	a=1.034, k=0.002434	0.9971	1.2483 x 10-4	0.01110	0.01947
5	a=-0.00197, b=1.056 x 10-6	0.9994	2.5937 x 10-5	0.00506	0.00405
6	a=1.328, c=-0.3151, k=0.001612	0.9997	1.4648 x 10-5	0.00379	0.00226
7	a=2.713, b=-1.707, k1=0.003481, k2=0.00441	0.9995	2.2264 x 10-5	0.00466	0.00338
8	a=0.0001208, k=19.05	0.9929	3.0901 x 10-4	0.01747	0.04821
9	a=0.01478, b=1.073, c=-0.08557, g=0.002574, h=0.03127, k=0.03148	0.9978	9.5854 x 10-5	0.00960	0.01419
10	a=1.011, b=-0.0001964, k=0.00174, n=1.02	0.9997	1.4556×10^{-5}	0.00377	0.00221
11	a=-1.36, b=0.7404, k=0.004676	0.9994	2.5175 x 10-5	0.00497	0.00388
12	a=0.0005609, g=0.002303, k=0.002305	0.9928	3.1168 x 10-4	0.01748	0.04800

Table 4.3 Curve fitting boundary of the semi-theoretical thin layer models for CPH at 70°C of operating temperature.

Model no	Model constants	R^2	χ^2	RMSE	SSE
	70°C				
1	k= 0.00316	0.9898	5.2184 x 10-4	0.02284	0.06991
2	k= 0.001385, n= 1.151	0.9979	1.0758 x 10-4	0.01037	0.01431
3	k= 0.0738, n= 0.04282	0.9898	5.2576 x 10-4	0.02293	0.06991
4	a= 1.051, k= 0.003403	0.9972	1.4406 x 10-4	0.01200	0.01916
5	a= -0.002755, b= 2.266 x 10-6	0.9959	2.0969 x 10-4	0.01448	0.02789
6	a=1.118, c= -0.07633, k= 0.003007	0.9976	1.2239 x 10-4	0.01106	0.01615
7	a=0.05359, b= 0.9937, k1= 0.003398, k2= 0.003385	0.9971	1.4828 x 10-4	0.01218	0.01942
8	a= 0.000316, k= 9.996	0.9897	5.3055 x 10-4	0.02303	0.07055
9	a=1.086, b= 0.5003, c= -0.5839, g= 0.0519, h= 0.04902, k= 0.003553	0.9992	4.2678 x 10-5	0.00653	0.00551
10	a=1.001, b= 0.0002907, k= 0.0008479, n= 1.281	0.9997	1.2895 x 10-5	0.00359	0.00169
11	a= -0.08671, b= 0.09683, k= 0.03671	0.9992	4.2007 x 10-5	0.00648	0.00554
12	a= 1.087, g= 0.03674, k= 0.003555	0.9992	4.2007 x 10-5	0.00648	0.00554

Figure 4.2 shows different selected model fits with moisture ratio versus drying time at each temperature 50, 60 and 70°C of the drying process. The prediction of moisture ratio during the drying process calculated from the selected models was both under and over the experimental data curve. Figure 4.3 compares the experimental and predicted moisture ratio values at different temperatures by the Midilli model. Results showed that the trending line concurred with the experimental data, with all magnitudes ranging around the 45° line as very good acceptance between predicted and experimental data (Celma et al., 2007). This result indicated that the Midilli model effectively forecast the mechanism of moisture evaporation of the CPH samples during the drying process and provided the highest value of desired values, as well as the lowest value of undesired statistical values. The Midilli model also provided the lowest value of the sum of residuals as most suitable for the CPH drying process.
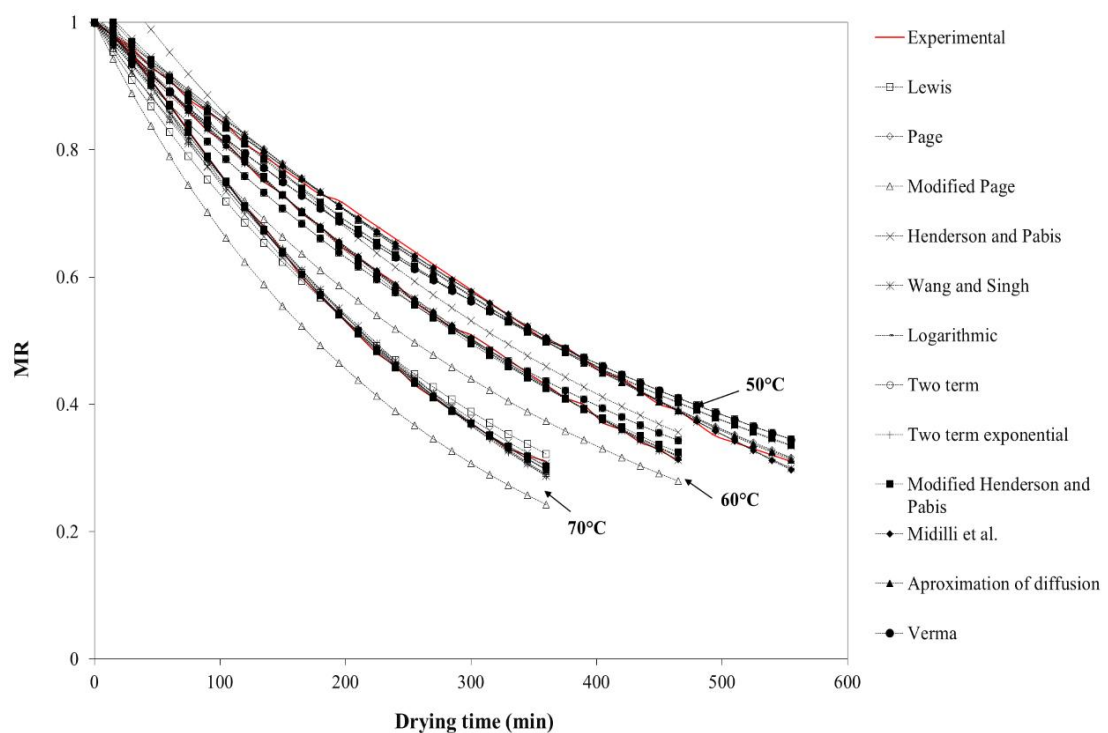
Figure 4.2 Variation of experimental and forecasted moisture ratio with drying time for different operating air temperatures
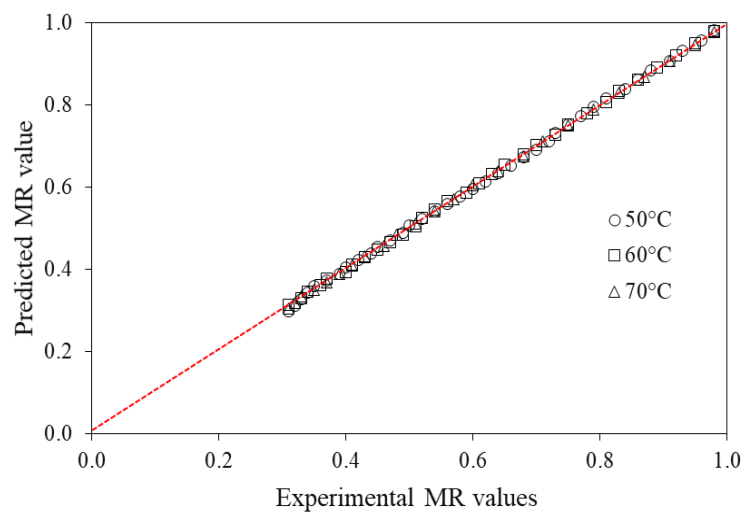
Figure 4.3 The experimental and predicted moisture ratio values at different temperatures by the Midilli model.

4.3 Determination of effective diffusivities

The experimental results can be explained by Fick's diffusion equation. Slab geometry is an assumption of materials at each temperature of the drying process. The diffusion coefficient was determined by plotting the result of the experiment in terms of ln (MR) as a function of drying time. Figure 4.4 shows a plot of ln(MR) as a sloped straight line. The slope values were used to calculate the effective diffusivities according to equation (3.13) as the measurement of the effective diffusivity. Effective diffusivities of dried CPH samples at each operating temperature of 50, 60 and 70°C were 7.979×10^{-10}, 9.499×10^{-10} and 13.298×10^{-10} m^2/s, respectively. As expected, the increment in the operating temperature generated D_e values which increased because the increase in operating temperature caused reduction in drying time. Values were in the typical range of 10^{-10} to 10^{-9} m^2/s for vegetables and agricultural materials and comparable to results in the literature as 1.6260×10^{-9} to 4.3612×10^{-9} m^2/s for drying apricots between 50 and 80°C (Faal et al., 2015), drying sludge from olive oil extraction range 2.224×10^{-10} to 6.993×10^{-10} m^2/s between 20 and 80°C (Celma et al., 2007) and drying apple pomace range 2.026×10^{-9} to 3.935×10^{-9} m^2/s between 75 and 105°C (Wang et al., 2007).
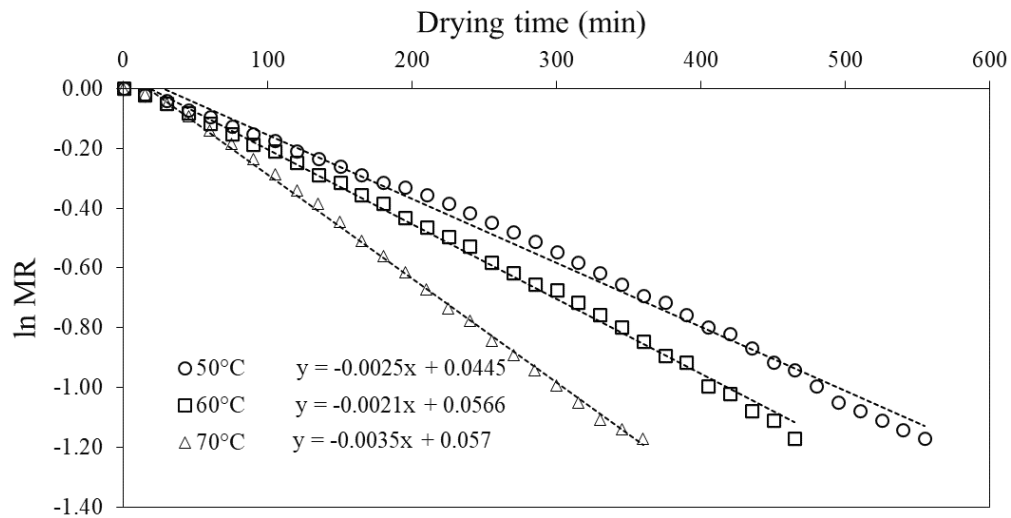
Figure 4.4 Plot of ln(MR) value with drying time.

4.4 Activation energy

Correlations between conditions of the drying process and calculated values of effective diffusivity (D_e) were expressed by an Arrhenius type equation according to equation 3.6 using the value of the gas constant 8.3143 kJ/kmol K. To obtain the magnitudes of the coefficients, ln D_e was plotted against the reciprocal of each operating temperature. The slope represented $-E_a$/R, while the intercept was $\ln(D_0$. The value of activation energy obtained from the calculation was 70.48 kJ/kmol, while the value of the Arrhenius pre-exponential factor was 4.814 x 10^{-6} m^2/s. This should be considered when designing drying machines and calculating the amount of energy required to remove moisture from the materials. Compares the activation energy estimated in our study and previous investigations of other materials such as sludge of olive extraction 15.77 kJ/mol (Celma et al., 2007), olive cake 26.71 kJ/mol (Doymaz et al., 2004), lemon basil leaf 32.34 kJ/mol (Mbegbu et al., 2021), okra 51.26 kJ/mol (Doymaz, 2005), green bun 39.47 kJ/mol (Senadeera et al., 2003), black tea 406.02 kJ/mol (Panchariya et al., 2002), thyme leaves 21.40 kJ/mol (Turan and Firatligil, 2019), red peppers 42.80 kJ/mol (Kaymak-Ertekin, 2002), and carrot 28.36 kJ/mol (Doymaz, 2004). Activation energy required for moisture diffusion of CPH was higher than other agricultural materials but lower than the activation energy of black tea. Activation energy consumption is influenced by the physical structure of the samples.

For example, CPH has a hard outer layer as a barrier for moisture diffusion and consists of high initial moisture content. This requires higher energy consumption than other materials.

4.5 Electrical energy consumption, drying time, and analysis of specific energy consumption (SEC)

Figure 4.5 shown the energy consumption from experiments, the energy consumption used for 50,60, and 70°C of drying process was 3.7, 5.0, and 5.4 kWh respectively, so the highest temperature of drying process consumed highest energy while the best result with concern to the energy consumption is founded from the 50°C of drying temperature.
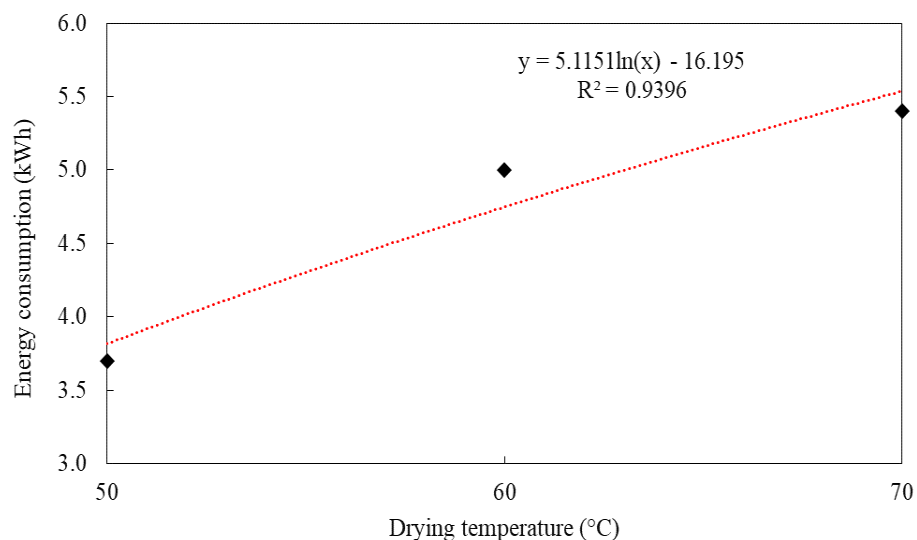
Figure 4.5 Energy consumption of CPH during drying under 50,60, and 70°C.

Figure 4.6 shows the specific energy consumption in each operation temperature of drying process. The difference of specific energy consumption occurred because of the first state of drying process. The moisture on the CPH surface is evaporated while the interior is still wet; the dry surface as outer layer resists the heat transport, causing in a reduction of drying and evaporation rate, also effecting long period of time to reach expected moisture content. Even though the lowest temperature in this study

required the longest drying time compared to the other values, it was still the optimal solution when the energy evaluation was taken into consideration.
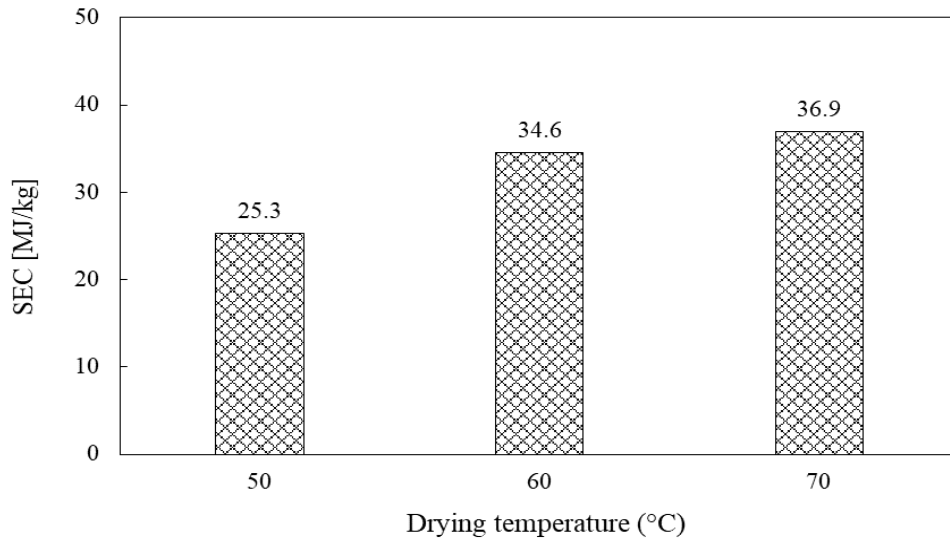
Figure 4.6 Specific energy consumption in each drying temperature.

In the initial phase of this study, the focus was on examining the drying characteristics of CPH. The results revealed that the model proposed by Midilli et al effectively predicted the moisture evaporation mechanism of the CPH samples during the drying process. This model exhibited the highest R^2 value, along with the lowest χ^2, RMSE, and SSE values when compared to other selected semi-theoretical mathematical models. The plots depicting the predicted values from the Midilli et al model closely aligned with the actual experimental data, forming a nearly straight line at a 45-degree angle, indicating very good agreement.

The effective diffusivity calculated using a modified Fick's diffusion equation, assuming a slab geometry for CPH, was found to be 7.979 x 10^{-10} m^2/s at 50°C, 9.944 x 10^{-10} m^2/s at 60°C, and 13.239 x 10^{-10} m^2/s at 70°C. The determination of the activation energy through an Arrhenius-type equation yielded a value of 70.48 kJ/kmol.

Regarding the SEC analysis, the obtained values were 25.3 MJ/kg, 34.6 MJ/kg, and 36.9 MJ/kg at operating temperatures of 50°C, 60°C, and 70°C, respectively.

Part II: Fermentation of Cocoa Pod Husk for Theobromine reduction, antioxidant enhancement, and total crude protein increase using RSM.

In Part II, the focus shifts towards determining the theobromine content, which poses harm to animal life. The emphasis lies in reducing the theobromine content under various fermentation conditions. Furthermore, the study examines antioxidant properties, including total phenolic content (TPC), total flavonoid content (TFC), and %DPPH scavenging activity. Following the identification of the optimal conditions leading to the lowest theobromine content, Response Surface Methodology (RSM) is employed to investigate the independent factors influencing the response, specifically the total crude protein content. The results of the study are presented below.

4.6   Theobromine in CPH reduction.

The HPLC analysis depicted in Figure 4.7(a) shows the standard theobromine peaks and theobromine contents in the CPH sample. The initial theobromine content in fresh CPH was measured at 59.50 ± 1.22 mg/100 g dry mass. However, fermentation with 4% molasses resulted in a significant reduction of theobromine content in CPH to 0.58 ± 0.02 mg/100 g dry mass. This decrease can be attributed to the growth of natural microorganisms during fermentation, which enhances the breakdown of theobromine into smaller molecules (Nieves et al., 2015). Xanthine, theophylline, and methylxanthines are some of the compounds formed through the destruction of theobromine (Brunetto et al., 2007). Although these compounds share structural similarities, they possess distinct chemical properties. The addition of water as a liquid medium in the fermentation reactor can accelerate the decomposition rate of theobromine in CPH, leading to its degradation over time (Seguine, 2009). Interestingly, the highest theobromine content was observed in the naturally degraded CPH sample, reaching 5.26 ± 0.27 mg/100 g dry mass. This can be attributed to the limited presence of microorganisms capable of decomposing the theobromine compound, compared to the sample with the lowest value that had additional molasses. Furthermore, theobromine is relatively stable under dry conditions (Izawa et al., n.d.). The HPLC analysis of the theobromine standard and fermented CPH extracts revealed a peak at 2.509 minutes, as illustrated in Figure 4.7(b).
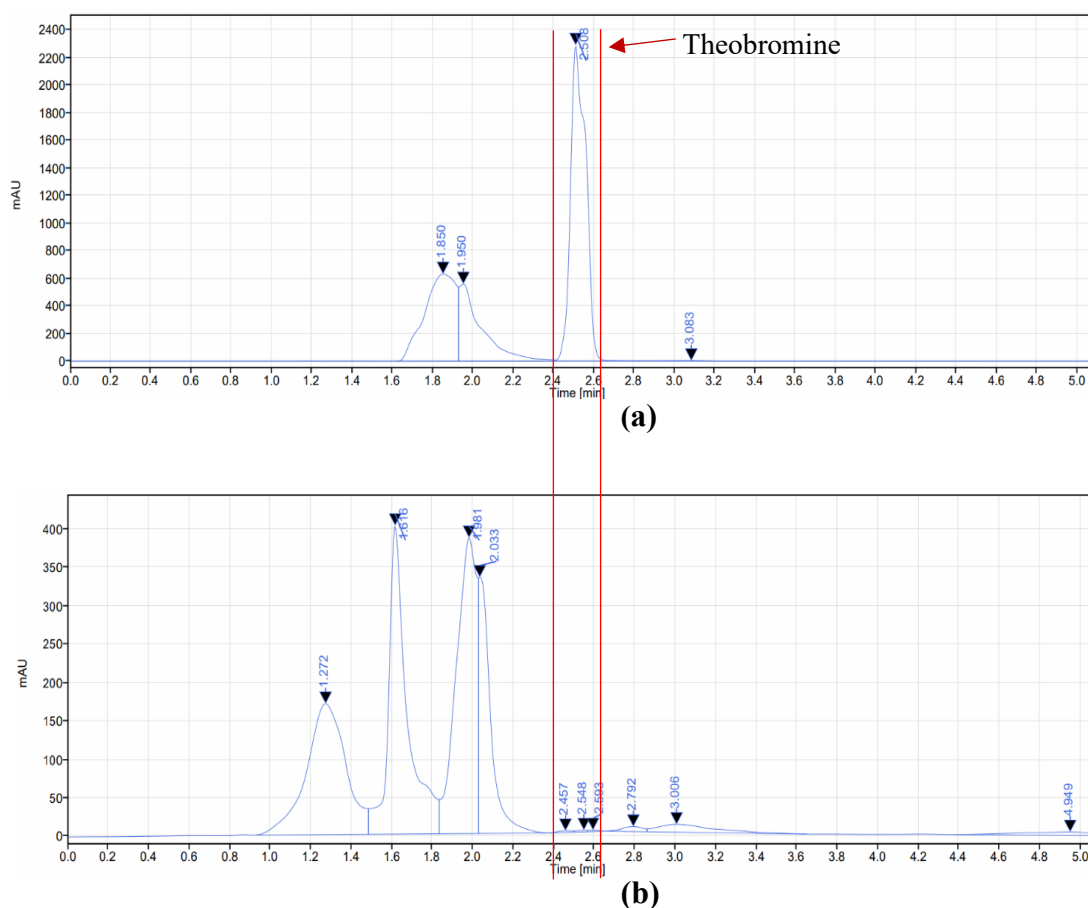
Figure 4.7 HPLC output for **(a)** calibration peak of theobromine substance at approximately 200 ppm, **(b)** CPH fermented with 4% of molasses

4.7 Antioxidants activity

4.7.1 Total phenolic content

The effect of different CPH fermentation conditions on the total phenolic content is presented in Table 4.4. Among the various fermentation conditions, fresh CPH fermentation with 4% molasses for 168 hours exhibited the highest total phenolic content, with a value of $2{,}127.76 \pm 19.29$ mgGAE/100g dry mass. The presence of molasses in the fermentation process can facilitate the breakdown of complex organic compounds into simpler compounds, leading to an increase in the total phenolic content (Brito et al., 2000b; Camu et al., 2008). This breakdown process allows larger phenolic compounds to be transformed into smaller, more bioavailable forms. A study conducted by Owusu, et al. (2017) investigated the effect of fermentation with

Lactobacillus plantarum on the phenolic content, antioxidant capacity, and bioactive compounds of cocoa pod husk from Ghana. Their results showed that the total phenolic content increased from 14.6 ± 0.3 mg GAE/g to 23.1 ± 0.4 mg GAE/g after 48 hours of fermentation (Ouattara et al., 2017). In comparison to these previous studies focusing on the fermentation of CPH, our study falls within the range of total phenolic content values reported. It is worth noting that this study did not specify the species of microorganisms used for fermentation, as all microorganisms were obtained from the CPH itself. Nevertheless, the optimum conditions for CPH fermentation from the southern parts of Thailand were determined based on the analysis results.

4.7.2 Total flavonoids content

The descriptive statistics for the total flavonoid content are presented in Table 4.4. The measurements of total flavonoids were normally distributed within a range of $1,618.42 \pm 178.12$ to $4,198.30 \pm 74.71$ mg/100g dry mass. Significant differences in the total flavonoid content were observed among the different fermentation conditions. Specifically, CPH fermented with 4% molasses exhibited the highest content of total flavonoids. This finding suggests that the fermentation process can enhance the overall flavonoid content, and the addition of 4% molasses (w/w) contributed to the highest value. Flavonoids, including flavanols, flavones, and condensed tannins, are known to increase during the fermentation process due to the growth of microorganisms. These microorganisms play a role in catalyzing the conversion of flavonoids into flavonoid derivatives (Hussain et al., 2022; Juan and Chou, 2010; Singleton et al., 1999b). Additionally, fermentation can influence the extraction and solubility of flavonoids within the fermented matrix. It has been observed that some flavonoids become more soluble in solvents compared to their non-fermented counterparts, which contributes to an increase in the measured total flavonoid content (Misnawi et al., 2002) .

4.7.3 %DPPH scavenging

In this investigation, the extracts of five samples were tested for their free radical scavenging potential using the DPPH assay. The %DPPH values ranged from $13.53 \pm 0.14\%$ to $89.57 \pm 14.64\%$. The highest %DPPH value was obtained from fresh CPH paste with an additional 4% molasses, while the lowest %DPPH value was obtained

from the decomposed sample. The addition of 4% molasses strongly influenced the change in %DPPH, as the molasses acted as a nutrient source for natural microorganisms, thereby activating their growth. The increased presence of microorganisms involved in fermentation can produce metabolites with antioxidant properties (Gan and Latiff, 2011). The increase in %DPPH can also be attributed to the formation of new bioactive compounds during fermentation or the breakdown of larger antioxidant molecules into smaller, more bioavailable forms, which enhances the %DPPH scavenging activity. On the other hand, in the case of the decomposed conditions, the lowest %DPPH value, the formation of reactive byproducts from the decomposition of antioxidants can have unintended effects on the body. These byproducts may exhibit pro-oxidant properties and have the potential to promote oxidative damage instead of providing protection. This phenomenon can occur when antioxidants undergo partial degradation or react with other compounds, leading to the formation of potentially harmful substances (Utami et al., 2016b).

Table 4.4 Quantification of antioxidants substance

#Exp.	Mean ± SD		
No	TPC (mg GAE/100g dry mass)	TFC (mg QE/ 100g dry mass)	%DPPH
1	626.66 ± 22.01	702.07 ± 124.53	79.58 ± 0.78
2	1,163.28 ± 59.22	1,618.42 ± 17.81	34.01 ± 0.03
3	2,127.76 ± 19.29	4,198.30 ± 24.71	88.33 ± 4.32
4	1,139.15 ± 14.81	1720.85 ± 218.67	81.18 ± 1.87
5	1,801.65 ± 26.62	908.40 ±192.39	56.08 ± 0.85
6	1411.24 ± 26.47	1917.22 ±84.47	13.53 ± 0.14

TPC, Total phenolic contents; SD, Standard deviation (n = 3); GAE, gallic acid equivalent; TFC, total flavonoids content; QE, Quercetin equivalent.

4.8 Analysis of response surfaces.

4.8.1 Statistical analysis of the model by ANOVA

The experimental results obtained in this study were shown in Table 4.5 below.

Table 4.5 Experiments result for the TCP content using the FCCD design-response surface method.

Run Order	Time (days) (X_1)	% Molasses (X_2)	L/S (ml/g) (X_3)	Actual value
1	14	10	7.5	6.73
2	21	10	0	7.85
3	14	5	0	6.89
4	7	10	15	6.53
5	14	5	7.5	5.93
6	21	10	15	5.21
7	7	5	7.5	6.03
8	7	10	0	7.33
9	14	0	7.5	4.87
10	14	5	7.5	6.12
11	21	5	7.5	5.87
12	21	0	0	6.28
13	21	0	15	4.12
14	7	0	0	5.12
15	14	5	15	5.15
16	7	0	15	4.82
17	14	5	7.5	6.15

The results demonstrated that the desired dependent variable was influenced by the main parameters of fermentation time, % molasses, and water to solid ratio. The mutual and simultaneous effects of these parameters were found to be significant in relation to the TCP content (%). The P-value of the model for the desired parameter was <0.0001, indicating the significance of the model and the obtained results. After eliminating the quadratic polynomial models, the equation () representing the most significant empirical relationship between the predictors (independent process variables) and their response, based on various criteria such as p-values, "lack of fit" p-value, highest R^2, predicted R^2, and adjusted R^2 values, is given in Table 4.6.

$$\mathbf{Y} = 4.60 + 0.0814X_1 + 0.2563 X_2 + 0.0378 X_3 - 0.0045 X_1 X_2 - 0.0088 X_1 X_3 - 0.0033 X_2 X_3 \quad (4.1)$$

Table 4.6 RSM quadratic model analysis of variance (ANOVA) of CPH fermentation experiments

TCP content (%).

Source	Sum of Squares	Df	Mean Square	F-value	p-value	
Model	15.02	6	2.50	134.47	< 0.0001	significant
X_1-Time	0.9283	1	0.9283	49.88	< 0.0001	
X_2-%molasses	2.27	1	2.27	121.71	< 0.0001	
X_3-liquid to solid ratio	0.1109	1	0.1109	5.96	0.0348	
X_1X_2	0.1984	1	0.1984	10.66	0.0085	
X_1X_3	1.71	1	1.71	91.95	< 0.0001	
X_2X_3	0.1200	1	0.1200	6.45	0.0294	
Residual	0.1861	10	0.0186			
Lack of Fit	0.1576	8	0.0197	1.38	0.4852	not significant
Pure Error	0.0285	2	0.0142			
Cor Total	15.20	16				
Std. Dev.	0.1364	**Mean**	5.94	**C.V. (%)**	2.30	
R²	0.9878	**Adjusted R²**	0.9804	**Predicted R²**	0.9683	
Adeq Precision	43.7059					

Table 4.6 displays the values of various terms associated with equation (4.1), including fermentation time, % of molasses added, and liquid to solid ratio for TCP content determination. The model presented in this table is considered significant based on the low p-value (<0.0001) and high F-value (134.47). The R^2 value of 0.9878 indicates good model accuracy, aligning with the theoretical method that favors lower p-values, higher F-values, and higher R^2 values to establish a significant and well-fitting model. Furthermore, the lack-of-fit test is nonsignificant for TCP content, while

the p-value (p = 0.4852) indicates that the quadratic models were statistically significant and can be used for further analysis. Additionally, a strong correlation between the experimental and predicted values was observed, as evidenced by R^2, R^2_{adj}, and $R^2_{predicted}$ values all exceeding 0.95, which signifies the adequacy and goodness-of-fit of the models (Aghel et al., 2014).

4.8.2 Accuracy check of the model using diagnostic charts

The normal distribution of the data can be assessed by examining the alignment of the points around a straight line the value of actual result and predict result were shown in Table 4.7 below. In the normal plot of the distribution, depicted in Figure 4.8 (a), the correlation between the variables is illustrated. The results closely follow the straight-line pattern, confirming that the data is normally distributed. Furthermore, when comparing the predicted vs residuals data in Figure 4.8(b) and predicted vs. run in Figure 4.8(c), it can be observed that the residuals vs. actual plot aligns closely with a straight line. This indicates that the results obtained from the experiments closely resemble the data generated from the runs, as depicted in Figure 4.8(d) these findings demonstrate the consistency between the predicted values and the values obtained from the experiments, thereby validating the accuracy of the designed model.

Table 4.7 The responses obtained from actual experiments were compared with the predicted outcomes generated using the FCCD design-response surface method, which was designed for varying the TCP content.

Run Order	Time (days) (X_1)	% Molasses (X_2)	L/S ratio (X_3)	Actual value	Predicted value
1	14	10	7.5	6.73	6.79
2	21	10	0	7.85	7.93
3	14	5	0	6.89	6.71
4	7	10	15	6.53	6.57
5	14	5	7.5	5.93	5.94
6	21	10	15	5.21	5.23
7	7	5	7.5	6.03	5.99
8	7	10	0	7.33	7.42
9	14	0	7.5	4.87	5.10
10	14	5	7.5	6.12	5.94
11	21	5	7.5	5.87	5.89
12	21	0	0	6.28	6.31
13	21	0	15	4.12	4.10
14	7	0	0	5.12	5.17
15	14	5	15	5.15	5.18
16	7	0	15	4.82	4.81
17	14	5	7.5	6.15	5.94
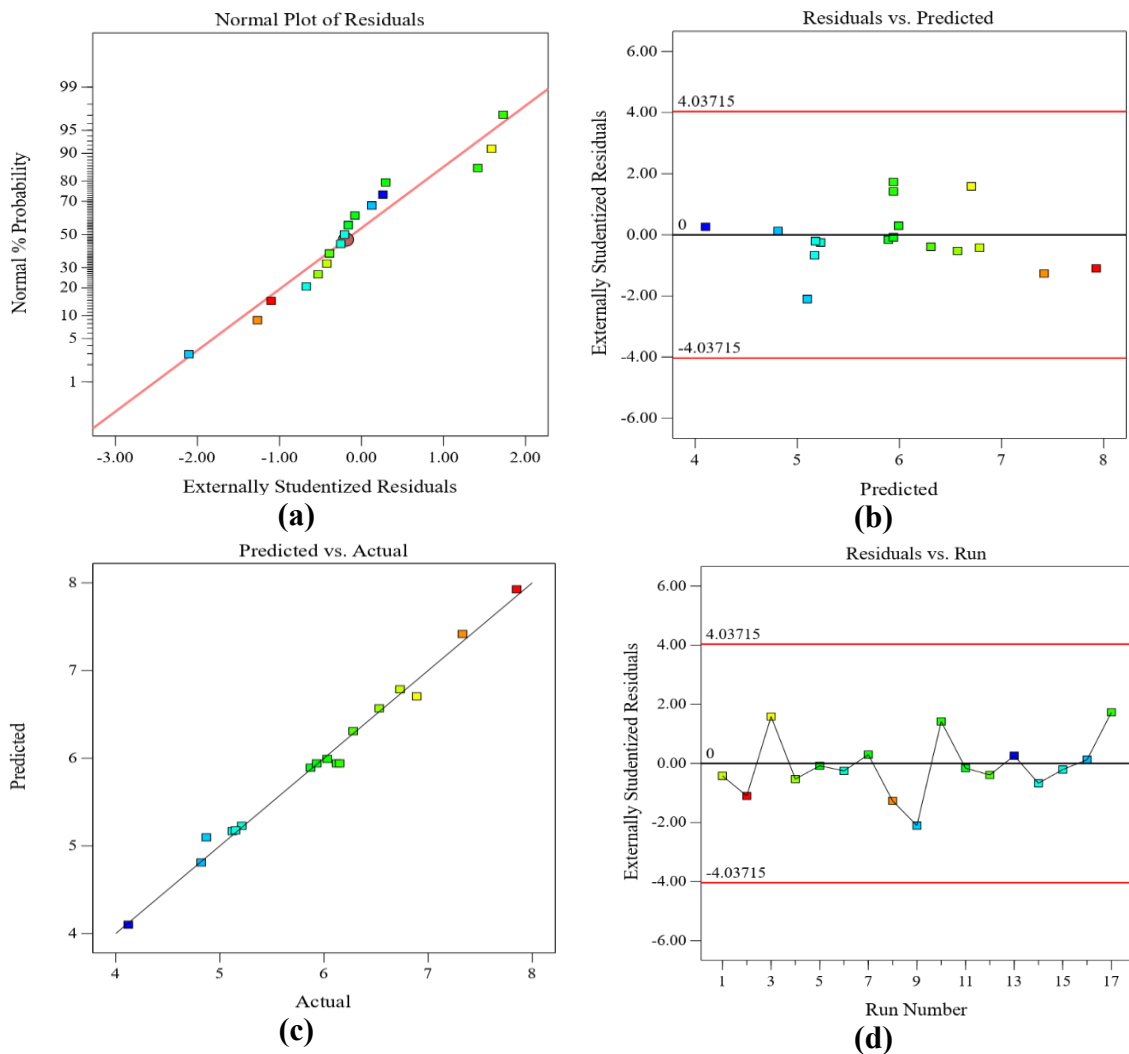
Figure 4.8 Distribution of data for TCP content; **(a)** Normal Plot of Residuals; **(b)** Predicted vs. Residuals; **(c)** Predicted vs. Actual; **(d)** Actual vs. Residuals.

4.8.3 Contour plots of variants parameters.

The impact of the selected input variables and their interactions on the percentage of TCP content was simulated. This is illustrated in Figure 4.9(a-c) which shows the variations in TCP content between two variables while keeping the third variable constant at its mean value. In Figure 4.9(a-c), the TCP content is depicted under different conditions. It was observed that fermentation time, %molasses, and L/S ratio had a significant influence on the TCP content. When the % molasses was increased from 0% to 10%, the TCP content rose from approximately 5% to 8%. On the other hand, increasing the L/S ratio initially resulted in a decrease in TCP content

from around 8% to 5%. Additionally, after 21 days of fermentation, the TCP content increased from approximately 5% to 8%. The initial TCP content in fresh CPH was approximately 4.75%. These findings demonstrate that the selected input variables, specifically fermentation time, %molasses, and L/S ratio, play a crucial role in determining the TCP content.
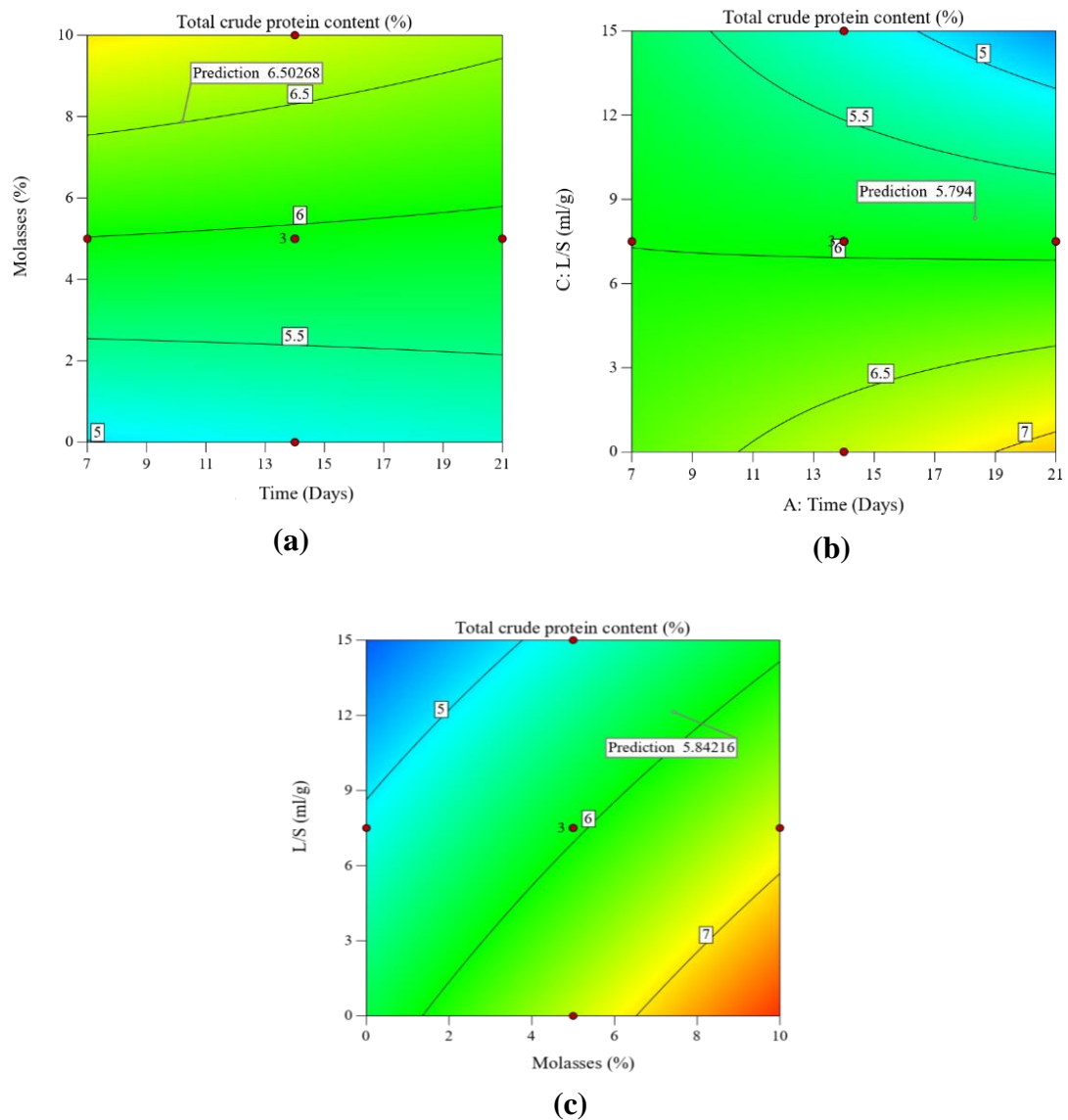

(a)

(b)

(c)

Figure 4.9 Contour plots depiciting the combined effect of two different variables on TCP **(a)** time vs. % molasses, **(b)** time vs. L/S ratio, and **(c)** % molasses vs. L/S ratio

4.8.4 Response surface plots and effects of variants variables.

The model equation indicates a positive correlation between TCP content and fermentation time as well as % molasses, while the L/S ratio has a negative effect. Graphs depicting the actual results against the predicted values for TCP content were generated using RSM in Design-Expert® software. The 3D surface plot illustrates the impact of fermentation time and % molasses on TCP content in Figure 4.10. TCP content increases significantly with longer fermentation time (from 7 days to 21 days) and the addition of molasses (from 0% to 10%). Natural microorganisms play a crucial role in biodegradation, breaking down organic materials into simpler compounds, and the addition of molasses provides a sufficient food source to activate their growth(Chebaibi et al., 2019a). Microorganisms synthesize proteins using the nutrients derived from the degradation of organic matter, and they also produce enzymes for biodegradation, many of which are proteins themselves (Chebaibi et al., 2019a). A high L/S ratio, referred to as submerged fermentation, significantly affects protein synthesis (Chebaibi et al., 2019a). Insufficient or imbalanced nutrients in the medium can limit the microorganisms' ability to efficiently produce protein, resulting in reduced TCP content. In this study, TCP content ranged from 4.12% to 7.85%. Through modeling calculations, the maximum predicted TCP content was 7.93% at 21 days of fermentation time with the addition of 10% molasses. Figure 4.11 displays the surface of CPH fermented under optimal conditions, which yielded the highest TCP. The microorganism Aspergillus. N played a crucial role in the decomposition process of CPH.
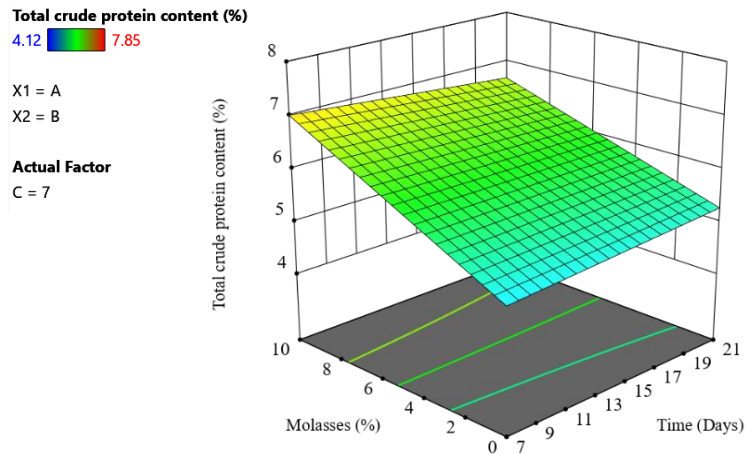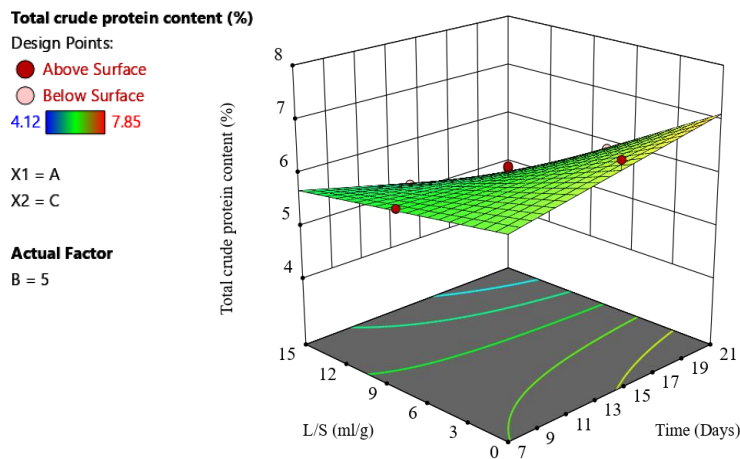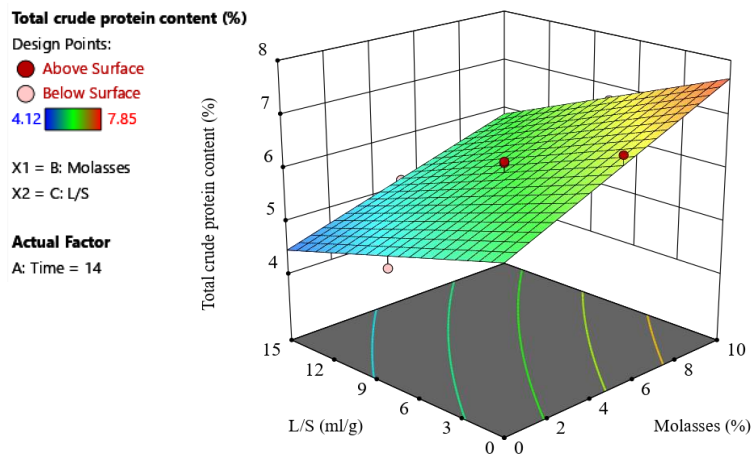
Figure 4.10 Response surface plots of the effects variants variables to TCP (%), **(a)** times vs. % molasses, **(b)** time vs. L/S ratio, and **(c)** % molasses vs. L/S ratio

Figure 4.11 The surface of CPH under the fermented conditions that yielded the highest TCP.

4.8.5 Optimal state validation

These optimal conditions were determined to be 21 days of fermentation time, 10% molasses added, and solid-state fermentation (L/S=0). The optimal conditions were determined through regression models with the inclusion of three specific constraints: fermentation times ranging from 7 to 21 days (X_1), additional molasses ranging from 0 to 10% (X_2), and extra water ranging from 0 to 15 ml/g (X_3). Following analysis in Design-Expert®, the optimal conditions were identified as stated above. To validate the model, the optimal predicted values generated by Design-Expert® software were compared with the actual values. The optimal predicted values are accompanied by a 95% confidence interval (CI). The comparison between the actual response values and the predicted response values is presented in table 4.8

Table 4.8 Comparison of the actual response value with the predicted response value

Response	Actual value	Predicted value	95% CI	
			Low	High
TCP content (%)	7.85 ± 0.02	7.93	7.67	8.19

Note: CI = Confidence interval

The second part of the study focuses on the fermentation process's impact on reducing the theobromine content, which is harmful to animal life. The fermentation screening aimed to identify the most effective fermentation types, including alkali

fermentation (using 1%, 2%, and 4% NaOH w/v), 4% molasses addition (w/v), and fresh CPH. All fermentation processes were conducted using submerged fermentation with the addition of 400 ml of water as the liquid medium. Following a 7-day fermentation period, the fermented samples underwent centrifugation, and the solid phase was subsequently dried for extraction. Theobromine content, total phenolic content (TPC), total flavonoid content (TFC), and %DPPH scavenging was utilized as standards for selecting optimal conditions.

The results revealed that the addition of 4% molasses yielded the lowest theobromine content, measuring 0.58 ± 0.02 mg/100 g dry mass. Meanwhile, this condition provided the highest TPC, TFC, and %DPPH values, measuring $2,127.76 \pm 19.29$ mgGAE/100g dry mass, $4,198.30 \pm 74.71$ mg/100g dry mass, and $89.57 \pm 14.64\%$, respectively. Upon determining the optimal conditions, the subsequent experiments focused on the total crude protein content (TCP) by extending the optimal conditions identified during the screening test.

The experimental design involved varying factors such as fermentation time (days), additional molasses (%), and liquid-to-solid ratio (ml/g). A total of 17 experimental runs were carried out using the FCCD method. Upon applying the principles of Response Surface Methodology (RSM), the results revealed that fermenting CPH for 21 days, with 10% molasses, and without the addition of extra liquid, resulted in the highest TCP content, measuring $7.85 \pm 0.02\%$. An analysis of variance (ANOVA) conducted using Design-expert® version 13 confirmed the reliability of the model predictions, which were supported by the goodness of fit parameters.

CHAPTER 5

CONCLUSION AND SUGGESTION

5.1 Conclusion

For part I, The CPH pieces (15 x 15 x 10 mm^3) obtained from the cocoa powder and chocolate process were successfully investigated using the drying process. The initial moisture content of CPH samples was 5.40 ± 0.5% kg$_{water}$/kg$_{dry\ matter}$. Twelve mathematical experimental models based on the assumption of thin layer drying kinetics were used to explain the drying behavior of CPH pieces and investigated in the temperature range 50-70°C. During the drying process, weight reduction is monitored using a load cell sensor in collaboration with an HX-711 module. The results revealed that the Midilli model exhibited the best drying characteristics of CPH pieces, with high statistical values of R square, RMSE, SSE and reduced chi-square. The rate of air ventilation was set at 3L/min and results showed that the operating temperature had an impact on drying time. Moisture ratio in the CPH pieces was reduced by increasing the drying temperature and time. The graphic of the drying curves showed that values of effective diffusivity ranged between 7.979 x 10^{-10} and 13.298 x 10^{-10} m^2/s with activation energy of CPH pieces 70.48 kJ/mol. The optimal drying conditions could be used to design an oven for a future pilot-scale test.

For Part II, the optimal fermentation conditions for reducing theobromine content were determined to be an L/S ratio of 8 as the liquid medium, 7 days of fermentation, and 4% molasses. These conditions resulted in a significant reduction of theobromine content from 59.50 ± 1.22 to 0.58 ± 0.02 mg/100 g dry mass. Notably, these optimal conditions not only minimized the theobromine content but also maximized the antioxidant activity, as indicated by the highest values of TPC, TFC content, and %DPPH, which were 2,114.88 ± 29.98 mg GAE/100g dry mass, 4,180.23 ± 21.69 mg QE/100g dry mass, and 89.57 ± 4.64%, respectively. Subsequently, the optimal conditions were employed as boundaries for independent parameters to be considered in relation to Total Crude Protein (TCP) content using Response Surface Methodology (RSM). The successful application of RSM allowed for the

determination of the influential variables on TCP content increase, supported by the statistical parameters confirmed by ANOVA. The quadratic model with R^2, R^2_{adj}, and a p-value of 0.9878, 0.9804, and <0.0001, respectively, proved its capability to predict the response. Fermentation time and % molasses exhibited positive effects on TCP content, while the L/S ratio had a strong negative effect. The highest predicted TCP content value of 7.93% was achieved under the optimal conditions of 21 days of fermentation, 10% molasses, and an L/S ratio of 0. These findings have significant implications for the potential utilization of CPH in various industries, particularly in the food and agriculture sectors. The developed model serves as a valuable tool for future research and large-scale implementation in the industrial domain.

The study of the drying characteristics of CPH provides insights into the drying behavior of these husks. This insight led to the design of a suitable oven for drying CPH, enabling the preservation of an optimal moisture content for the CPH during seasons of low CPH yield. In the second part of the study, concerning the fermentation process, a satisfactory conclusion can be drawn regarding the augmentation of TCP in CPH. This augmentation deems the CPH appropriate as a replacement for expensive livestock feed. The outcomes of both studies are anticipated to benefit cocoa farmers, allowing them to enhance the value of their agricultural waste, an economically viable utilization. This approach also contributes to cost effective resource employment and positively impacts sustainable agriculture.

5.2 Suggestions

- Varying the air ventilation values in the drying conditions for model fitting is essential to ensure the suitability of the Midilli et al. model for explaining the drying characteristics of CPH.

- To establish the robustness of the fit, the single perforated tray should be replaced with a multi-layer perforated tray, affirming that the statistical parameters favor the Midilli et al. model.

- Expanding the size of the lab oven is necessary to accommodate industrial sector requirements.

- Specifying the natural microorganism species is crucial for enhancing clarity in understanding.

- The focus should also extend to aerobic microorganisms since this study exclusively concentrates on microorganisms. This issue becomes critical when conducting economic assessments within the industrial sector.

- Changes in other chemical compositions, such as total crude protein content during the fermentation process, warrant focused investigation.

REFERENCES

Adeoye AA, Akegbejo-Samsons Y, Fawole FJ, Olatunji PO, Muller N, Wan AHL, et al. From waste to feed: Dietary utilisation of bacterial protein from fermentation of agricultural wastes in African catfish (Clarias gariepinus) production and health. Aquaculture 2021;531:735850. https://doi.org/https://doi.org/10.1016/j.aquaculture.2020.735850.

Aghel B, Rahimi M, Sepahvand A, Alitabar M, Ghasempour HR. Using a wire coil insert for biodiesel production enhancement in a microreactor. Energy Convers Manag 2014;84:541–9. https://doi.org/https://doi.org/10.1016/j.enconman.2014.05.009.

Al-Amin M, Hossain MdS, Iqbal A. Effect of Pre-treatments and Drying Methods on Dehydration and Rehydration Characteristics of Carrot. Universal Journal of Food and Nutrition Science 2015;3:23–8. https://doi.org/10.13189/ujfns.2015.030201.

Ali M, Kumar A, Yvaz A, Salah B. Central composite design application in the optimization of the effect of pumice stone on lightweight concrete properties using RSM. Case Studies in Construction Materials 2023;18. https://doi.org/10.1016/j.cscm.2023.e01958.

Anees Ali Jafri S, Mehmood Khalid Z, Rizwan Khan M, Ashraf S, Ahmad N, Mahmoud Karami A, et al. Evaluation of some essential traditional medicinal plants for their potential free scavenging and antioxidant properties. J King Saud Univ Sci 2023;35. https://doi.org/10.1016/j.jksus.2023.102562.

B SR, LSS VR, S S. Chocolate Poisoning In A Dog. International Journal of Veterinary Health Science & Research 2013:16–7. https://doi.org/10.19070/2332-2748-130004.

Barroca MJ, Guiné RPF. Study of Drying Kinetics of Quince. Proceedings (Electronic) Da 362 International Conference of Agricultural Engineering CIGR-AgEng2012 2012:2–7.

Bhatia SK, Jagtap SS, Bedekar AA, Bhatia RK, Patel AK, Pant D, et al. Recent developments in pretreatment technologies on lignocellulosic biomass: Effect of key parameters, technological improvements, and challenges. Bioresour Technol 2020;300. https://doi.org/10.1016/j.biortech.2019.122724.

Brito E, García N, Gallao M, Cortelazzo A, Fevereiro P, Braga M. Structural and chemical changes in cocoa (Theobroma cacao L) during fermentation, drying and roasting. J Sci Food Agric 2000a;81:281–8. https://doi.org/10.1002/1097-0010(20010115)81:2<281::AID-JSFA808>3.0.CO;2-B.

Brito E, García N, Gallao M, Cortelazzo A, Fevereiro P, Braga M. Structural and chemical changes in cocoa (Theobroma cacao L) during fermentation, drying and roasting. J Sci Food Agric 2000b;81:281−8. https://doi.org/10.1002/1097-0010(20010115)81:2<281::AID-JSFA808>3.0.CO;2-B.

Bruce DM. Exposed-layer barley drying: Three models fitted to new data up to 150°C. Journal of Agricultural Engineering Research 1985;32:337−48. https://doi.org/10.1016/0021-8634(85)90098-8.

Brunetto M del R, Gutiérrez L, Delgado Y, Gallignani M, Zambrano A, Gómez Á, et al. Determination of theobromine, theophylline and caffeine in cocoa samples by a high-performance liquid chromatographic method with on-line sample cleanup in a switching-column system. Food Chem 2007;100:459−67. https://doi.org/10.1016/j.foodchem.2005.10.007.

Campos-Vega R, Nieto-Figueroa KH, Oomah BD. Cocoa (Theobroma cacao L.) pod husk: Renewable source of bioactive compounds. Trends Food Sci Technol 2018;81:172−84. https://doi.org/10.1016/j.tifs.2018.09.022.

Camps-Bossacoma M, Pérez-Cano FJ, Franch àngels, Castell M. Theobromine is responsible for the effects of cocoa on the antibody immune status of rats. Journal of Nutrition 2018;148:464−71. https://doi.org/10.1093/jn/nxx056.

Camu N, Winter T, Addo S, Takrama J, Bernaert H, De Vuyst L. Fermentation of cocoa beans: Influence of microbial activities and polyphenol concentrations on the flavour of chocolate. J Sci Food Agric 2008;88:2288−97. https://doi.org/10.1002/jsfa.3349.

Celma AR, Rojas S, López F, Montero I, Miranda T. Thin-layer drying behaviour of sludge of olive oil extraction. J Food Eng 2007;80:1261−71. https://doi.org/10.1016/j.jfoodeng.2006.09.020.

Chebaibi S, Leriche Grandchamp M, Burgé G, Clément T, Allais F, Laziri F. Improvement of protein content and decrease of anti-nutritional factors in olive cake by solid-state fermentation: A way to valorize this industrial by-product in animal feed. J Biosci Bioeng 2019a;128:384−90. https://doi.org/10.1016/j.jbiosc.2019.03.010.

Chebaibi S, Leriche Grandchamp M, Burgé G, Clément T, Allais F, Laziri F. Improvement of protein content and decrease of anti-nutritional factors in olive cake by solid-state fermentation: A way to valorize this industrial by-product in animal feed. J Biosci Bioeng 2019b;128:384−90. https://doi.org/10.1016/j.jbiosc.2019.03.010.

Cimrin T, Avsaroglu MD, Ivgin Tunca R, Kandir S, Ayasan T. Effects of the dietary supplementation of layer diets with natural and synthetic antioxidant additives on yolk lipid

peroxidation and fatty acid composition of eggs stored at different temperatures and duration. Rev Bras Cienc Avic 2019;21:1–10. https://doi.org/10.1590/1806-9061-2019-0991.

Dahunsi SO, Adesulu-Dahunsi AT, Izebere JO. Cleaner energy through liquefaction of Cocoa (Theobroma cacao) pod husk: Pretreatment and process optimization. J Clean Prod 2019a;226:578–88. https://doi.org/10.1016/j.jclepro.2019.04.112.

Dahunsi SO, Osueke CO, Olayanju TMA, Lawal AI. Co-digestion of Theobroma cacao (Cocoa) pod husk and poultry manure for energy generation: Effects of pretreatment methods. Bioresour Technol 2019b;283:229–41. https://doi.org/10.1016/j.biortech.2019.03.093.

Donkoh A, Atuahene CC, Wilson BN, Adomako D. Chemical composition of cocoa pod husk and its effect on growth and food efficiency in broiler chicks. Anim Feed Sci Technol 1991;35:161–9. https://doi.org/10.1016/0377-8401(91)90107-4.

Doymaz I. Drying characteristics and kinetics of okra. J Food Eng 2005;69:275–9. https://doi.org/10.1016/j.jfoodeng.2004.08.019.

Doymaz I. Convective air drying characteristics of thin layer carrots. J Food Eng 2004;61:359–64. https://doi.org/10.1016/S0260-8774(03)00142-0.

Doymaz I, Gorel O, Akgun NA. Drying characteristics of the solid by-product of olive oil extraction. Biosyst Eng 2004;88:213–9. https://doi.org/10.1016/j.biosystemseng.2004.03.003.

Eryasar-Orer K, Karasu-Yalcin S. Bioproduction of Xylitol From Chestnut Shell Hydrolysate: Optimization of Fermentation Parameters. vol. 46. 2019.

Eteng MU, Ettarh RR. Comparative effects of theobromine and cocoa extract on lipid profile in rats. Nutrition Research 2000;20:1513–7. https://doi.org/https://doi.org/10.1016/S0271-5317(00)80032-9.

Faal S, Tavakoli T, Ghobadian B. Mathematical modelling of thin layer hot air drying of apricot with combined heat and power dryer. J Food Sci Technol 2015;52:2950–7. https://doi.org/10.1007/s13197-014-1331-9.

Gan C-Y, Latiff A. Extraction of antioxidant pectic-polysaccharide from mangosteen (Garcinia mangostana) rind: Optimization using response surface methodology. Carbohydr Polym 2011;83:600–7. https://doi.org/10.1016/j.carbpol.2010.08.025.

Gervasi T, Pellizzeri V, Calabrese G, Di Bella G, Cicero N, Dugo G. Production of single cell protein (SCP) from food and agricultural waste by using Saccharomyces cerevisiae. Nat Prod Res 2018;32:648–53. https://doi.org/https://doi.org/10.1080/14786419.2017.1332617.

Gumus RH. Drying Characteristics and Kinetics of Bitter leave (Vernonia amygdalina) and Scent leave (Ocimum gratissimum). Chemical and Process Engineering Research 2015;32:1−11.

Gupta R, Hemansi, Gautam S, Shukla R, Kuhad RC. Study of charcoal detoxification of acid hydrolysate from corncob and its fermentation to xylitol. J Environ Chem Eng 2017;5:4573−82. https://doi.org/https://doi.org/10.1016/j.jece.2017.07.073.

Hartog LA den, Sijtsma SR. Challenges and opportunities in animal feed and nutrition. 11th World Conference on Animal Production 2013:1−15.

Henderson SM. Progress in Developing the Thin Layer Drying Equation. Transactions of the American Society of Agricultural Engineers 1974;17:1−3. https://doi.org/10.13031/2013.37052.

Hernández-Mendoza AG, Saldaña-Trinidad S, Martínez-Hernández S, Pérez-Sariñana BY, Láinez M. Optimization of alkaline pretreatment and enzymatic hydrolysis of cocoa pod husk (Theobroma cacao L.) for ethanol production. Biomass Bioenergy 2021;154. https://doi.org/10.1016/j.biombioe.2021.106268.

Hu Z, Tang X, Liu J, Zhu Z, Shao Y. Effect of parboiling on phytochemical content, antioxidant activity and physicochemical properties of germinated red rice. Food Chem 2017a;214:285−92. https://doi.org/https://doi.org/10.1016/j.foodchem.2016.07.097.

Hu Z, Tang X, Liu J, Zhu Z, Shao Y. Effect of parboiling on phytochemical content, antioxidant activity and physicochemical properties of germinated red rice. Food Chem 2017b;214:285−92. https://doi.org/https://doi.org/10.1016/j.foodchem.2016.07.097.

Hussain OA, Abdel Rahim EA, Badr AN, Hathout AS, Rashed MM, Fouzy ASM. Total phenolics, flavonoids, and antioxidant activity of agricultural wastes, and their ability to remove some pesticide residues. Toxicol Rep 2022;9:628−35. https://doi.org/10.1016/j.toxrep.2022.03.038.

Hutjens MF, Baltz JH. SYMPOSIUM : KEEPING EXTENSION PROGRAMS CURRENT Keeping Extension Programs Current in Order to Meet the Needs of a Dynamic Dairy Industry. J Dairy Sci 2000;83:1412−7. https://doi.org/10.3168/jds.S0022-0302(00)75010-7.

Izawa K, Amino Y, Kohmura M, Ueda Y, Kuroda M. 4.16 Human-Environment Interactions-Taste. n.d.

Jacobs S. The determination of nitrogen in organic compounds by the indanetrione hydrate method. Analyst 1960;85:257−64. https://doi.org/10.1039/AN9608500257.

Jönsson LJ, Martín C. Pretreatment of lignocellulose: Formation of inhibitory by-products and strategies for minimizing their effects. Bioresour Technol 2016;199:103−12. https://doi.org/10.1016/j.biortech.2015.10.009.

Juan MY, Chou CC. Enhancement of antioxidant activity, total phenolic and flavonoid content of black soybeans by solid state fermentation with Bacillus subtilis BCRC 14715. Food Microbiol 2010;27:586−91. https://doi.org/10.1016/j.fm.2009.11.002.

Júnior PCG, dos Santos VB, Lopes AS, de Souza JPI, Pina JRS, Chagas Júnior GCA, et al. Determination of theobromine and caffeine in fermented and unfermented Amazonian cocoa (Theobroma cacao L.) beans using square wave voltammetry after chromatographic separation. Food Control 2020;108:106887. https://doi.org/https://doi.org/10.1016/j.foodcont.2019.106887.

Karathanos VT. Determination of water content of dried fruits by drying kinetics. J Food Eng 1999;39:337−44. https://doi.org/10.1016/S0260-8774(98)00132-0.

Kaymak-Ertekin F. Drying and rehydrating kinetics of green and red peppers. J Food Sci 2002;67:168−75. https://doi.org/10.1111/j.1365-2621.2002.tb11378.x.

Khan S, Das P, Thaher MI, AbdulQuadir M, Mahata C, Al Jabri H. Utilization of nitrogen-rich agricultural waste streams by microalgae for the production of protein and value-added compounds. Curr Opin Green Sustain Chem 2023;41:100797. https://doi.org/https://doi.org/10.1016/j.cogsc.2023.100797.

KIM H, KEENEY PG. (-)-Epicatechin Content in Fermented and Unfermented Cocoa Beans. J Food Sci 1984;49:1090−2. https://doi.org/https://doi.org/10.1111/j.1365-2621.1984.tb10400.x.

L SS, K G S, B M C, Koushik, M A S, karthik J. Experimental investigation and optimization of light transmitting brick using ANOVA method of regression using minitab software. Mater Today Proc 2023. https://doi.org/https://doi.org/10.1016/j.matpr.2023.06.176.

Lorenci Woiciechowski A, Dalmas Neto CJ, Porto de Souza Vandenberghe L, de Carvalho Neto DP, Novak Sydney AC, Letti LAJ, et al. Lignocellulosic biomass: Acid and alkaline pretreatments and their effects on biomass recalcitrance − Conventional processing and recent advances. Bioresour Technol 2020;304. https://doi.org/10.1016/j.biortech.2020.122848.

Mbegbu NN, Nwajinka CO, Amaefule DO. Thin layer drying models and characteristics of scent leaves (Ocimum gratissimum) and lemon basil leaves (Ocimum africanum). Heliyon 2021;7:e05945. https://doi.org/10.1016/j.heliyon.2021.e05945.

Mehmood T, Fareed S, Iqbal M, Naseem A, Siddique F. Utilization of Agro-waste and Non-conventional Eruca sativa Seed Oil for Getting Optimized Process to Acquire Better Yield of Biodiesel by Using Response Surface Methodology (RSM). vol. 45. 2018a.

Mehmood T, Fareed S, Iqbal M, Naseem A, Siddique F. Utilization of Agro-waste and Non-conventional Eruca sativa Seed Oil for Getting Optimized Process to Acquire Better Yield of Biodiesel by Using Response Surface Methodology (RSM). vol. 45. 2018b.

Midilli A, Kucuk H, Yapar Z. A new model for single-layer drying. Drying Technology 2002;20:1503–13. https://doi.org/10.1081/DRT-120005864.

Misnawi, Selamat J, Bakar J, Saari N. Oxidation of polyphenols in unfermented and partly fermented cocoa beans by cocoa polyphenol oxidase and tyrosinase. J Sci Food Agric 2002;82:559–66. https://doi.org/10.1002/jsfa.1075.

Mohammed Raffic N, Mohammed Khondoker A, Mohammed Ali Kaabi A, Ali Hamad Majrashi A, Yhaya Mohammed Qusadi I, Ibrahim Mohamed Moawad F, et al. Utilization of ANOVA analysis in identifying the effects of various parameters on the corrosion behaviour of 7021 Al alloys in simulated RED SEA conditions. Mater Today Proc 2023. https://doi.org/https://doi.org/10.1016/j.matpr.2023.06.278.

Muharja M, Darmayanti RF, Fachri BA, Palupi B, Rahmawati I, Rizkiana MF, et al. Biobutanol production from cocoa pod husk through a sequential green method: Depectination, delignification, enzymatic hydrolysis, and extractive fermentation. Bioresour Technol Rep 2023;21. https://doi.org/10.1016/j.biteb.2022.101298.

Nag S, Dash KK. Mathematical modeling of thin layer drying kinetics and moisture diffusivity study of elephant apple. Int Food Res J 2016;23:2594–600.

Nair KPP. Cocoa (Theobroma cacao L.). 2010. https://doi.org/10.1016/b978-0-12-384677-8.00005-9.

Najari Z, Khodaiyan F, Yarmand MS, Hosseini SS. Almond hulls waste valorization towards sustainable agricultural development: Production of pectin, phenolics, pullulan, and single cell protein. Waste Management 2022;141:208–19. https://doi.org/https://doi.org/10.1016/j.wasman.2022.01.007.

Nguyen TH, Sunwoo IY, Jeong GT, Kim SK. Detoxification of Hydrolysates of the Red Seaweed Gelidium amansii for Improved Bioethanol Production. Appl Biochem Biotechnol 2019;188:977–90. https://doi.org/10.1007/s12010-019-02970-x.

Nieves LM, Panyon LA, Wang X. Engineering sugar utilization and microbial tolerance toward lignocellulose conversion. Front Bioeng Biotechnol 2015;3. https://doi.org/10.3389/fbioe.2015.00017.

Oddoye EOK, Agyente-Badu CK, Gyedu-Akoto E. Cocoa and its by-products: Identification and utilization. Chocolate in Health and Nutrition, Humana Press Inc.; 2013, p. 23–37. https://doi.org/10.1007/978-1-61779-803-0_3.

Oduro-Mensah D, Ocloo A, Nortey T, Antwi S, Okine LK, Adamafio NA. Nutritional value and safety of animal feed supplemented with Talaromyces verruculosus-treated cocoa pod husks. Sci Rep 2020;10. https://doi.org/10.1038/s41598-020-69763-9.

de Oliveira PZ, de Souza Vandenberghe LP, Rodrigues C, de Melo Pereira GV, Soccol CR. Exploring cocoa pod husks as a potential substrate for citric acid production by solid-state fermentation using Aspergillus niger mutant strain. Process Biochemistry 2022;113:107–12. https://doi.org/https://doi.org/10.1016/j.procbio.2021.12.020.

Omolola AO, Jideani AIO, Kapila PF. Drying kinetics of banana (Musa spp.). Interciencia 2015;40:374–80.

Osei SA, Atuahene CC, Heathcote D, Frimpong EB, Adomako D. Cocoa pod-and-husk meal as a feed ingredient in layer diets. Anim Feed Sci Technol 1991;35:283–8. https://doi.org/10.1016/0377-8401(91)90134-E.

Ouattara H, G. Honoré O, Droux M, Reverchon S, Nasser W, Niamke S. Lactic acid bacteria involved in cocoa beans fermentation from Ivory Coast: Species diversity and citrate lyase production. Int J Food Microbiol 2017;256:11–9. https://doi.org/10.1016/j.ijfoodmicro.2017.05.008.

Ouattara HG, Niamké SL. Mapping the functional and strain diversity of the main microbiota involved in cocoa fermentation from Cote d'Ivoire. Food Microbiol 2021;98. https://doi.org/10.1016/j.fm.2021.103767.

Page GE. Factors influencing the maximum rates of air drying shelled corn in thin layers. M.S. Thesis 1949:1–65.

Panchariya PC, Popovic D, Sharma AL. Thin-layer modelling of black tea drying process. J Food Eng 2002;52:349–57. https://doi.org/10.1016/S0260-8774(01)00126-1.

Perry TW. Nutrient Requirements of Beef Cattle. Beef Cattle Feeding and Nutrition 1995:351–69. https://doi.org/10.1016/b978-012552052-2/50026-3.

Rachmawaty, Halifah P, Hartati, Zulkifli M, Madihah MS. Optimization of chitinase production by trichoderma virens in solid state fermentation using response surface methodology. Materials Science Forum, vol. 967 MSF, Trans Tech Publications Ltd; 2019, p. 132–42. https://doi.org/10.4028/www.scientific.net/MSF.967.132.

Roelofsen PA. Fermentation, Drying, and Storage of Cacao Beans. Adv Food Res 1958;8:225—96. https://doi.org/10.1016/S0065-2628(08)60021-X.

Roy S, Kr Saha A, Panda S, Dey G. Optimization of turmeric oil extraction in an annular supercritical fluid extractor by comparing BBD-RSM and FCCD-RSM approaches. Mater Today Proc 2023a;76:47—55. https://doi.org/https://doi.org/10.1016/j.matpr.2022.09.039.

Roy S, Kr Saha A, Panda S, Dey G. Optimization of turmeric oil extraction in an annular supercritical fluid extractor by comparing BBD-RSM and FCCD-RSM approaches. Mater Today Proc 2023b;76:47—55. https://doi.org/https://doi.org/10.1016/j.matpr.2022.09.039.

Secrist DS. "Effect of corn particle size on feedlot steer performance and carcass characteristics. Research Report." Concept and Communication 2019;null:301—16. https://doi.org/10.15797/concom.2019..23.009.

Seguine ES. Evidence for the Effect of the Cocoa Bean Flavour Environment during Fermentation on the Final Flavour Profile of Cocoa Liquor and Chocolate. 2009.

Senadeera W, Bhandari BR, Young G, Wijesinghe B. Influence of shapes of selected vegetable materials on drying kinetics during fluidized bed drying. J Food Eng 2003;58:277—83. https://doi.org/10.1016/S0260-8774(02)00386-2.

Sharaf-Eldeen YI, Blaisdell JL, Hamdy MY. Model for Ear Corn Drying. Transactions of the American Society of Agricultural Engineers 1980;23. https://doi.org/10.13031/2013.34757.

Singleton VL, Orthofer R, Lamuela-Ravent6s RM. 52 POLYPHENOLS AND FLAVONOIDS [14] [14] Analysis of Total Phenols and Other Oxidation Substrates and Antioxidants by Means of Folin-Ciocalteu Reagent. 1999a.

Singleton VL, Orthofer R, Lamuela-Ravent6s RM. 52 POLYPHENOLS AND FLAVONOIDS [14] [14] Analysis of Total Phenols and Other Oxidation Substrates and Antioxidants by Means of Folin-Ciocalteu Reagent. 1999b.

Thabti I, Marzougui N, Elfalleh W, Ferchichi A. Antioxidant composition and antioxidant activity of white (Morus alba L.), black (Morus nigra L.) and red (Morus rubra L.) mulberry l e a v e s . A c t a B o t a n i c a G a l l i c a 2 0 1 1 ; 1 5 8 : 2 0 5 — 1 4 . https://doi.org/10.1080/12538078.2011.10516267.

Togrul IT, Pehlivan D. Mathematical modelling of solar drying of apricots in thin layers. J Food Eng 2002;55:209—16. https://doi.org/10.1016/S0260-8774(02)00065-1.

Tunde-Akintunde TY, Ogunlakin GO. Mathematical modeling of drying of pretreated and untreated pumpkin. J Food Sci Technol 2013;50:705—13. https://doi.org/10.1007/s13197-011-0392-2.

Turan OY, Firatligil FE. Modelling and characteristics of thin layer convective air-drying of thyme (Thymus vulgaris) leaves. Czech Journal of Food Sciences 2019;37:128–34. https://doi.org/10.17221/243/2017-CJFS.

Utami RR, Armunanto R, Rahardjo S, Supriyanto. Effects of cocoa bean (Theobroma cacao L.) fermentation on phenolic content, antioxidant activity and functional group of cocoa bean shell. Pakistan Journal of Nutrition 2016a;15:948−53. https://doi.org/10.3923/pjn.2016.948.953.

Utami RR, Armunanto R, Rahardjo S, Supriyanto. Effects of cocoa bean (Theobroma cacao L.) fermentation on phenolic content, antioxidant activity and functional group of cocoa bean shell. Pakistan Journal of Nutrition 2016b;15:948−53. https://doi.org/10.3923/pjn.2016.948.953.

Valadez-Carmona L, Plazola-Jacinto CP, Hernández-Ortega M, Hernández-Navarro MD, Villarreal F, Necoechea-Mondragón H, et al. Effects of microwaves, hot air and freeze-drying on the phenolic compounds, antioxidant capacity, enzyme activity and microstructure of cacao pod husks (Theobroma cacao L.). Innovative Food Science and Emerging Technologies 2017;41:378−86. https://doi.org/10.1016/j.ifset.2017.04.012.

Vásquez ZS, de Carvalho Neto DP, Pereira GVM, Vandenberghe LPS, de Oliveira PZ, Tiburcio PB, et al. Biotechnological approaches for cocoa waste management: A review. Waste Management 2019;90:72−83. https://doi.org/10.1016/j.wasman.2019.04.030.

Wang Z, Sun J, Liao X, Chen F, Zhao G, Wu J, et al. Mathematical modeling on hot air drying of thin layer apple pomace. Food Research International 2007;40:39−46. https://doi.org/10.1016/j.foodres.2006.07.017.

White GM, Ross IJ, Poneleit CG. Fully-Exposed Drying of Popcorn. Paper - American Society of Agricultural Engineers 1979:466−9.

Yaldiz O, Ertekin C, Uzun HI. Mathematical modeling of thin layer solar drying of sultana grapes. Energy 2001;26:457−65. https://doi.org/10.1016/S0360-5442(01)00018-4.

Yaya OL, Kouadio Appiah KE, Doudjo S, Mahamane Nassirou AK, Didier FG, Benjamin YK, et al. Multi-response and multi-criteria optimization of acid hydrolyzate detoxification of cocoa pod husks: Effect on the content of phenolic compounds and fermentable sugars. Heliyon 2023;9. https://doi.org/10.1016/j.heliyon.2023.e15409.

Appendix A

CHEMICAL PREPARATIONS AND CALCULATIONS

Initial moisture content

Initial Moisture Content (%) = (Mass of Water / Initial Mass of Material) * 100

For example, in the case of CPH, the initial weight was 100 g. After being dried at 80°C for 72 hours, the weight of the dried CPH was 15.87 g. The initial moisture content of the CPH can be calculated as follows.

Initial Moisture Content (%) = [(100-15.87)/100]*100

= 84.13%

Moisture ratio of CPH (Dry basis)

The moisture ratio of CPH which used to fit with the selected mathematical model was shown below. The moisture ratio on a dry basis is a measure of the amount of moisture present in a material relative to the dry weight of the material. It's often used in drying processes to understand the extent of moisture removal. The formula for calculating the moisture ratio on a dry basis is:

Moisture Ratio (Dry Basis) = (Weight of Water / Dry Weight of Material)

Calculate Dry Weight: Subtract the weight of water that has been removed from the initial weight of the material to get the dry weight. The initial weight of CPH was 100 g, and the weight of dried CPH was 15.87 g. So, the dry weight of the CPH would be 100 g – 84.13 = 15.87 g.

Calculate Weight of Water: The weight of water that was removed during drying is the initial weight of the material minus the weight of dried material. In this case, it's 100 g - 15.87 g = 84.13 g.

Calculate Moisture Ratio (Dry Basis): Use the formula mentioned above to calculate the moisture ratio on a dry basis.

$$\text{Moisture Ratio (Dry Basis)} = (\text{Weight of Water} / \text{Dry Weight of Material})$$
$$= (84.13 \text{ g} / 15.87 \text{ g})$$
$$= 5.30$$

Reagents used for the reaction.

1. 0.5 M Na_2CO_3 500 mL

: Weigh 57.5 g of Na_2CO_3, then dissolved in 500 mL of HPLC water.

2. 5% $NaNO_2$ in 100 mL

: Weigh 5g of $NaNO_2$ g dissolved in 100 mL.

3. 40% NaOH (w/v)

: Weigh NaOH 400 g dissolved in 1000 mL.

4. 0.1N HCL

: Take 2.1 ml of concentrated HCl with a pipet, and dilute to 250 ml with distilled water in a 250ml-volumetric flask.

5. 4% boric acid

: Weigh 4 g of boric acid and dissolved in 100 mL.

Mobile phase

Mobile phase A: Distilled water for HPLC analysis

Mobile phase B: 100% Acetonitrile

Standard substance

1. Theobromine substance (HPLC grade with 98.5% purity)

HPLC condition

1. C_{18} column (Hypersil ODS, 5 μm, 4.0 x 250 mm cartridge

2. Flow rate 1.0 mL/min at 35 ºC

3. Fluorescence detector : Excit 274 nm

4. Isocratic mode

5. Injection program

    5.1 Injection volume 50 μL

5.2 Wash vial No. 91

5.3 The retention time was set to 5 minutes

Method for making calibration curve of theobromine standard solution.

1. Prepare theobromine standard solutions at concentrations of 0, 50, 100, 200, 300, and 400 mg/L.

2. Use a syringe to aspirate the solution at various concentrations, then filter into a 2 mL vial through Syringe Filters with a filtration medium of 0.45 µm.

3. The reagent and mobile phase were filtered through 0.2 µm filter paper.

4. Theobromine was analyzed by HPLC using the conditions described above. Theobromine peaks at approximately 2.509 minutes.

5. The area under the graph was integrated at the peak of theobromine at various concentrations. Then plot the graph where the x-axis is the theobromine concentration (mg/L), the y-axis is the area under the curve, the calibration curve of the theobromine standard solution is obtained, as shown in Figure A-1.
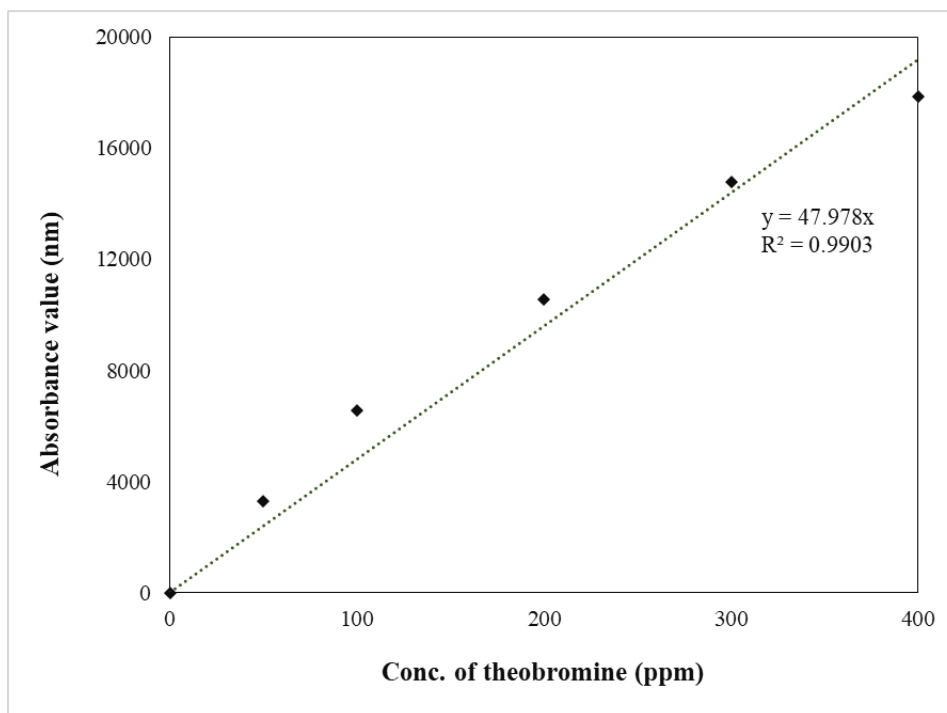

Figure A-1 Calibration curve of theobromine standard solution for theobromine

analysis

Calculation of theobromine content

From the calibration curve of the theobromine standard solution, the linear equation is

y = 47.978x

From the equation $y = 47.978x$

Replace y = 14.3

Then x = 0.298 mg theobromine/ml

The theobromine content in the extract was equal to:

$$0.298 \frac{\text{mg theobromine}}{1 \text{ L}} \times \frac{45 \text{ ml}}{1.5 \text{ g dry powder}} \times \frac{1 \text{ L}}{1000 \text{ ml}}$$

$$= 0.00894 \frac{\text{mg Theobromine}}{\text{g dry powder}}$$

Total phenolic content (TPC) determination

The TPC analysis of the extracts was performed according to the Folin-Ciocalteu assay, which was adapted from the method of Hatami et al. (2014).

Plotting of calibration curve of gallic acid standard solution.

1. Prepare gallic acid standards at the concentrations of 0.05, 0.10, 0.20, 0.40, and 0.50 mg/mL.

2. The 0.1 mL of various concentrations of gallic acid standard solutions were pipetted into the test tubes. Then added 5 mL of diluted solution of Folin-Ciocalteu reagent.

3. The 3.5 ml of sodium carbonate solution was added in test tubes. Then shake to mix well.

4. The mixture was incubated in a water bath at 40°C for 1 hour.

5. The absorbance was measured at a wavelength of 738 nm with a UV-Vis spectrophotometer at a wavelength of 738 nm. Then take the absorbance value to create a calibration curve. The phenolic content was calculated from the gallic acid calibration curve and expressed as mg gallic acid equivalent (mg GAE / 100 g dry powder)

Calibration curve
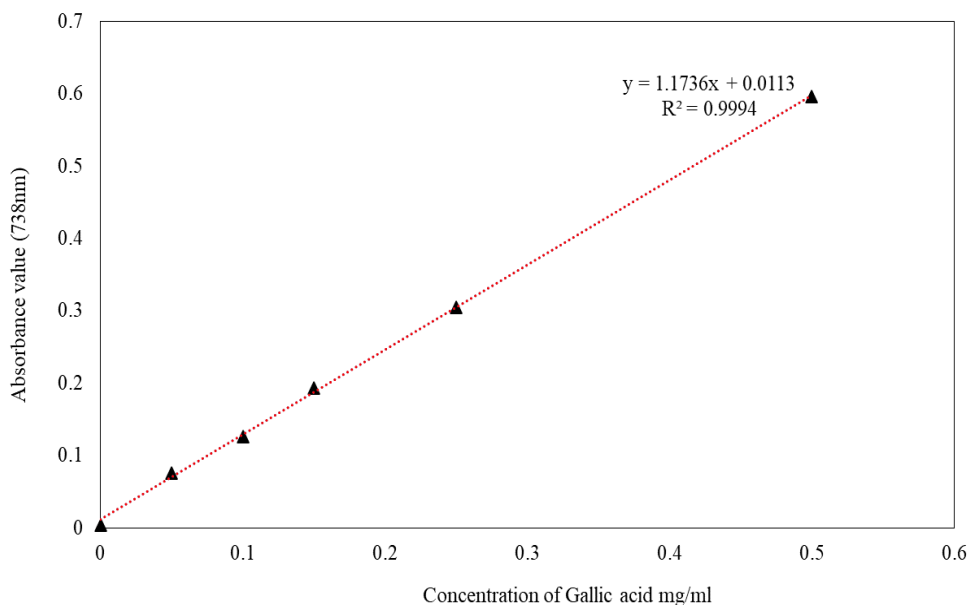
Figure A-2 Calibration curve of gallic acid solution for TPC determination

Calculation of TPC

From the calibration curve of the gallic acid solution, the linear equation is $y = 1.1736x + 0.00113$

The samples used in the calculation were obtained from experiments, with a fixed solvent-to-dried sample ratio of 30:1 (ml/g). Following the extraction process, the solutions containing the extracts were analyzed using a UV-vis spectrophotometer, and the absorbance values were subsequently calculated.

From the equation $y = 1.1736x + 0.00113$

Replace $y = 0.517$

Then $x = 0.440$ mg GAE/mL

The TPC in the extract was equal to:

$$0.440 \frac{\text{mg GAE}}{\text{mL}} \times \frac{45 \text{ mL}}{1.5 \text{ g dry powder}} = 13.2 \frac{\text{mg GAE}}{\text{g dry powder}}$$

Total flavonoid content (TFC) analysis

The TFC analysis method used in this study was adapted from the method by Hu et al. (2017).

Plotting of calibration curve of quercetin standard solution

1. Prepare quercetin standard solution at concentrations of 0.05, 0.2, 0.4, 0.6, 0.8 and 1.2 mg/mL.

2. Pipette 0.5 mL of various concentrations of quercetin standard solution into the test tube.

3. Pipette 100 µL of 5% $NaNO_2$ solution into the test tube. After that, shake it for 5 minutes.

4. Pipette 1 mL of 10% $AlCl_3$ solution into the test tube. After that, shake for 5 minutes and set aside.

5. Pipette 1 mL of 1 M of NaOH solution and 3 mL of distilled water into the test tube. Then set it aside for 10 minutes.

6. The absorbance was measured at a wavelength of 510 nm with a UV-Vis spectrophotometer. Then take the absorbance value to create a calibration curve. The results were reported in a form (mg QE / g dry powder)
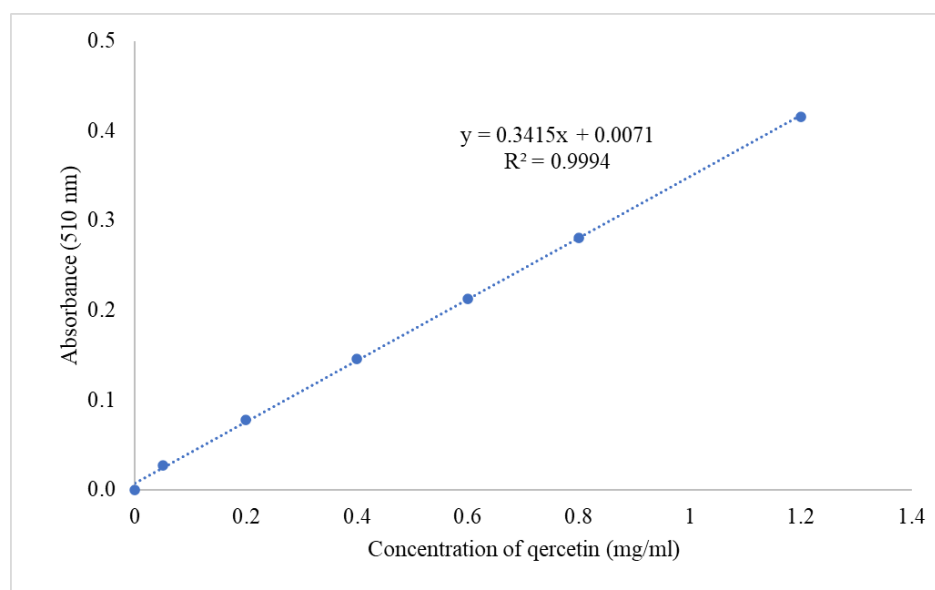
Calibration curve

Figure A-3 Calibration curve of quercetin solution for TFC analysis

Calculation of TFC

From the calibration curve of the quercetin solution, the linear equation is $y = 0.3415x + 0.0071$

The samples used in the calculation were obtained from experiments, with a fixed solvent-to-dried sample ratio of 30:1 (ml/g). Following the extraction process, the solutions containing the extracts were analyzed using a UV-vis spectrophotometer, and the absorbance values were subsequently calculated.

From the equation $y = 0.3415x + 0.0071$

Replace y $= 0.192$

Then x $= 0.541$ mg QE/mL

The TFC in the extract was equal to:

$$0.541 \frac{\text{mg QE}}{\text{mL}} \times \frac{45 \text{ mL}}{1.5 \text{ g powder}} = 16.23 \frac{\text{mg QE}}{\text{g powder}}$$

2,2 diphenyl--1picryhydrazyl scavenging activity (DPPH) analysis

The 2,2-diphenyl-1-picrylhydrazyl (DPPH) radical scavenging activity of the extract was evaluated using Thabti et al (2011).

1. 2.0 mL of DPPH solution (0.2 mM DPPH in 95% ethanol) was thoroughly mixed with 1.0 mL of extract at concentration of 300 µg/mL in screw cap tubes

2. The mixture was forcefully shaken and stored at room temperature for 30 minutes in the dark.

3. A UV-vis spectrophotometer was used to detect the absorbance at 517 nm.

4. The blank control was 95% ethanol.

5. The DPPH scavenging activity (%) was calculated according to the following equation:

DPPH scavenging activity (%) = (($A_{control}$- A_{sample}) / $A_{control}$) x 100%

when

$A_{control}$ = Light absorption value of DPPH solution

A_{sample} = The light absorbance value of the extract mixed with DPPH solution

Calculation of DPPH scavenging activity (%)

From the experiment at optimal condition using solvent extraction method, the results were $A_{control}$ = 1.066 and A_{sample} = 0.1502 When calculated according to the above formula, the value of DPPH scavenging activity (%) is as follows:

$$\text{DPPH scavenging activity (\%)} = \left[\frac{1.066-0.1502}{1.066}\right] \times 100$$

DPPH scavenging activity (%) = 85.90%

Appendix B

THE RAW DATA OF EXPERIMENTS

Table B-1 The data of moisture ratio of CPH under 50, 60, and 70ºC of operating temperature

Time (minutes)	70ºC (%dry basis)	60 ºC(%dry basis)	50 ºC(%dry basis)
0	540.03	540.03	540.03
15	529.49	530.25	530.40
30	511.66	513.90	517.61
45	489.98	497.81	503.57
60	468.33	481.75	490.64
75	447.11	465.27	476.84
90	426.08	450.04	464.54
105	405.01	434.98	451.97
120	385.16	420.50	439.32
135	365.65	406.12	427.66
150	344.71	392.49	415.87
165	326.44	378.28	405.02
180	309.30	365.18	393.35
195	293.27	351.68	386.27
210	275.49	339.46	376.12
225	261.59	327.85	364.65
240	246.76	316.40	353.98
255	232.50	304.65	344.32
270	221.18	294.09	333.68
285	209.07	283.18	322.92
300	198.54	272.77	313.08
315	189.35	262.39	302.63
330	180.39	251.60	292.20

345	173.80	242.30	282.18
360	166.31	231.88	272.35
375	-	223.34	262.66
390	-	214.49	253.33
405	-	201.25	244.31
420	-	191.73	234.94
435	-	183.77	226.06
450	-	176.69	216.99
465	-	171.49	208.37
480	-	165.57	200.15
495	-	164.62	191.67
510	-	-	184.21
525	-	-	179.03
540	-	-	172.00
555	-	-	165.05

Table B-2 The data of moisture content (%dry basis), and drying rate (g water/ g dry matter*m) as function of drying time (mins)

Time (mins)	Moisture content (% dry basis)			DR (g water/ g dry matter*m)		
	50°C	60°C	70°C	50°C	60°C	70°C
0	540	540	540	0	0	0
15	530	530	529	0.297	0.304	0.324
30	518	514	512	0.395	0.508	0.548
45	504	498	490	0.433	0.500	0.667
60	491	482	468	0.399	0.499	0.666
75	477	465	447	0.426	0.513	0.653
90	465	450	426	0.380	0.473	0.647
105	452	435	405	0.388	0.468	0.648
120	439	420	385	0.390	0.450	0.610
135	428	406	366	0.360	0.447	0.600
150	416	392	345	0.364	0.424	0.644
165	405	378	326	0.335	0.442	0.562
180	393	365	309	0.360	0.407	0.527
195	386	352	293	0.219	0.420	0.493
210	376	339	275	0.313	0.380	0.547
225	365	328	262	0.354	0.361	0.428
240	354	316	247	0.329	0.356	0.456
255	344	305	233	0.299	0.365	0.439
270	334	294	221	0.328	0.328	0.348
285	323	283	209	0.332	0.339	0.372
300	313	273	199	0.304	0.324	0.324
315	303	262	189	0.323	0.323	0.283
330	292	252	180	0.322	0.336	0.276
345	282	242	174	0.309	0.289	0.203
360	272	232	166	0.304	0.324	0.230
375	263	223	-	0.299	0.266	-
390	253	214	-	0.288	0.275	-

405	244	201	-	0.278	0.412	-
420	235	192	-	0.289	0.296	-
435	226	184	-	0.274	0.248	-
450	217	177	-	0.280	0.220	-
465	208	171	-	0.266	0.233	-
480	200	166	-	0.254	0.220	-
495	192	165	-	0.262	0.214	-
510	184	-	-	0.230	-	-
525	179	-	-	0.160	-	-
540	172	-	-	0.217	-	-
555	165	-	-	0.215	-	-

Table B-3 The list of selected mathematical models used for predicting the moisture ratio of CPH

Model number	Model name
1	Lewis
2	Page
3	Modified Page
4	Henderson and Pabis
5	Wang and Singh
6	Logarithmic
7	Two term
8	Two term exponential
9	Modified Henderson and Pabis
10	Midilli et al.
11	Approximation of diffusion
12	Verma

Table B-4 The predicted data obtained from mathematical modeling in terms of the reduced moisture ratio of CPH during the drying process at an operating temperature of 50°C and an air ventilation rate of 3 L/min.

Time (mins)	50°C											
	Model number											
	1	2	3	4	5	6	7	8	9	10	11	12
0	1.00	1.00	1.00	1.04	1.00	1.00	1.00	1.00	1.03	1.01	1.00	1.00
15	0.97	0.98	0.98	1.00	0.98	0.98	0.97	0.97	1.00	0.98	0.98	0.97
30	0.94	0.96	0.96	0.97	0.95	0.95	0.94	0.94	0.97	0.96	0.96	0.94
45	0.92	0.94	0.94	0.95	0.93	0.93	0.92	0.92	0.94	0.93	0.93	0.92
60	0.89	0.92	0.92	0.92	0.91	0.91	0.89	0.89	0.91	0.91	0.91	0.89
75	0.87	0.89	0.89	0.89	0.88	0.88	0.87	0.87	0.89	0.88	0.89	0.87
90	0.84	0.87	0.87	0.86	0.86	0.86	0.84	0.84	0.86	0.86	0.87	0.84
105	0.82	0.85	0.85	0.84	0.84	0.84	0.82	0.82	0.83	0.84	0.84	0.82
120	0.79	0.82	0.82	0.81	0.82	0.82	0.79	0.79	0.81	0.82	0.82	0.79
135	0.77	0.80	0.80	0.79	0.80	0.80	0.77	0.77	0.78	0.80	0.80	0.77
150	0.75	0.78	0.78	0.76	0.78	0.77	0.75	0.75	0.76	0.77	0.78	0.75
165	0.73	0.76	0.76	0.74	0.75	0.75	0.73	0.73	0.74	0.75	0.76	0.73
180	0.71	0.73	0.73	0.72	0.73	0.73	0.71	0.71	0.72	0.73	0.73	0.71

195	0.69	0.71	0.71	0.70	0.71	0.71	0.69	0.69	0.70	0.71	0.71	0.69
210	0.67	0.69	0.69	0.68	0.69	0.69	0.67	0.67	0.67	0.69	0.69	0.67
225	0.65	0.67	0.67	0.66	0.67	0.67	0.65	0.65	0.65	0.67	0.67	0.65
240	0.63	0.65	0.65	0.64	0.65	0.65	0.63	0.63	0.63	0.65	0.65	0.63
255	0.61	0.63	0.63	0.62	0.63	0.63	0.61	0.61	0.62	0.63	0.63	0.61
270	0.60	0.61	0.61	0.60	0.61	0.61	0.60	0.60	0.60	0.61	0.61	0.60
285	0.58	0.59	0.59	0.58	0.60	0.59	0.58	0.58	0.58	0.60	0.59	0.58
300	0.56	0.57	0.57	0.56	0.58	0.58	0.56	0.56	0.56	0.58	0.57	0.56
315	0.55	0.55	0.55	0.55	0.56	0.56	0.55	0.55	0.55	0.56	0.55	0.55
330	0.53	0.53	0.53	0.53	0.54	0.54	0.53	0.53	0.53	0.54	0.53	0.53
345	0.52	0.52	0.52	0.51	0.52	0.52	0.52	0.52	0.51	0.52	0.52	0.52
360	0.50	0.50	0.50	0.50	0.50	0.50	0.50	0.50	0.50	0.51	0.50	0.50
375	0.49	0.48	0.48	0.48	0.49	0.49	0.49	0.49	0.48	0.49	0.48	0.49
390	0.47	0.47	0.47	0.47	0.47	0.47	0.47	0.47	0.47	0.47	0.47	0.47
405	0.46	0.45	0.45	0.45	0.45	0.45	0.46	0.46	0.45	0.45	0.45	0.46
420	0.45	0.44	0.43	0.44	0.44	0.44	0.45	0.45	0.44	0.44	0.43	0.45
435	0.43	0.42	0.42	0.43	0.42	0.42	0.43	0.43	0.43	0.42	0.42	0.43
450	0.42	0.41	0.40	0.41	0.40	0.40	0.42	0.42	0.42	0.41	0.40	0.42

465	0.41	0.39	0.39	0.40	0.39	0.39	0.41	0.41	0.40	0.39	0.39	0.41
480	0.40	0.38	0.38	0.39	0.37	0.37	0.40	0.40	0.39	0.37	0.38	0.40
495	0.39	0.37	0.36	0.38	0.36	0.36	0.39	0.39	0.38	0.36	0.36	0.39
510	0.38	0.35	0.35	0.37	0.34	0.34	0.38	0.38	0.37	0.34	0.35	0.38
525	0.37	0.34	0.34	0.36	0.33	0.33	0.37	0.37	0.36	0.33	0.34	0.37
540	0.35	0.33	0.33	0.35	0.31	0.31	0.36	0.35	0.35	0.31	0.32	0.35
555	0.34	0.32	0.32	0.33	0.30	0.30	0.35	0.34	0.34	0.30	0.31	0.34

Table B-5 The predicted data obtained from mathematical modeling in terms of the reduced moisture ratio of CPH during the drying process at an operating temperature of 60°C and an air ventilation rate of 3 L/min.

Time (mins)	60°C											
	Model number											
	1	**2**	**3**	**4**	**5**	**6**	**7**	**8**	**9**	**10**	**11**	**12**
0	1.00	1.00	1.00	1.10	1.00	1.01	1.01	1.00	1.00	1.01	1.00	1.00
15	0.97	0.98	0.96	1.06	0.97	0.98	0.98	0.97	0.99	0.98	0.97	0.97
30	0.93	0.95	0.92	1.03	0.94	0.95	0.95	0.93	0.97	0.95	0.95	0.93
45	0.90	0.92	0.88	0.99	0.91	0.92	0.92	0.90	0.94	0.92	0.92	0.90

60	0.87	0.89	0.85	0.95	0.89	0.89	0.89	0.87	0.91	0.89	0.89	0.87
75	0.84	0.87	0.81	0.92	0.86	0.86	0.86	0.84	0.88	0.86	0.86	0.84
90	0.81	0.84	0.78	0.89	0.83	0.83	0.84	0.81	0.85	0.83	0.84	0.81
105	0.79	0.81	0.75	0.85	0.80	0.81	0.81	0.79	0.82	0.81	0.81	0.79
120	0.76	0.78	0.72	0.82	0.78	0.78	0.78	0.76	0.79	0.78	0.78	0.76
135	0.73	0.76	0.69	0.79	0.75	0.75	0.75	0.73	0.76	0.75	0.76	0.73
150	0.71	0.73	0.66	0.77	0.73	0.73	0.73	0.71	0.73	0.73	0.73	0.71
165	0.68	0.70	0.64	0.74	0.70	0.70	0.70	0.68	0.70	0.70	0.70	0.68
180	0.66	0.68	0.61	0.71	0.68	0.68	0.68	0.66	0.67	0.68	0.68	0.66
195	0.64	0.65	0.59	0.69	0.66	0.65	0.65	0.64	0.65	0.66	0.66	0.64
210	0.62	0.63	0.56	0.66	0.63	0.63	0.63	0.62	0.62	0.63	0.63	0.62
225	0.60	0.61	0.54	0.64	0.61	0.61	0.61	0.60	0.60	0.61	0.61	0.60
240	0.58	0.58	0.52	0.62	0.59	0.59	0.58	0.58	0.58	0.59	0.59	0.58
255	0.56	0.56	0.50	0.59	0.57	0.57	0.56	0.56	0.56	0.57	0.56	0.56
270	0.54	0.54	0.48	0.57	0.55	0.54	0.54	0.54	0.54	0.54	0.54	0.54
285	0.52	0.52	0.46	0.55	0.52	0.52	0.52	0.52	0.52	0.52	0.52	0.52
300	0.50	0.50	0.44	0.53	0.50	0.50	0.50	0.50	0.50	0.50	0.50	0.50
315	0.48	0.48	0.42	0.51	0.48	0.48	0.48	0.48	0.48	0.48	0.48	0.48

330	0.47	0.46	0.41	0.49	0.46	0.47	0.46	0.47	0.46	0.47	0.46	0.47
345	0.45	0.44	0.39	0.48	0.45	0.45	0.44	0.45	0.44	0.45	0.44	0.45
360	0.44	0.43	0.37	0.46	0.43	0.43	0.43	0.44	0.42	0.43	0.43	0.44
375	0.42	0.41	0.36	0.44	0.41	0.41	0.41	0.42	0.41	0.41	0.41	0.42
390	0.41	0.39	0.34	0.43	0.39	0.39	0.39	0.41	0.39	0.39	0.39	0.41
405	0.39	0.38	0.33	0.41	0.38	0.38	0.38	0.39	0.38	0.38	0.38	0.39
420	0.38	0.36	0.32	0.40	0.36	0.36	0.36	0.38	0.36	0.36	0.36	0.38
435	0.37	0.35	0.30	0.38	0.34	0.34	0.35	0.37	0.35	0.34	0.35	0.37
450	0.35	0.33	0.29	0.37	0.33	0.33	0.33	0.35	0.34	0.33	0.33	0.35
465	0.34	0.32	0.28	0.36	0.31	0.31	0.32	0.34	0.32	0.31	0.32	0.34

Table B-6 The predicted data obtained from mathematical modeling in terms of the reduced moisture ratio of CPH during the drying process at an operating temperature of 70°C and an air ventilation rate of 3 L/min.

Time (mins)	70°C											
	Model number											
	1	2	3	4	5	6	7	8	9	10	11	12
0	1.00	1.00	1.00	1.05	1.00	1.04	1.00	1.00	1.01	1.00	1.00	1.00
15	0.95	0.97	0.94	1.00	0.96	0.99	0.98	0.97	0.98	0.98	0.98	0.98

30	0.91	0.94	0.89	0.95	0.92	0.94	0.95	0.93	0.94	0.94	0.95	0.95
45	0.87	0.90	0.84	0.90	0.88	0.90	0.91	0.90	0.91	0.91	0.91	0.91
60	0.83	0.86	0.79	0.86	0.85	0.86	0.87	0.86	0.87	0.87	0.87	0.87
75	0.79	0.82	0.74	0.81	0.81	0.82	0.83	0.82	0.83	0.83	0.83	0.83
90	0.75	0.78	0.70	0.77	0.77	0.78	0.79	0.79	0.79	0.79	0.79	0.79
105	0.72	0.75	0.66	0.73	0.74	0.74	0.75	0.75	0.75	0.75	0.75	0.75
120	0.69	0.71	0.62	0.70	0.71	0.71	0.71	0.71	0.71	0.71	0.71	0.71
135	0.65	0.68	0.59	0.66	0.67	0.67	0.67	0.68	0.67	0.67	0.67	0.67
150	0.62	0.64	0.55	0.63	0.64	0.64	0.64	0.65	0.64	0.64	0.64	0.64
165	0.59	0.61	0.52	0.60	0.61	0.61	0.60	0.61	0.60	0.60	0.60	0.60
180	0.57	0.58	0.49	0.57	0.58	0.58	0.57	0.58	0.57	0.57	0.57	0.57
195	0.54	0.55	0.46	0.54	0.55	0.55	0.54	0.55	0.54	0.54	0.54	0.54
210	0.52	0.52	0.44	0.51	0.52	0.52	0.51	0.52	0.51	0.51	0.51	0.51
225	0.49	0.49	0.41	0.49	0.50	0.49	0.49	0.49	0.48	0.48	0.49	0.49
240	0.47	0.46	0.39	0.46	0.47	0.47	0.46	0.46	0.46	0.46	0.46	0.46
255	0.45	0.44	0.37	0.44	0.44	0.44	0.44	0.44	0.43	0.43	0.44	0.44
270	0.43	0.41	0.35	0.42	0.42	0.42	0.41	0.41	0.41	0.41	0.41	0.41
285	0.41	0.39	0.33	0.40	0.39	0.39	0.39	0.39	0.39	0.39	0.39	0.39
300	0.39	0.37	0.31	0.38	0.37	0.37	0.37	0.37	0.37	0.37	0.37	0.37

315	0.37	0.35	0.29	0.36	0.35	0.35	0.35	0.35	0.35	0.35	0.35	0.35
330	0.35	0.33	0.27	0.34	0.33	0.33	0.33	0.32	0.33	0.33	0.33	0.33
345	0.34	0.31	0.26	0.32	0.31	0.31	0.31	0.31	0.32	0.32	0.31	0.31
360	0.32	0.29	0.24	0.31	0.29	0.29	0.30	0.29	0.30	0.30	0.30	0.30

Table B-7 The moisture ratio of CPH was measured under operating temperatures of 50°C, 60°C, and 70°C through experiments, and these results were compared with predictions from the Midilli et al. model.

Time	Experimental			Midilli et al.		
(mins)	50°C	60°C	70°C	50°C	60°C	70°C
0	1.00	1.00	1.00	1.01	1.01	1.00
15	0.98	0.98	0.98	0.98	0.98	0.98
30	0.96	0.95	0.95	0.96	0.95	0.94
45	0.93	0.92	0.91	0.93	0.92	0.91
60	0.91	0.89	0.87	0.91	0.89	0.87
75	0.88	0.86	0.83	0.88	0.86	0.83
90	0.86	0.83	0.79	0.86	0.83	0.79
105	0.84	0.81	0.75	0.84	0.81	0.75
120	0.81	0.78	0.71	0.82	0.78	0.71
135	0.79	0.75	0.68	0.80	0.75	0.67
150	0.77	0.73	0.64	0.77	0.73	0.64
165	0.75	0.70	0.60	0.75	0.70	0.60
180	0.73	0.68	0.57	0.73	0.68	0.57
195	0.72	0.65	0.54	0.71	0.66	0.54
210	0.70	0.63	0.51	0.69	0.63	0.51
225	0.68	0.61	0.48	0.67	0.61	0.48
240	0.66	0.59	0.46	0.65	0.59	0.46
255	0.64	0.56	0.43	0.63	0.57	0.43
270	0.62	0.54	0.41	0.61	0.54	0.41
285	0.60	0.52	0.39	0.60	0.52	0.39
300	0.58	0.51	0.37	0.58	0.50	0.37
315	0.56	0.49	0.35	0.56	0.48	0.35
330	0.54	0.47	0.33	0.54	0.47	0.33
345	0.52	0.45	0.32	0.52	0.45	0.32
360	0.50	0.43	0.31	0.51	0.43	0.30
375	0.49	0.41	-	0.49	0.41	-

390	0.47	0.40	-	0.47	0.39	-
405	0.45	0.37	-	0.45	0.38	-
420	0.44	0.36	-	0.44	0.36	-
435	0.42	0.34	-	0.42	0.34	-
450	0.40	0.33	-	0.41	0.33	-
465	0.39	0.31	-	0.39	0.31	-
480	0.37	-	-	0.37	-	-
495	0.35	-	-	0.36	-	-
510	0.34	-	-	0.34	-	-
525	0.33	-	-	0.33	-	-
540	0.32	-	-	0.31	-	-
555	0.31	-	-	0.30	-	-

Table B-8 The data of ln (MR) value at 50, 60, and 70°C of operating temperature

Drying time	ln (MR)		
(mins)	50°C	60°C	70°C
0	0.00	0.00	0.00
15	-0.02	-0.02	-0.02
30	-0.04	-0.05	-0.05
45	-0.07	-0.08	-0.09
60	-0.09	-0.12	-0.14
75	-0.13	-0.15	-0.19
90	-0.15	-0.19	-0.24
105	-0.17	-0.21	-0.29
120	-0.21	-0.25	-0.34
135	-0.24	-0.29	-0.39
150	-0.26	-0.31	-0.45
165	-0.29	-0.36	-0.51
180	-0.31	-0.39	-0.56
195	-0.33	-0.43	-0.62
210	-0.36	-0.46	-0.67

225	-0.39	-0.49	-0.73
240	-0.42	-0.53	-0.78
255	-0.45	-0.58	-0.84
270	-0.48	-0.62	-0.89
285	-0.51	-0.65	-0.94
300	-0.54	-0.67	-0.99
315	-0.58	-0.71	-1.05
330	-0.62	-0.76	-1.11
345	-0.65	-0.80	-1.14
360	-0.69	-0.84	-1.17
375	-0.71	-0.89	-
390	-0.76	-0.92	-
405	-0.80	-0.99	-
420	-0.82	-1.02	-
435	-0.87	-1.08	-
450	-0.92	-1.11	-
465	-0.94	-1.17	-
480	-0.99	-	-
495	-1.05	-	-
510	-1.08	-	-
525	-1.11	-	-
540	-1.14	-	-
555	-1.17	-	-

Table B-9 The data for energy consumption during the CPH drying process in a laboratory oven are provided for operating temperatures of 50°C, 60°C, and 70°C.

Operating temperature (°C)	Energy consumption (kWh)
50	3.7
60	5.0
70	5.4

Table B-10 The data for specific energy consumption (SEC) during the CPH drying process in a laboratory oven are provided for operating temperatures of 50°C, 60°C, and 70°C.

Operating temperature (°C)	Specific energy consumption (MJ/kg)
50	25.3
60	34.6
70	36.9

Table B-11 The data of the theobromine content of the extracts analyzed by HPLC at 7 days of fermentation time, ambient temperature extracted by the solvent extraction method, 55% ethanol concentration, ratio of 1: 30 g/mL.

Bottle No.	Theobromine content (mg/L)			
	1st	2nd	3rd	Average
1	54.50	60.20	63.80	59.50
2	21.44	29.44	25.44	25.44
3	0.46	0.65	0.63	0.58
4	20.95	14.07	17.51	17.51
5	6.08	9.04	7.56	7.56
6	20.10	27.03	23.57	23.57

Table B-12 The statistical data obtained from the regression analysis using ANOVA in Design-Expert® were utilized to confirm the goodness of fit.

Run Order	Actual Value	Predicted Value	Residual	Leverage	Internally Studentized Residuals	Externally Studentized Residuals	Cook's Distance	Influence on Fitted Value DFFITS	Standard Order
1	6.73	6.79	-0.0552	0.159	-0.441	-0.422	0.005	-0.184	15
2	7.85	7.93	-0.0767	0.734	-1.089	-1.101	0.467	-1.828	6
3	6.89	6.71	0.1848	0.159	1.477	1.585	0.059	0.689	16
4	6.53	6.57	-0.0387	0.734	-0.550	-0.529	0.119	-0.879	3
5	5.93	5.94	-0.0112	0.059	-0.084	-0.080	0.000	-0.020	11
6	5.21	5.23	-0.0187	0.734	-0.265	-0.253	0.028	-0.419	4
7	6.03	5.99	0.0388	0.159	0.310	0.296	0.003	0.129	7
8	7.33	7.42	-0.0867	0.734	-1.232	-1.268	0.597	-2.106[1]	1
9	4.87	5.10	-0.2272	0.159	-1.816	-2.104	0.089	-0.914	13
10	6.12	5.94	0.1788	0.059	1.351	1.418	0.016	0.354	12
11	5.87	5.89	-0.0212	0.159	-0.169	-0.161	0.001	-0.070	2
12	6.28	6.31	-0.0287	0.734	-0.407	-0.390	0.065	-0.647	8

13	4.12	4.10	0.0193	0.734	0.275	0.261	0.030	0.434	10
14	5.12	5.17	-0.0487	0.734	-0.692	-0.672	0.188	-1.116	5
15	5.15	5.18	-0.0272	0.159	-0.217	-0.207	0.001	-0.090	14
16	4.82	4.81	0.0093	0.734	0.132	0.126	0.007	0.209	9
17	6.15	5.94	0.2088	0.059	1.578	1.727	0.022	0.432	17

[1] Exceeds limits.

Table B-13. The changes in samples were observed during each period throughout the fermentation process for the collected samples at 7 days.

Conditions	1st day	3rd day	7th day
$X_1 = 7$ day $X_2 = 0\%$ $X_3 = 15$ ml/g			
$X_1 = 7$ day $X_2 = 0\%$ $X_3 = 0$ ml/g			
$X_1 = 7$ day $X_2 = 5\%$ $X_3 = 7.5$ ml/g			
$X_1 = 7$ day $X_2 = 10\%$ $X_3 = 0$ ml/g			

| $X_1 = 7$ day $X_2 = 10\%$ $X_3 = 15$ ml/g | | | |

Table B-14 The changes in samples were observed during each period throughout the fermentation process for the collected samples at 14 days.

Conditions	1st day	3rd day	14th day
$X_1 = 14$ day $X_2 = 5\%$ $X_3 = 0$ ml/g			
$X_1 = 14$ day $X_2 = 5\%$ $X_3 = 7.5$ ml/g			
$X_1 = 14$ day $X_2 = 0\%$ $X_3 = 7.5$ ml/g			

$X_1 = 14$ day $X_2 = 5\%$ $X_3 = 7.5$ ml/g			
$X_1 = 14$ day $X_2 = 5\%$ $X_3 = 15$ ml/g			
$X_1 = 14$ day $X_2 = 5\%$ $X_3 = 7.5$ ml/g			
$X_1 = 14$ day $X_2 = 10\%$ $X_3 = 7.5$ ml/g			

Table B-15 The changes in samples were observed during each period throughout the fermentation process for the collected samples at 21 days.

Conditions	1st day	3rd day	21st day
$X_1 = 21$ day $X_2 = 10\%$ $X_3 = 15$ ml/g			
$X_1 = 21$ day $X_2 = 5\%$ $X_3 = 7.5$ ml/g			
$X_1 = 21$ day $X_2 = 0\%$ $X_3 = 0$ ml/g			
$X_1 = 21$ day $X_2 = 0\%$ $X_3 = 15$ ml/g			

$X_1 = 21$ day $X_2 = 10\%$ $X_3 = 0$ ml/g			
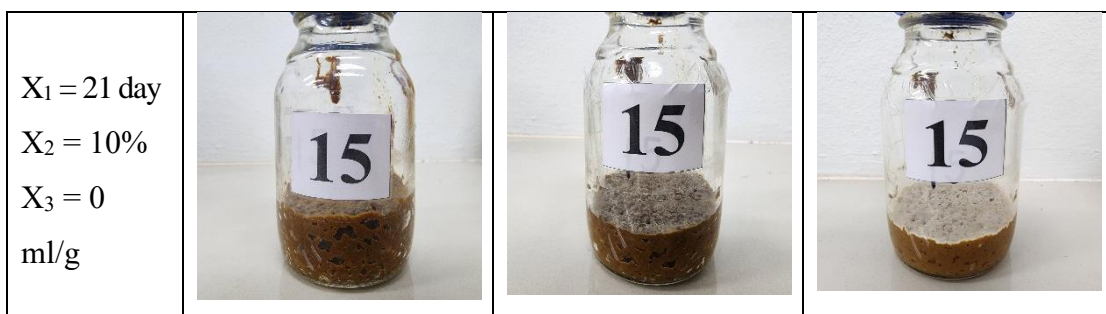
VITAE

Name   Mr. Nattawut Sianoun

Student ID   6110130022

Educational Attainment

Degree	Name of Institution	Year of Graduation
Bachelor of Engineering (Chemical engineering)	Prince of Songkla University	2017

Scholarship Awards during Enrolment

- The Faculty of Engineering's Graduate Study Scholarship

- The Graduate School of Prince of Songkla University (PSU)